Universidad Pontificia Comillas
Escuela Técnica Superior de Ingeniería (ICAI)
Instituto de Investigación Tecnológica (IIT)

Improvements in Intraoperative Neurophysiological Monitoring towards a wireless Technology

Avances en Monitorización Neurofisiológica Intraoperatoria hacia una tecnología inalámbrica

Autor: Eduardo Alonso Rivas
Directores: Dr. D. Carlos Rodríguez-Morcillo García
Dr. D. Romano Giannetti

MADRID | Marzo 2023

Universidad Pontifica Comillas
Escuela Técnica Superior de Ingeniería ICAI

Improvements in Intraoperative Neurophysiological Monitoring towards a wireless technology

Avances en Monitorización Neurofisiológica Intraoperatoria hacia una tecnología inalámbrica

PhD Candidate
Eduardo Alonso Rivas

Supervisors
Carlos Rodríguez-Morcillo García, PhD
Romano Giannetti, PhD

Submitted in part fulfillment of the requirements for the degree of
Doctor of Philosophy in Engineering Systems Modeling of Universidad Pontificia Comillas
March 2023

Resumen

La Monitorización Neurofisiológica Intraoperatoria (MNIO) se define como un conjunto de técnicas consistentes en el registro de la actividad eléctrica generada por las estructuras del sistema nervioso durante las operaciones quirúrgicas. Se trata de una rama de la medicina que está ganando cada vez más prominencia y relevancia, ya que se ha mostrado como una herramienta de mucha utilidad para evitar efectos adversos y complicaciones derivadas de intervenciones quirúrgicas. Este tipo de técnicas son utilizadas principalmente por el equipo de Neurofisiología y/o por los cirujanos para apoyar la toma de decisiones durante las cirugías para minimizar los riesgos de lesión sobre tejidos o estructuras que afecten al sistema nervioso.

El trabajo de investigación recogido en esta tesis surge como respuesta a la identificación de un área de mejora dentro de la tecnología actual dedicada a la MNIO. La monitorización de la respuesta del sistema nervioso conlleva en la mayoría de los casos el registro de un gran número de señales eléctricas derivadas de las distintas estructuras que se desean controlar y estimular, lo que implica la disposición de un gran número de electrodos de registro en distintas zonas del cuerpo del paciente, así como la interconexión de distintos elementos hardware del sistema de monitorización. Esto supone una gran cantidad de cableado y conexiones que quedan normalmente cubiertas y parcialmente inaccesibles durante las cirugías. La eliminación o reducción de este cableado se ha identificado como un avance tecnológico relevante que supondría no sólo un aumento en la ergonomía y confort para el equipo médico en la preparación del escenario, sino también un ahorro en tiempo, coste y la reducción de posibles fuentes de ruido en las señales registradas.

La motivación de esta tesis es por tanto la aplicación de tecnología inalámbrica a esta rama de la Neurofisiología, desarrollando un sistema que sea capaz de cumplir con las características de los sistemas actuales de monitorización intraoperatoria reduciendo o eliminando conexiones cableadas. Para ello, se propusieron una serie de objetivos, listados a continuación:

- Desarrollo y prototipado de un front-end analógico que cumpla con los requisitos de impedancia de entrada, bajo ruido y tasa de muestreo de los sistemas actuales. Este desarrollo irá incluido dentro de un dispositivo transmisor, autónomo y alimentado por batería, encargado de registrar las señales biológicas de interés.

- Desarrollo y prototipado de un dispositivo receptor, encargado de reconstruir la señal analógica que se ha recibido de manera inalámbrica, de modo que ésta pueda ser registrada por el sistema de monitorización empleado.
- Desarrollo de un enlace de comunicación inalámbrico bidireccional entre ambos dispositivos, para el envío de señales muestreadas y mensajes de configuracion.
- Desarrollo y validación de un prototipo funcional, incluyendo la implementación hardware y software del sistema completo de transmisión/recepción, y la realización de pruebas en un entorno de trabajo equivalente a las condiciones en las que se utilizan los equipos comerciales actuales.

Debido a su importancia para una correcta adquisición de señal, los dispositivos dedicados al registro de bioseñales están equipados con un sistema de medida de impedancia de contacto entre los electrodos y el tejido de interés. La tecnología actual hace uso de métodos activos, que implican la inyección de corriente hacia el paciente, lo cual presenta ciertas desventajas para dispositivos portátiles. Con el fin de solventarlas, se añadió un objetivo a la investigación:

- Desarrollo e implementación de un método novedoso de medida de la impedancia de contacto entre los electrodos y el tejido objeto de la medida. El objetivo en este caso es obtener un sistema pasivo, más adecuado para un dispositivo inalámbrico y autónomo, alimentado por lo tanto con batería.

La adición de este método de medida de impedancia al sistema mostró un efecto adverso: debido a los cambios necesarios en la entrada de la adquisición, se producen transitorios muy lentos en la señal de salida, lo que da lugar a que la medida requiera un gran cantidad de tiempo para llevarse a cabo. Para solventar este efecto, se añadió otro objetivo a la investigación:

- Desarrollo de un método novedoso para el establecimiento rápido de la señal mediante el control de la frecuencia de corte del filtro de entrada. Se propone una solución novedosa para sistemas diferenciales que adapta un diseño existente en la literatura para amplificadores unipolares.

El cuerpo principal de la tesis, formado por el compendio de tres publicaciones en revistas con índice de impacto en JCR, recoge los desarrollos y resultados fundamentales de esta.

En el primero de ellos, *E. Alonso, R. Giannetti, C. Rodríguez-Morcillo, J. Matanza, and J. D. Muñoz-Frías, "A Novel Passive Method for the Assessment of Skin-Electrode Contact Impedance in Intra-operative Neurophysiological Monitoring Systems," Scientific Reports, vol. 10, no. 1, pp.1–11, 2020*, se define la impedancia de contacto que se genera entre la superficie del electrodo de registro y el tejido del que se quiere obtener la respuesta eléctrica; y se destaca su importancia y efecto en la medida. En la práctica médica, la medida de esta impedancia sirve para evaluar si la conexión de los electrodos de registro es correcta y por tanto la medida fiable. Se propone un nuevo método de medida de la impedancia basado en un modelo pasivo (sin inyección de corriente), que consiste en analizar la variación de la señal medida cuando se conecta y desconecta, de manera controlada, una carga resistiva de valor conocido a la entrada del circuito de adquisición. Esta metodología ha sido contrastada con un modelo matemático, a través de simulación, y por último mediante medidas tomadas tanto en laboratorio como en un entorno hospitalario con la ayuda de un prototipo. Los resultados muestran que es posible evaluar la bondad de la conexión de los electrodos con respecto al valor de referencia ($5\,\mathrm{k}\Omega$, según la literatura).

Este nuevo método presenta una serie de ventajas relacionadas con el hecho de que no se emplee inyección de corriente como en los sistemas actuales. La primera de ellas es que resulta más adecuado para sistemas alimentados con batería, ya que reduce el consumo energético para la realización de la medida. El uso de corriente hacia el paciente implica también un riesgo de abrasión o lesión, lo que hace que la clasificación del equipo varíe según la normativa de dispositivos médicos y sea más restrictiva, de manera que un método pasivo simplifica el proceso de validación de este. El hecho de que se utilice únicamente la señal registrada para evaluar (sin hardware adicional) la impedancia de contacto, produce un efecto no deseado que consiste en la aparición de transitorios de larga duración cada vez que se realiza una conmutación de la carga, debido a los escalones de tensión que se originan a la entrada de la etapa de adquisición.

Para superar este efecto adverso, en *E. Alonso Rivas, G. Scandurra, C. Ciofi, C. Rodríguez-Morcillo García, and R. Giannetti, "A novel approach for the design of fast-settling amplifiers for biosignal detection," Electronics (Switzerland), vol. 10, no. 21, pp. 1–14, 2021.*, se propone una nueva topología para obtener un filtrado variable y configurable en función de la etapa de medida deseada.

El potencial de contacto es un efecto que se produce entre los electrodos de registro y los tejidos en los que se insertan. La diferencia de este potencial entre los distintos electrodos necesarios para la medida puede producir una componente DC que enmascare la señal AC que se desea registrar o bien que se sature la etapa de amplificación de la adquisición. Por ello, es necesario que los equipos de medida de bioseñal cuenten con un filtro paso alto para eliminar esa componente DC indeseada, normalmente consistente en una red RC con una muy baja frecuencia de corte, y por tanto una gran constante de tiempo. Si bien esto no supone un problema durante la monitorización de señales, cuando se realizan cambios en la configuración de entrada se producen variaciones de tensión con largos tiempos de establecimiento que es necesario tener en cuenta a la hora de interpretar las señales, como es el caso de la implementación del método de medida de impedancia descrito.

En este caso se propone un filtro ajustable mediante tensión que modifica de manera controlada la frecuencia de corte del filtro de entrada, y por tanto la constante de tiempo. Esta metodología se ha probado mediante simulación y con la ayuda de un prototipo del que se han obtenido medidas en laboratorio, en conjunto con el método de medida de impedancia propuesto. Los resultados obtenidos son similares a los logrados con el filtro convencional RC, consiguiendo una reducción del tiempo necesario para la estabilización de la medida en torno a un orden de magnitud, manteniendo la capacidad de realizar la medida con la misma señal registrada.

Estos resultados cubren dos de los objetivos planteados para el desarrollo de esta tesis: la implementación de un método novedoso de medida de la impedancia y el desarrollo de un método para el establecimiento rápido de la señal en sistemas de adquisición de señales biológicas. El resto de ellos se abordan mediante el prototipo presentado en *E. Alonso Rivas, R. Giannetti, C. Rodríguez-Morcillo García, J. Matanza Domingo, J. D. Muñoz Frías, G. Scandurra, C. Ciofi, L. Vega-Zelaya, and J. Pastor, "A Quasi-Wireless Intraoperatory Neurophysiological Monitoring System," Electronics (Switzerland), vol. 11, no. 23, pp. 1–19, 2022.*

Este artículo, que recoge los resultados más importantes del trabajo de investigación, muestra el diseño del prototipo desarrollado, que consta de dos elementos: Transmisor y Receptor, que se comunican mediante un enlace de radiofrecuencia bidireccional que permite, por un lado, el envío de las muestras adquiridas por el Transmisor; y por otro, la modificación de la configuración de la etapa analógica de adquisición en función de los comandos del panel de control instalado en el dispositivo Receptor.

De manera general, el dispositivo Transmisor se encarga de registrar las señales mediante electrodos convencionales, y contiene las etapas de amplificación, filtrado y conversión analógico/digital previas a la transmisión de las muestras obtenidas a través de la comunicación vía radio. Además, cuenta con la inclusión del método de medida de impedancia propuesto dentro de la etapa de adquisición. Este dispositivo está alimentado por una batería y está concebido para colocarse en la mesa quirúrgica lo más cerca posible del paciente, de manera que se pueda reducir la longitud del cableado necesario para la conexión de los electrodos.

El dispositivo Receptor, por su parte, se encarga de recibir la información enviada por el Transmisor, procesarla y reconstruir la señal registrada de manera que esta pueda ser recogida por un sistema de MNIO convencional. La inclusión de conectores estándar tanto en el Transmisor como en el Receptor permite que sea posible su utilización con cualquier sistema comercial actual. Así, se forma un puente inalámbrico transparente entre la bioseñal de interés y el sistema de monitorización que se desea emplear. Este módulo está pensado para colocarse cerca del sistema de registro, de manera más accesible para el personal médico, por lo que incluye un panel de control para modificar tanto el tipo de medida (registro o medida de impedancia), como la configuración de los canales, que puede ser diferencial o referencial. Los cambios en la configuración se transmiten igualmente mediante un transmisor de radio en sentido opuesto, en dirección hacia el Transmisor, ya que es este último el que contiene el hardware necesario para hacer las modificaciones correspondientes. La transmisión de la configuración incluye un protocolo de confirmación para asegurar la correcta recepción de la trama y así evitar interpretaciones erróneas de las señales registradas.

El sistema cuenta también con dos algoritmos implantados mediante software. El primero de ellos permite lidiar con la posible pérdida de muestras enviadas, evitando que se produzcan discontinuidades en las señales reconstruidas. El segundo algoritmo permite la variación en tiempo real de la ganancia de la etapa de amplificación, de manera que ésta sea óptima para la señal registrada.

El sistema ha sido validado mediante pruebas de laboratorio, así como a través de medidas tomadas en entorno hospitalario, comparando la salida del dispositivo Receptor con la señal registrada en paralelo por un sistema comercial de monitorización intraoperatoria. Las pruebas, tal y como se recogen en el artículo, se han realizado para un amplio espectro de técnicas de monitorización, que incluyen señales con distinto rango de frecuencia y amplitud. La única

diferencia significativa entre la señal original registrada y la reconstruida es un retraso constante (e inevitable debido a las distintas etapas del sistema), cuyo valor está en torno a 1.5 ms, lo cual se demuestra aceptablemente bajo para las aplicaciones probadas.

El dispositivo desarrollado, además de suponer una contribución a nivel científico debido a las novedosas soluciones aportadas, se presenta también como un elemento innovador con potencial contribución comercial dentro de un ámbito, el de la MNIO, que se encuentra en fase de crecimiento a nivel global. Tal es así que partes del sistema se han incluido en una solicitud de patente que está en fase de evaluación.

Si bien el trabajo contenido en esta tesis deja margen para futuros desarrollos, se han cubierto los objetivos iniciales de la tesis, dando respuesta a una necesidad no resuelta por la tecnología comercial actual, que consiste en la incorporación de soluciones inalámbricas para una mejora de la ergonomía y un incremento de la eficiencia coste-tiempo de la que puedan beneficiarse tanto el personal médico que participa en los procesos quirúrgicos y de la monitorización intraoperatoria, como los pacientes implicados en los mismos.

Summary

Intraoperative Neurophysiological Monitoring (IONM) is defined as a set of techniques consisting of recording the electrical activity generated by the nervous system structures during a surgical operation. This branch of medicine is gaining more and more prominence and relevance, since it is seen as a powerful tool to prevent pernicious effects and complications derived from surgical procedures. These kind of techniques are utilized mainly by the Neurophysiologists and/or the Surgeons to support the decision-making process during operations, in order to minimize injuries over tissues or structures related to the nervous system.

The research work summarized in this dissertation arises as a response to the recognition of an area with room for improvement within the current technology dedicated to IONM. Monitoring of the nervous system activity implies in most cases recording a large amount of electrical signals from the different structures to be controlled and/or stimulated. This involves the arrangement of a substantial amount of electrodes in different areas of the body of the patient; as well as the connection of several hardware elements, resulting in a considerable quantity of cabling that normally remains covered and partially inaccessible during surgeries. Eliminating or diminishing this cabling is seen as a relevant technological step forward that may contribute to increasing ergonomics and easiness for the medical staff in the preparation of the montage, as well as reducing possible sources of noise on the recorded signals in a more cost and time-effective manner.

The main motivation of the thesis is the application of wireless technology to this branch of Neurophysiology, developing a wireless system able to pair the characteristics of the current commercial IONM systems. To this effect, a set of specific objectives were proposed:

- Development and prototyping of an analog front-end that complies with the requirements of current monitoring systems in terms of input impedance, low noise and sampling rate. This setup will be embedded in an autonomous, battery-powered transmitter device, in charge of recording the biological signals of interest and transmitting them through a wireless medium.

- Development and prototyping of a receiver, responsible for reconstructing the original signal received wirelessly, so that it can be acquired by any monitoring system utilized.

- Development of a bidirectional wireless communication link between both devices for signal samples and configuration message transmission.
- Development and validation of a functional prototype, entailing a complete transmission/reception hardware and software implementation and testing it in a work environment equivalent to the one where current commercial systems are utilized.

Due to its importance for a correct signal acquisition, current systems are equipped with a technical solution to measure the contact impedance between the electrodes and the tissue of interest. These methods are active, injecting electrical current to the patient, what has proved to present drawbacks. To overcome this, a new objective arose:

- Development of a novel methodology for the measurement of the contact impedance between the electrode and the tissue from where the signal is recorded. The objective in this case is the development of a passive method, more suitable for a wireless, battery-powered device.

The inclusion of this novel methodology led to a disadvantage: due to the necessary changes in the input of the acquisition stage, slow transients appear in the output signal, entailing a long time to take the measurement. To tackle this difficulty, a new objective was added to the initial ones:

- Proposing a novel approach for fast-settling of biosignals in acquisition systems based on differential amplifiers. An original methodology has been designed and tested, adapting a solution for a single-ended amplifier existing in the literature.

The main body of the thesis, made up of the compendium of three publications in journals with impact index in JCR, entails the fundamental developments and results of this piece of research.

The first one, *E. Alonso, R. Giannetti, C. Rodríguez-Morcillo, J. Matanza, and J. D. Muñoz-Frías, "A Novel Passive Method for the Assessment of Skin-Electrode Contact Impedance in Intra-operative Neurophysiological Monitoring Systems," Scientific Reports, vol. 10, no. 1, pp.1–11, 2020*, describes the contact impedance generated between the surface of the recording

electrode and the tissue under examination. In medical practise, this measurement is utilized to assess if the connection of the electrodes is correct and consequently the measurement is reliable. A new methodology is proposed, consisting in a passive approach (without injection of current), that takes advantage of the variation suffered by the measured signal when a known resistive load is connected and disconnected in a controlled fashion at the input of the amplification circuit. This methodology has been evaluated with a mathematical model, a simulation model and by measurements obtained in laboratory and in a hospital environment with a prototype. The results show that it is possible to evaluate the goodness of the connection of the electrodes with respect to the reference value (5 kΩ, according to literature).

This new methodology presents some advantages because it does not use any current injection. Fist of all, it is more suitable for battery-powered devices, since power consumption is reduced. Secondly, the injection of current to the patient also brings a risk of injure or abrasion, that modifies the classification of the system and imposes more restrictive conditions according to medical device regulations. A passive method will facilitate the validation of a medical system. Analyzing only the registered signal for the impedance measurement (without additional hardware) produces the unwanted effect of long transients because of the load commutation at the input stage.

To overcome this adverse effect, publication *E. Alonso Rivas, G. Scandurra, C. Ciofi, C. Rodríguez-Morcillo García, and R. Giannetti, "A novel approach for the design of fast-settling amplifiers for biosignal detection," Electronics (Switzerland), vol. 10, no. 21, pp. 1–14, 2021.*, presents a new topological approach to obtain a configurable input filter, which can be changed depending on the desired measurement stage.

Contact potential is an effect produced between the recording electrodes and the tissue where they are placed. The differences between this potential among the electrodes used for the measurement may provoke a DC component that can cover up the wanted AC signal or can saturate the amplification stage. Thus, it is necessary that the biosignal acquisition system presents a high-pass filter to eliminate the aforementioned DC component, normally consisting of a RC net with a very low cutoff frequency and, consequently, a large time constant. Even though this does not pose a problem during signal monitoring, changes in the input configuration might lead to voltage variations with long settling times. Such is the case of the impedance measurement method previously described.

This works proposes an adjustable filter that modifies the cutoff frequency and therefore the time constant by means of a voltage control. This method has been assessed by simulation and laboratory measurements obtained from a prototype tested in combination with the impedance measurement method proposed. The results obtained are similar to the ones gathered with the conventional RC filter, with the advantage of a drastic reduction of the time required for the measurement, maintaining the ability of performing the impedance measurement with the same recorded signal.

These results fulfill two of the objectives of this thesis: Developing of a novel methodology for the measurement of the contact impedance and proposing a new approach for the fast-settling of biosignal acquisition systems. The rest of them are addressed with the prototype presented in *E. Alonso Rivas, R. Giannetti, C. Rodríguez-Morcillo García, J. Matanza Domingo, J. D. Muñoz Frías, G. Scandurra, C. Ciofi, L. Vega-Zelaya, and J. Pastor, "A Quasi-Wireless Intraoperatory Neurophysiological Monitoring System," Electronics (Switzerland), vol. 11, no. 23, pp. 1–19, 2022.*

This paper outlines the design of the prototype developed, consisting of two elements: Transmitter and Receiver, that communicate through a bidirectional radio frequency (RF) link. This connection allows: (a) sending the signal samples gathered by the Transmitter; and (b) modifying the analog input configuration depending on the commands of the control panel installed in the Receiver device.

In brief, the Transmitter device is in charge of recording the signals obtained from standard electrodes, and contains the amplification, filtering and analog/digital conversion stages, as well as transmitting the samples via radio. Moreover, it is equipped with the proposed impedance measurement method. This device is battery-powered and is intended to be located in the surgical table as close as possible to the patient, so that the necessary cabling for the electrode connection can be reduced.

The Receiver device is in charge of receiving the information sent by the Transmitter, process it and reconstruct the registered signal so that it can be recorded by conventional IONM systems. Due to the utilization of standard connectors, it is possible to utilize the devices proposed with any current commercial system. In this way, a wireless transparent bridge is established between the biosignal of interest and the monitoring device. The Receiver is designed to be located close to the monitoring unit, more accessible to the medical staff. It includes a control

panel to modify the type of measurement (recording or impedance) and the configuration of the channels (differential or referential). The changes in the configuration are transmitted also trough a RF in the opposite direction, towards the Transmitter, because this is the device that contains the hardware needed to carry out the corresponding modifications. The configuration message transmission includes an assessment protocol to ensure the correct reception of the frame in order to prevent misinterpretations of the recorded signals.

The system also includes two software algorithms. The first one allows managing the possible loss of samples transmitted, preventing discontinuities in the reconstructed signals. The second algorithm permits the variation in real time of the gain of the amplification stage, adapting it optimally to the recorded signal.

The system has been validated with laboratory tests, as well as with real measurements taken in a hospital environment, comparing the output signal of the Receiver with the original signal recorded in parallel by means of a commercial intraoperative monitoring system. As presented in the paper, tests have been carried out for a broad set of monitoring techniques, including signals with different amplitude and frequency ranges. The only significant difference between the original signal and the reconstructed one is a constant delay with a value close to 1.5 ms, which is acceptable for the applications tested.

The device developed not only entails a scientific progress due to the novel solutions provided, but it is also presented as an innovative component with commercial potential in the realm of IONM, that is currently undergoing a global growing stage. Proof thereof is the fact that parts of the system proposed have been included in a patent submission that is in course of evaluation.

Even though the work described in this dissertation leaves room for future developments, the initial objectives of the thesis have been fulfilled, providing a solution to a gap in current commercial technology, consisting of the addition of wireless solutions for an improvement in ergonomics and an increased cost-time efficiency; with the aim of benefiting both the medical staff and the patients involved in surgical procedures and intraoperative monitoring.

Agradecimientos

El trabajo recogido en este documento es el resultado de varios años de investigación, y aunque firmada por un autor, esta *Tesis* no es sino un compendio del esfuerzo y contribución conjunta de varias personas e instituciones a los que es necesario mencionar y reconocer.

En primer lugar, y más importante, a mis Directores. Al Dr. Carlos Rodríguez-Morcillo por la cercanía, el trabajo abnegado y por aportar la exactitud y minuciosidad necesaria en este tipo de tareas tras horas en el laboratorio; por prestarse a tantas y tantas pruebas en el hospital en pro de la investigación. Al Dr. Romano Giannetti, por su ayuda esencial con los prototipos y medidas, por su gran involucración y por siempre sacar tiempo para que este trabajo fuera lo más enriquecedor y completo posible. A ambos gracias por aportar orientación, paciencia y comprensión desde la amistad.

Especial mención merece el Dr. Sadot Alexandres, la persona que me dio la oportunidad de formar parte del IIT, y que habría firmado esta tesis como Director si el destino nos lo hubiera permitido. Siempre recordaré su constante buen humor, su optimismo y sus consejos mientras dirigía mi Proyecto Fin de Carrera. Donde estés, gracias.

Al Dr. Carmine Ciofi y la Dra. Graziella Scandurra, por su crucial colaboración en este proyecto desde la distancia, y por formar con nosotros un productivo equipo de trabajo.

Al Dr. José Daniel Muñoz y al Dr. Javier Matanza, por su gran disposición a echar una mano en todo momento, por participar de manera activa desde el inicio de este proyecto y por crear un tan necesario ambiente de equipo en torno al laboratorio de investigación, que fue mi casa tanto tiempo. Al Dr. Aurelio García, por sus provechosas contribuciones en los últimos pasos de este largo camino.

A Jose y Antonio, responsables del taller de los laboratorios de ICAI, por su inestimable ayuda con el montaje de los prototipos, y por surtirnos siempre de los consejos, herramientas y materiales adecuados. Sin ellos, una modificación, corrección o reparación nos habría llevado lustros.

Al Servicio de Neurofisiología del Hospital Universitario de La Princesa, en especial al Dr. Jesús Pastor y a la Dra. Lorena Vega-Zelaya por sus consejos y su guía en la toma de decisiones de

diseño, y por su indispensable colaboración y apoyo para la toma de medidas. Gracias por cedernos tiempo y espacio de trabajo.

A Soinde S.L. por financiar este proyecto de investigación, y en especial a Eduardo Jiménez-Carlés, cuya visión de negocio proporcionó la idea germen de esta tesis.

A la Asociación de Ingenieros del ICAI, por su financiación y compromiso con la investigación.

También me gustaría recordar a los que fueron mis compañeros del IIT durante mis años en el Instituto, con los que a diario me tomaba un respiro de la rutina del laboratorio. Aunque la mayoría ya no estén allí, espero que ese espíritu de grupo se mantenga.

Por último, a todo el personal del IIT y de ICAI, por mantener una visión que considera la investigación como parte fundamental de la educación, y por promover de manera ejemplar la colaboración entre academia e industria con el fin de lograr resultados productivos y cuyo fin último sea el de crear un mundo mejor.

A todos, y a los que no he nombrado, **Gracias**.

A mi familia

Contents

Resumen i

Summary vii

Agradecimientos xiii

List of Figures xix

List of Tables xxi

1 Introduction 1

1.1 Introduction 1

1.2 Current technology of IONM systems 4

1.3 State of the Art 8

1.4 Motivation and Objectives of the Thesis 20

1.5 Outline of the Thesis 22

2 Publications 23

2.1 A Novel Passive Method for the Assessment of skin-electrode contact impedance in IONM Systems 25

2.2 A Novel Approach for the Design of Fast-Settling Amplifiers for Biosignal Detection . 39

2.3 A Quasi-Wireless Intraoperatory Neurophysiological Monitoring System 55

3 Conclusion 77

3.1 Contributions 78

3.2 Future Work 80

Bibliography 83

List of Figures

1.1 Example of commercial IONM systems. *Cadwell* system on the left, *inomed* system on the right. Images obtained from the web pages of the manufacturers. 5

1.2 Example of cabling during a surgery preparation with IONM. Note the bundle of coloured cables (electrodes) and the adapters of the monitoring system. [7] . . 6

1.3 Schematic of the different elements of a biological signal acquisition system. . . . 8

1.4 Frequency and voltage range of some biopotential signals [1]. *EOG* is the *Electro-oculogram* and *AAP* is the *axon action potential.* 12

List of Tables

1.1 Technical characteristics of biopotential signal acquisition systems 16
1.2 Comparison of wireless EEG systems [56] 16
1.3 Comparison of wereable biosensor systems 17

Chapter 1

Introduction

1.1 Introduction

Modern medicine makes use of a broad diversity of techniques in order to obtain useful information from the human body. With the help of different types of sensors, physiological properties such as temperature, pressure, flow, chemical concentration or biopotential can be measured out direct or indirectly from the body. Among them, bioelectric potentials are the result of electrochemical activity of a class of cells called *excitable cells*, present in different tissues such as nervous, medular or glandular. These cells present two different states: a resting state, with a steady potential difference between internal and external environments, and an active state, which is defined as the ability of the cell to conduct an action potential when stimulated [1].

This bioelectrical response was found to be useful for the diagnosis and identification of different states of the nervous and muscular system. As a result, diverse techniques were developed, such as the following:

- *Electrocardiogram (ECG)* permits recording the electrical events related to the different types of tissues the heart is comprised of [1]. It allows the identification of conduction patterns and characteristic action potentials that may exhibit malfunctions.

- *Electroencephalography (EEG)* is a medical technique that reads electrical activity generated by brain structures. The electrical activity observed and recorded varies according to the functional status of the brain, with changes correlated to the cognitive state. Among others, EEG can be used for the following clinical applications: monitor of alertness, locate damaged areas in the neural system, investigate epilepsy or sleep disorders [2]. The recording electrodes are commonly placed in the scalp of the subject; if they are located in the cortical surface, it is called *Electrocorticography (ECoG)*.

- *Electromyography (EMG)* records local bioelectrical activity from small regions within the muscle in which recording electrodes are inserted (normally needle electrodes) [1]. Abnormal values in nerve conduction can reveal if the motor nerves are compromised by disease or injury [3]. Besides, it allows the identification of changes in cranial or peripheral nerves [4]. *Stimulated EMG*, obtained as a response to electrical stimulus, is also utilized for functional mapping of the nerve structures during surgeries.

- *Evoked potentials (EP)* provide noninvasive methods of assessing the neural activity of the nervous system by recording the electrical response to an adequate stimulus. EP represent an important resource for detecting and locating neurological disorders or abnormal conduction of the sensory system, like auditory or visual, that are not detected through other methods.

Among all the branches of physiology and medicine that take advantage of these techniques, this work focuses on Neurophysiology, that studies the functionality of the nervous system. Neurophysiology plays an increasing and prominent role as a powerful tool for surgical procedures in which the nervous structures are affected or at risk. The application of different sets of techniques in order to assess the integrity of such structures during surgeries is known as **Intraoperative Neurophysilogical Monitoring (IONM)**. IONM presents several applications. For example, it permits warning the surgeon if a complication occurs in time to intervene and correct the problem before it may cause a permanent harm to the patient through the monitoring of the bioelectrical responses of the corresponding structures. It can also identify systemic problems that need to be corrected. Additionally, some techniques are also used to obtain a

topographic identification of the areas or nerves of interest (mapping). In general, IONM increases the confidence and comfort of the medical staff being aware of the patient's neurological safety and state, so that the risks of surgery are significantly reduced [5].

Broadly speaking, the techniques utilized in IONM can be categorized as *free-running*, if they read continuously the spontaneous electrical activity from the brain (EEG) or muscle cells (EMG); or *Evoked Potentials*, if the activity recorded is the result of the application of a stimulus. The most common EP recorded during a surgery are Motor Evoked Potentials (MEP) and Somato-sensory evoked potentials (SSEP). The former is obtained from the muscles of interest in response to an electrical stimulus typically derived transcranially. SSEP, on the contrary, are registered normally in the scalp as a response to an electrical stimulation on the peripheral nerves, and are used to monitor the somato-sensory pathways.

Additionally, and depending on the area that may be affected during the surgical procedure, AEP (auditory evoked potentials) or VEP (visually evoked potentials) are utilized to assess the integrity of the auditory and visual pathways and nerves, respectively. In both cases, the stimulus are not electrical. A sound/pressure transducer is utilized to induce the response in the AEP, and a visual pattern or specific LED goggles are used in the VEP. The recording is normally carried out on the scalp.

1.2 Current technology of IONM systems

With regard to commercial systems, the market is shared out among several major players, some of them listed here: *inomed*, *Medtronic*, *Natus*, *Nihon Kohden*, *Cadwell*, *Dr. Langer*. Each of them presents a different IONM system which technology features are, of course, proprietary and confidential. Nevertheless, there are some general characteristics that are common to all of them, and can be utilized as a starting point for the study of this technology:

- Hardware setup: As can be seen in Fig. 1.1, all the systems converge to a similar solution: they present a central unit (PC) with a dedicated software that receives the monitoring data from one or several modular amplifiers arranged in a medical degree equipment cart in order to ease the movement and positioning of the system in the operating room (OR). For the purpose of gathering the signals from the electrodes located in the patient, they make use of several adaptor boxes that are designed to be located in the surgical table and are connected to the system through a long hose that permits flexibility in the connection of all the elements of the chain. Besides, they are supplied with a stimulator module controlled via software.

- Number of channels: The standard is a number of channels multiple of 8, with typical configurations starting on 16 channels and up to 64 in current setups.

- Bandwidth: Taking into account the range of the signals needed, they all present configurable filters, spanning from 0.5 Hz to 5 kHz in most of the systems.

- Resolution and sampling rate: The analog-to-digital-converter (ADC) conversion resolution is typically 16 bits, with sampling rates reaching up to approximately 20 kHz.

- Input impedance: As a common figure in acquisition devices, the input impedance is, at least, 100 MΩ for most systems.

- Input connections: All the systems utilize *touchproof* standard 1.5 mm connectors (DIN 42802), that is the prevailing option for the commercial available electrodes. Since both

differential and referential measurements are needed, the systems present either dedicated inputs or non-differentiated configurable inputs.

- Impedance measurement: Imperatively, it must be ensured a good positioning and contact of the electrodes before and during the monitoring. To this end, all the systems are equipped with an impedance measurement option, normally activated via software, that requires halting the monitoring.

Figure 1.1: Example of commercial IONM systems. *Cadwell* system on the left, *inomed* system on the right. Images obtained from the web pages of the manufacturers.

Although these systems are conceived as a powerful tool to be utilized inside the OR, with hardware robustness and signal integrity as main design factors, the current dependency on wired technology present a significant drawback. Due to the large amount of signals needed during a surgery, the number of wired electrodes and cords of the input adaptors represent a cause of uneasiness for the medical personnel, as can be seen in Fig.1.2. Although shielded, malfunction in these cabling, connections or location close to strong sources of interference (power sources or high-frequency surgical equipment) may be a cause of noise in the signals. Moreover, they are subject to EMI interference [6].

Figure 1.2: Example of cabling during a surgery preparation with IONM. Note the bundle of coloured cables (electrodes) and the adapters of the monitoring system. [7]

Thus, **developing a system able to reduce the cabling of IONM systems is the main objective of this thesis**. This work focuses on the development of a significant advance to this type of technology to ease the utilization of these kind of devices in the OR providing an enhancement in ergonomics, offering benefits for both the medical staff and the patients.

Intraoperative Neuromonitoring is an increasing field of medicine, with an estimated global market value over $3 billion in 2020 and $4 billion in 2021, depending on the source. Moreover, the forecasted annual growth rate is expected to be between 4% and 7%, reaching a value of up to $9 billion in 2028. The largest market with respect to IONM is USA, with Asia and Pacific as the fastest growing markets in this field [8], [9], [10].

Considering this, any advancement applied to IONM technology may result in a significantly valuable impact for the industry. The pieces of research and results obtained in the thesis here presented entail not only a step forward in the technology utilized, but a move towards a paradigm shift in IONM.

Since the aim of this thesis is the development of a wireless solution for IONM, we had to focus on the existing technology and literature to reach this aim. As it was previously stated, the specifications of current commercial systems are not available due to confidentiality. Therefore, scientific literature regarding biopotential acquisition must be utilized as reference.

1.3 State of the Art

Literature is scarce with respect to wireless approaches to Intraoperative Monitoring. The works presented in [6], [11], [12], and [13] show the results obtained under different conditions for a wireless IONM prototype, although the results are mainly focused on the benefit with respect to the EMI interference suffered by the cabling. These pieces of research yet promising, have only been tested with MEP signals which are the least demanding signals that can be monitored during a surgery. Other limitations of the design shown in these publications are the ADC conversion rate (8 bits) and the number of channels (4).

Several studies describe wired and wireless technology applied to EEG devices. The broad range of applications of EEG grants a lot of interest in the development of solutions and research in different fields. In medical practice, EEG is utilized for diagnosis and treatment. These references can be considered as a starting point for the development of a novel wireless system.

In recent years, the progress in design of sensors and system techniques have made it possible to integrate sensors into portable acquisition devices to measure a wide variety of physiological signals [14]. These sensor systems can be made comfortably wearable in caps, headbands and headsets, and thus potentially usable in a wide range of settings [15]. Regarding the medical realm, portability and wireless transmission capability in patient monitoring systems is highly desirable to enhance patient's comfort and convenience [16].

Typically, a biopotential acquisition system encompasses the elements shown in Fig. 1.3. See the specific case of an EEG system in [2]. These elements are described below.

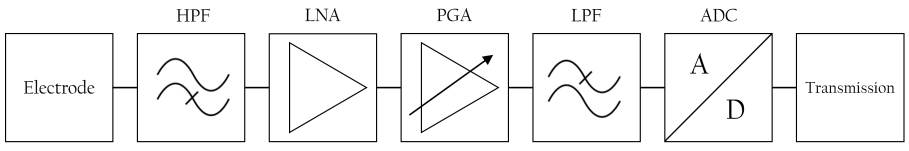

Figure 1.3: Schematic of the different elements of a biological signal acquisition system.

Electrodes

Electrodes (sensors) can be divided into two groups:

(a) Wet sensors; normally disposable pre-gelled or needle electrodes. These are the most commonly utilized sensors, but present the handicap of requiring skin preparation that can be uncomfortable for the user, as well as degrade the skin-electrode impedance.

(b) Dry biosensors, which prevent the problems of skin preparation with an acceptable performance in measuring signals when applied to hairless parts of the body.

In opposition to commonly utilized $Ag/AgCl$ electrodes, and in order to overcome the problems of wet electrodes in long-term signal acquisition, different technologies for dry electrodes have emerged in recent years. In [17], some of these technologies are reviewed: invasive microneedle electrodes, surface dry electrodes and capacitive electrodes, concluding a similar performance than wet electrodes. In this line, reference [18] presents a new design of a current-to-voltage capacitive electrode for a variety of biosignals. These type of electrodes are well suited for wireless applications.

Textile electrodes are another alternative specially interesting for wearable systems. In [19], it is presented a configuration to obtain ECG signals from dry conductive textile electrodes, focusing on the effect of the skin-electrode interface impedance in the quality of ECG signal registered. A review of the current trends on textile electrodes can be found in [20], reporting applications in ECG, EEG, EMG and even Electrooculography (EOG).

Depending on the type of biosignal of interest, acquisition arrangements can be referential (monopolar) or differential. Differential recordings are made between a pair of electrodes: active (signal), and reference electrode. Additionally, there is a third electrode (ground) that is needed to reduce the common mode voltage on the differential pair, as well as the interferences [2]. Modern EEG systems are able to record from 128 to 256 electrodes [21], [22], with an increasing number of channels of interest [23].

Analog front end (amplifier + filters)

Literature is prolific in low-noise, low-power biosignal amplifiers, mostly oriented to the development of VLSI (very large scale integration) ICs (integrated circuits) for implantable devices [24], [25], [26], [27].

The parameters that need to be satisfied simultaneously in a correct design of an analog front-end for biomedical applications are listed in [28]. Among others, DC offset rejection, high CMRR, high input impedance, low noise and low power. As stated in the same reference, all these parameters may not be optimized in one stage simultaneously. Consequently, common arrangements for biosignal are designed in two stages. Power, noise and input impedance are dealt with in the first one, and linearity, gain and dynamic range in the second one.

Basically, the structure of an analog front end consists of a low-noise instrumentation pre-amplifier with fixed gain, followed by a PGA or VGA (programmable/variable gain amplifier) which output is connected to an analog-to-digital-converter. Since the difference between the contact potential between the recording electrodes and the tissue may generate a DC signal much larger than the signal of interest, a high-pass filter is included as the first state of the acquisition set up. An IONM amplifier must amplify very small signals and its gain must be suitable to deal with microvolts or below. Moreover, all components of this element must be chosen in order to minimize thermal noise and other types of electronic noise. To improve the signal-to-noise ratio, a low-pass filter is also included in the signal path [29]. Regarding the conversion resolution, most commercial EEG units use ADCs with 16 or more sampling bits [22].

In [30], the typical structure of a biosignal acquisition system is presented, comprised of an instrumentation amplifier, low-pass filter, programmable gain amplifier and ADC. In this work, the implementation is optimized for ECG and EEG, with bandwidths of $0.1-150\,\mathrm{Hz}$ and $0.3-100\,\mathrm{Hz}$, respectively. Due to the wide range of different biosignals that can be registered, it is desirable to have an analog front-end able to cope with all of them optimally. For this purpose, [31] and [32] present two configurable approaches. In the former, both the variable gain

amplifier and the subsequent low-pass filter are tunable in the bands 70−400 Hz and 1.2−7 kHz, depending if the application is utilized for free running registers (EMG, EEG, ECG) or EP. On the other hand, the approach described in [32] is intended for several measurements such as ECG, bio-impedance or general-purpose analog signals. For this, a combined on-chip setup of a current generator and configurable instrumentation amplifier is proposed. The combination of different configurations is obtained by transmission gate implemented switches, that allow the system to measure voltage, current or impedance of the subject without affecting greatly the analog performance metrics.

When conditioning the signal for biopotential acquisition, the first hurdle is the DC offset generated at the skin-electrode interface between electrodes, that can reduce the CMRR of the front-end and even the saturation of the signal [33]. To overcome this, the most typical solution is utilizing a RC high-pass filter with a very low cutoff frequency. An innovative solution to this is presented in [34], where an active loopback is used to compensate the DC component in a monopolar low noise measurement. A thorough study of the different LNA topologies for recording neural signals with differential amplifiers is presented in [35], where each architecture offers a different transfer function, proposing also a two amplifier stages to create a double pole in the corner frequency of the filter desired.

Since the signals registered are normally in the range of a few tens of microvolts, high quality low-noise amplifier are required for biomedical applications. Commonly, the first stage preamplifier determines the signal-to-noise-ratio (SNR) of the whole chain, so it is essential to have low input referred noise (typically $<10\,\mu V$ RMS integrated over the entire frequency spectrum) [36].

The work presented in [37] focuses on the power consumption of low-noise designs oriented to wearable biosignal acquisition systems. The authors present a dynamic instrumentation amplifier that makes uses of a clock to modulate the input signal (in this case an ECG) in order to reduce the current consumed. This dynamic stage is followed by a PGA and a low-pass filter to remove the noise of the signal. In [33], a low-noise PGA circuit is presented for EEG, that utilizes three amplification stages to improve CMRR.

For the wireless monitoring system described in [38], the stages of the front end specified are an instrumentation amplifier followed by two-stage amplifiers (for a total gain of 2047 V/V). Then the signals pass through a high-pass filter to remove low frequency artifacts. In a similar work from the same authors, the front-end described in [6] consists of a high pass filter with a cut-off frequency of 3 Hz, followed by an instrumentation amplifier (with a gain of 20 dB), active band-pass filter (100−1000 Hz) and a second amplification stage (34 dB) up to an 8 bit ADC that samples the signal at 6.2 Hz.

Frequency and amplitude range of some typical biopotential measurements is shown in Fig. 1.4. Below, filter span and amplitude display resolutions are listed as a rule of thumb for most common signals [4]. Note the variability in order of magnitude in frequency and amplitude:

- EMG: filter: 10−3000 Hz, 50 µV/div.
- EEG: filter: 0.5−30 Hz, 10 µV/div.
- ECoG: filter: 0.5−100 Hz, 1000 µV/div.
- SSEP: filter: 10−1500 Hz, 0.1−2 µV/div.
- MEP: filter: 0.5−100 Hz, 50−500 µV/div.
- sEMG: filter: 50−3000 Hz, 30−50 µV/div.

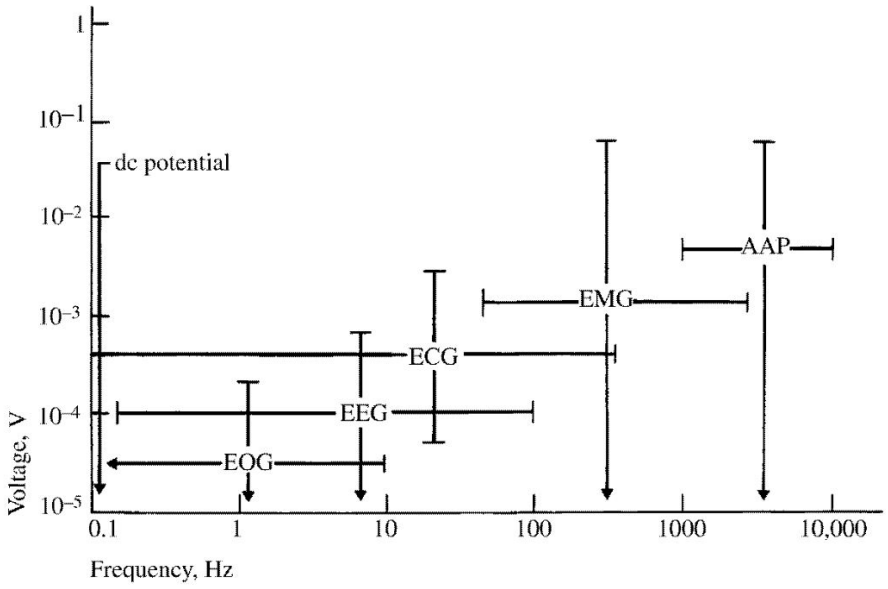

Figure 1.4: Frequency and voltage range of some biopotential signals [1]. *EOG* is the *Electro-oculogram* and *AAP* is the *axon action potential*.

Taking into account these ranges, the acquisition system has to deal with RMS levels in the µV range, making noise rejection critical for a correct design. Ranges of operation are proposed in [2] for the analog front-end stage in EEG systems. The amplifier gain should be between 100 and 100.000 V/V, presenting a high input impedance. The sampling frequency of the device, given the characteristics of the input signals, should be between 128 and 1024 Hz. Although a 200 Hz sampling rate frequency is recommended, it is not uncommon to offer sampling frequencies above 1 kHz [22].

For the system proposed in the work presented here, a modular unit of 8 channels is selected, with an ADC resolution of 16 bits per channel. Due to implementation constraints, the cycle acquisition time of the samples is 112 µs, for a sample frequency of 8.9 kHz. As described in [7], we have selected LNA AD8429 followed by a programmable gain amplifier, with a high-pass filter and anti-aliasing filter setting a bandwidth from 0.1 Hz to 5 kHz. To modify the gain of the amplification stage, the system is equipped with a software algorithm that automatically adapts the gain of the PGA depending on the amplitude of the signal, in order to obtain an optimal resolution for a dynamic range that spans from ±180 µV to ±36 mV.

Transmission medium

Once the analog signal has been converted to a digital data stream, signal transmission can be classified into two categories: wired or wireless. Currently, most existing IONM systems have been constructed with wired connections, which results in heavy, impractical and limiting devices. Wireless transmission technology can eliminate this limitation and offer more ergonomic and flexible solutions [39]. This technology is utilized in implantable [40], [41] and non-invasive devices [42], but not yet in commercial monitoring systems.

In this work, we investigate different wireless alternatives that permit obtaining a wireless, light, battery-powered and low cost solutions for IONM.

Broadly used protocols as Bluetooth or Zigbee are commonly utilized in wireless EEG devices or WBSN (Wireless Body Sensor Networks). Bluetooth is a technology standard for exchanging data wirelessly over short distances, invented by Ericsson in 1994. Bluetooth low energy (BLE)

was developed in 2010 with a new protocol stack for rapid transmission of simple links, with wider communication range and reduced power consumption [43]. ZigBee specification was released firstly in 2004 [44], and is aimed for low-data rate monitoring applications. Wi-Fi is another wireless technology designed to provide high-speed connectivity to devices operating in Local Area Networks [45].

ZigBee presents some advantages, like higher efficiency, a smaller stack and larger coverage with respect to other solutions [46]. On the other hand, it lacks of user interface [47], has a reduced compatibility and is more power consuming than Bluetooth and BLE, depending on the application [45]. Due to its higher data rate and high compatibility, Bluetooth seems to be a good solution for a portable device, but it presents a heavier stack, higher power consumption and shorter coverage range, although its compatibility permits its use with devices such as a cellphone acting as data receiver [42]. Because of its low power requirements, BLE appears to be a better option, since it allows the utilization of smaller batteries and hence designing smaller devices. This technology is intended for sensors that transmit data periodically, making it more prone to disconnections [48]. Moreover, the low power consumption is the result of the operation mode, that keeps the device in sleep mode until a connection is initiated by a host [49].

Several studies related to smart sensors compare these technologies. With respect to data rate, Bluetooth presents the highest, with up to 3 Mbit/s, followed by BLE (1 Mbit/s) and ZigBee (250 kbit/s) [44], [47]. Following [43], taking into account the stack and protocol, the application throughput is reduced up to 2.1 Mbit/s for Bluetooth and 0.27 Mbit/s for BLE. Although depending on the application Wi-Fi technology can reach more than 1 Gbit/s, the cost of deployment and higher power consumption makes this technology less suitable for the application intended [50], [51].

The literature presents some examples of the utilization of wireless technology for biological monitoring. In [50], an IoT solution is provided to collect sensor data of the body and send it to a smartphone. For this solution, BLE is selected over ZigBee and Bluetooth because of its lower consumption. In [52] a wireless stethoscope is presented. BLE is also selected because

of its convenience for audio transmissions. In [53] and [54], wearable sensors for recording ECG and respiratory signals are described. In the latter, a queue based transmission protocol is implemented to prevent packet loss and obtain real-time data transfer. Several samples are buffered before requesting the BLE host to start the communication, that remains in idle state the rest of the time. In [55], a custom RF solution is selected in order to optimize power consumption for a wireless EEG/EMG real time acquisition recorder. However, data is sampled at 500 Hz at most.

Given the amount of data to be transmitted in multichannel systems (with up to 256 channels), compression techniques or digital modulation can be used to reduce data rate [56]. The literature offers some examples along this line. For example, [22] presents a study of the power trade-off between compression algorithm complexity and reduction in data rate and [16] presents a lossless data compression algorithm implemented in a VLSI device. In [57], a wearable ECG monitoring system for remote monitoring is presented, making use of Zigbee technology. ECG data are compressed and buffered before been sent, keeping the transmission idle while samples are not transmitted. In [58], a Bluetooth implementations is described where muscular information is coded by mimicking the neural spikes by digital pulses. This way, the amount of data to be transmitted is reduced. Nevertheless, in this case latencies of $100-300$ ms are acceptable for the application. Signals of interest for IONM are random or quasi random, so they are not prone to be compressed as ECG signals. The complexity of a system of this kind, that requires software and hardware elements, the low compression ratios, and the energy consumption lead to the consideration of another solution when transmitting data.

Tables 1.1 and 1.2 summarize some technical features regarding the data acquisition chain in systems proposed or analyzed in the literature. As shown in these tables, sampling rate and bandwidth present a high difference between implantable and non-invasive devices. Reference [41] in Table 1.2 (obtained from [56]) presents the highest values of both features, but the digital resolution is limited to 8 bits, and the RF transmission proposed requires the use of digital modulation techniques. More recent studies for wearable sensors are included in Table 1.3, showing again values of sampling rate and bandwidth far from the type of signals registered during an intraoperative monitoring.

Reference	Device type	#Channels	Sampling rate [Sps]	Coding bits	Voltage range [uVpp]	Bandwidth [Hz]	Gain	Transmission
[59]	Implantable	-	40,000	12	50-800	450-5000	-	Wired
[60]	Noninvasive	3	200	-	-	0.5-30	-	Wired
[61]	Noninvasive	32	500	16	-	0.5-100	-	RF/ Bluetooth
[23]	Noninvasive	128	250	16	-	0.1-100	-	-
[62]	Noninvasive	8	512	12	-	1-50	6000	Bluetooth
[42]	Noninvasive	4	-	16	-	0.7-159	-	Bluetooth
[63]	-	16	-	-	-	0.3-150	500x [1-10]	-
[64]	Implantable	32	15,700	10	-	0.1-5000	-	RF (FSK)-345,6kbps
[65]	Implantable	32	30,000	12	-	0.05-5000	-	RF (FSK)-24Mbps
[14]	Noninvasive	3	256	12	-	0.5-50	5500	Bluetooth
[41]	Implantable	64	62,500	8	20-500	100-10,000	-	RF (FSK)–1Mbps
[26]	(Front-end)	-	-	-	0,3-350	390-2500	-	-
[66]	Noninvasive	16	1000	12	-	0,5-100	-	-
[29]	Implantable	16	-	10	-	0-15,500	-	Wireless

Table 1.1: Technical characteristics of biopotential signal acquisition systems

	Reference						
	Chi et al. [67]	Lin et al [62]	Wang et al. [68]	Torfs et al. [69]	Riera et al. [70]	Matthews et al. [71]	Brown et al. [72]
Appearance	Headband	Headband	Headband	Headphone	Cap	Helmet	Headset
Signal	EEG/ECG	EEG	SSVEP	EEG	EEG/ECG	EEG	EEG
Number of channels	4	8	4	2	4	12	8
Gain [V/V]	10000	6000	8000	-	-	-	4000
Sampling Rate [Hz]	343	512	128	256	256	4000	500/1000
Filter [Hz]	0.7-159	1-50	0.01-50	-	0.1-100	1-50	-
Resolution of A/D [bit]	16	12	12	12	16	16	11
Transmission	Bluetooth	Bluetooth	Bluetooth	RF transmitter	Zigbee	RF transmitter	RF transmitter
Controller	PIC24	Micro-controller	MSP430	MSP430	-	-	MSP430

Table 1.2: Comparison of wireless EEG systems [56]

	Reference						
	Spano et al. [57]	Malwade et al [52]	Di Pascoli et al. [55]	Rossi et al. [58]	De Vito et al. [54]	Lee et al. [53]	Joaquinito et al. [73]
Signal	ECG	Stethoscope (Audio)	EEG EMG	EMG	ECG	ECG Respiration	ECG
Transmission technology	ZigBee	BLE	RF	BLE	BLE	BLE	BLE
Sampling Rate [Hz]	320	-	500	1000	256	400	100
Filters / BW [Hz]	0.05-150	20-250	0.1-100	30-400	0.5-40	0.03-155	0.5-400

Table 1.3: Comparison of wereable biosensor systems

The system developed in the work reported here implies sensing, sampling, transmitting and reconstructing signals in real time in order to be registered back in a commercial IONM system. This requires continuous transmission of samples and a latency as low and constant as possible. Bearing in mind that some evoked responses have to be evaluated in the scale of milliseconds, latencies above that range are not acceptable for the application intended.

Reference [74] presents a study of different wireless technologies applied to smart agriculture. For some of the solutions compared, the latency is up to 30 ms for ZigBee and up to 50 ms for Wi-Fi.

Latency is not a constraint in [53], since sampling period of one of the biosensors is 12.5 ms. In [75], an implantable BCI (brain-computer interface) neural stimulation device is presented, but in this case only stimulation burst commands are sent via Bluetooth with expected total delays of up to 10 ms.

Considering all these aspects, we will utilize a RF solution with custom protocol, similarly to [55]. Indeed, in this reference, the comparison of power/data rate is clearly favourable to the same transceiver with respect to ZigBee and Bluetooth, making it more suitable for our application.

As detailed in [7], a Nordic Semiconductor nRF24L01 transceiver is selected to implement the wireless communication link with a custom protocol. This device works in the ISM (Industrial, Scientific and Medical) band at 2.4−2.48 GHz width a bandwidth of 2 Mbit/s.

The number of bits transmitted in the data frame takes into account the ADC resolution (16 bits/channel), number of channels of the device (8 channels), and the information required

for the codification of the scale selected for the variable gain amplification stage (4 bits per channel). This information has to be transmitted since the receiver device has to replicate the amplification of the input stage in the analog attenuator. Additionally, a sequential header is included on each sample. Considering the sampling rate of the device and address and CRC bytes added by the transceiver, the total bit rate needed for this application is 1.923 Mbit/s, which is compatible with the RF transceiver selected.

The data frame is inserted (via SPI) in the transmission FIFO of the RF transceiver byte per byte and, after every acquisition cycle (each time one sample is obtained per channel), the frame is transmitted to the receiver in a continuous and uninterrupted manner. In that device, data is parsed and buffered in real time. The receiver also counts with an algorithm that analyzes the header of the frames received in order to cope with sample loss.

Electrode-skin impedance measurement

Achieving a low contact impedance between the surface of the electrode and the skin is of paramount importance in order to ensure sufficient quality in the measurement taken, both to reduce the thermal noise injected and to avoid power line interference.

In [19], the error rate of associated to the skin-electrode impedance is analyzed in the case of textile electrodes, showing its impact in the quality and shape of the signal. The EEG data quality with respect to scalp-electrode impedance is analyzed in [23].

In order to prevent signal distortion, impedance at each electrode contact with the scalp should be as low as possible, and always below 5 kΩ, approximately [2]. Therefore, measuring the impedance of the contact while obtaining data is a key component of a monitoring system.

Impedance monitors are built in commercially available EEG and IONM devices. This measurement is ideally performed by injecting a known current across the interface between the electrode and the tissue and then by measuring the voltage difference between points above the electrode and below the scalp [23], [76], [77], [78]. In [54], the bio-impedance signal acquisition of the proposed wearable monitoring device is provided by a commercial integrated circuit MAX3001, driving a current of 32 µA at 80 kHz, that also senses the resulting voltage

signal. In [79], a wireless system is proposed to measure biopotential recordings (ECG) and electrode-tissue impedance to analyse the correlation between motion artifacts (not desired in the registered signal), and the impedance.

Bio-impedance is also a source of information of physiological conditions that are of interest for monitoring different bio-markers. The works in [80] and [81] present different approaches to obtain impedance information (magnitude and phase) for implantable devices. In both cases, current is injected to the tissue.

According to [80], the medical standard IEC60601-1 [82] defines the maximum amplitude and frequency of the current that can be used. Injection of a current in the subject of study presents safety and power consumption issues. Firstly, medical regulation restricts the application of active current into the patient, and classifies medical devices with this feature as Class B or Class C (if they may cause a potential injury) [83], and they have to deal with strict regulatory aspects. Secondly, the utilization of current generators implies a power consumption that may compromise the performance of batteries in wireless systems.

To overcome these disadvantages, as previously described, a passive approach that avoids current injection is designed and presented in this work [84].

1.4 Motivation and Objectives of the Thesis

In brief, the motivation of this thesis arises from the dependency of current commercial IONM systems on wired transmission technologies. This feature limits the flexibility and ergonomics of this kind of devices in the OR. Although wireless solutions are found in the literature and industry for biopotential acquisition devices, they are mainly circumscribed to EEG, ECG or EMG. Wireless transmission in non-implantable devices is limited to protocols like Bluetooth, BLE or ZigBee; and in the case of implantable devices, RF technology is commonly used in order to undertake research, clinical, entertainment or industrial applications. The requirements of the diverse biosignals registered during an intraoperative monitoring are much more demanding than the ones needed for these free running techniques.

Consequently, the main focus of this work will be the fulfilment of the gap between existing wireless solutions for biopotential acquisition and current intraoperative monitoring systems. A system that improves the technical features of current wireless biosignal acquisition devices, has been developed. The design of such device has been tackled as follows:

- Designing and prototyping of an analog front-end that complies with the low-noise, impedance and sampling rate characteristics. A biomedical signal acquisition setup is designed based on literature arrangements to comply with the bandwidth and dynamic range of the signals of interest. This design has been embedded in a transmitter device able to send the sampled data.

- Designing and prototyping of a receiver device to reconstruct the sensed signal, capable of connecting to current commercial systems, establishing a transparent bridge between the patient electrodes and the monitoring equipment.

- Developing a bidirectional high-speed RF communication system. Unlike in current systems, a raw data link has been used to avoid the utilization of data compression techniques or digital signal modulation.

- Developing and testing of a functional prototype. This objective entails the management of the whole system through digital implementation, complying with the hard time constraints for both data acquisition and wireless transmission. It is also necessary to fulfill the requirements for medical devices such as the isolation between the patient and any possible source of voltage risk [82].

For a correct functionality and compliance with common medical industry standards, an electrode-skin impedance measurement method should be embedded in any system of this kind. During the development of the system, power consumption and regulatory constraints of current methods were identified as drawbacks for portable devices. To overcome them, a new objective arose:

- Proposing a novel impedance measurement method to measure the skin-electrode contact impedance with the patient. A novel methodology has been developed and implemented in the device. In comparison to current technology, this method will be passive (without the injection of current).

As it will be seen, the inclusion of this novel methodology led to a disadvantage: because of the changes in the input loads, slow transients appear in the output signal, entailing a long time to take the measurement. To tackle this difficulty, a new objective was added to the initial ones:

- Proposing a novel approach for fast-settling of signal for acquisition systems with differential amplifiers. An original methodology has been designed and tested, adapting an existing solution from the literature for a single-ended amplifier to a differential one.

1.5 Outline of the Thesis

This thesis is presented as a compendium of three papers, that encompass the research, design and testing carried out in order to fulfill the objectives listed above:

- Reference [84] presents a solution to overcome the drawbacks of the injection of current when measuring the contact impedance between electrode and tissue. The design of a novel passive methodology is presented, together with laboratory and field test results.
- The work in [85] can be seen as an improvement of the novel methodology presented in [84]. It presents a new approach for the input filter of the acquisition system that can be used to reduce long transients when a steep change in the DC component of signals takes place. This approach has the potential to reduce substantially the time required for the impedance measurement.
- In [7] the authors describe the problem that serves as starting point of this work as well as the design and different elements of the prototype developed. In addition, the paper includes laboratory tests and on-site results of the prototype under real working conditions. They validate the technology conceived for the various types of signal that it was intended.

Chapter 2

Publications

2.1 A Novel Passive Method for the Assessment of Skin-Electrode Contact Impedance in Intraoperative Neurophysiological Monitoring Systems

SCIENTIFIC REPORTS
nature research

OPEN

A Novel Passive Method for the Assessment of Skin-Electrode Contact Impedance in Intraoperative Neurophysiological Monitoring Systems

Eduardo Alonso[1,2], Romano Giannetti[1,2*], Carlos Rodríguez-Morcillo[1,2], Javier Matanza[1,2] & José Daniel Muñoz-Frías[1,2]

Intraoperative Neurophysiological Monitoring is a set of monitoring techniques consisting of reading electrical activity generated by the nervous system structures during surgeries. In order to guarantee signal quality, contact impedance between the sensing electrodes and the patient's skin needs to be as low as possible. Hence, monitoring this impedance while signals are measured is an important feature of current medical devices. The most commonly used technique involves injection of a known current and measurement of the voltage drop in the contact interface. This method poses several problems, such as power consumption (critical in battery-powered systems), frequency dependency and regulation issues, which are overcome by using a passive method. The fundamentals of the method proposed in this paper are based on the utilization of the variation suffered by the input random signal when a known resistance is connected in parallel to the input terminals of the low-noise amplifier (LNA) of the analog front-end of the acquisition system. Controlling the connection of the resistors and computing the root mean square of the LNA output voltage has been proved to be a useful tool to assess that the contact impedance is suitably low, allowing the user to know if the neural measurements obtained are valid.

Intraoperative Neurophysiological Monitoring (IONM) is a set of techniques that provide increased functional knowledge of the nervous system structures during a surgical operation. These powerful tools allow the surgeon to identify and prevent possible injuries during the medical procedure[1]. The IONM denomination includes stimulus-based techniques, such as evoked potentials (that measure the response to a previous stimulation), and free running techniques, which can be acquired continuously without any stimulus, including Electroencephalography (EEG), Electromyography (EMG) and Electrocorticography (ECoG), and several other.

Due to the context of utilization, it is of paramount importance to guarantee the accuracy of the biological signals acquired. Therefore, limiting the noise sources and their effects over the measurements is a critical aspect of IONM.

A common source of signal quality degradation is the contact impedance that appears in the interface between the electrode and the patient's tissues[2]. Commonly, IONM techniques use needle electrodes and/or wet adhesive electrodes for the connections, creating an interface between the metal end of the electrode and the biological tissue. The electrical behaviour of this interface is normally represented following the Webster model[3], as can be seen in Fig. 1.

A large contact impedance may lead to a system more susceptible to power line interferences and motion artefacts[4,5]; additionally, the voltage drop on the same impedance results in signal attenuation[6]. Kappenman and Luck[7] highlight the importance of electrode impedance on data quality for event-related potentials (ERP) and EEG signals. Sagha *et al.*[8] include high electrode impedance as a source of signal degradation for EEG utilized in

[1]Institute for Research in Technology, ICAI School of Engineering, Pontifical Comillas University, Madrid, Spain. [2]These authors contributed equally: Eduardo Alonso, Romano Giannetti, Carlos Rodríguez-Morcillo, Javier Matanza, José Daniel Muñoz-Frías. *email: romano@comillas.edu

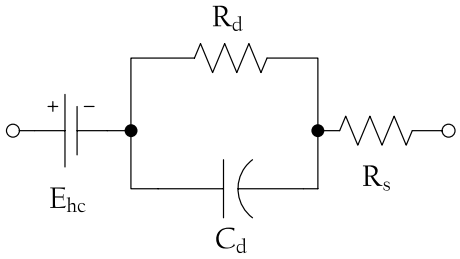

Figure 1. Equivalent circuit for a biopotential electrode-tissue impedance. E_{hc} is the half-cell potential, R_d and C_d the impedance due to the electrode-electrolyte and polarization effects, and R_s models the interface effects due to the resistance of the electrolyte[3].

brain-computer interfaces. In order to avoid these pernicious effects, the literature sets the limit for the impedance value around 5 kΩ for EEG[6,9–12] and for evoked potentials[1].

Typically, the first stage of a biopotential monitoring system consists of a low-noise amplifier (LNA) that receives the analog signal sensed by several electrodes connected to the patient. A high-impedance first stage is necessary for a system of this kind[13], because it minimizes the effect of the contact impedance. Nevertheless, and due to the half-cell potential that occurs in the interface between the electrode and the biological tissues (E_{hc} in Fig. 1), it is necessary to remove the DC component to prevent the signal from saturating the output of the amplifier. The design of a passive high pass filter (HPF) with a low cutoff frequency requires the use of a parallel resistor that lowers the input impedance of the system in several orders of magnitude with respect to the input impedance of the LNA.

The common method for measuring the electrode-tissue impedance consists of injecting a known AC current[14] (usually a square wave) and measuring the differential voltage between the electrodes[6,15]; this methodology is applied to measure bio-impedance in general. For example, Zamani *et al.*[16] present a bio-impedance measurement system for cardiac tissues, and Rodriguez *et al.*[17] describe a wireless sensor suitable for implantable devices. Multifrequency analysis can be found in the literature, applied for example to cardiac tissues[18], in order to extend the analysis of the impedance to the range of frequencies of the measured signals. Kubendran *et al.*[19] highlight the drawbacks of using sinusoidal sources or square waves when performing an analysis of this kind.

Current injection presents several problems. Firstly, the application of an active current into the patient is restricted due to regulation of medical devices, implying a thorough validation process for Class B or Class C devices (those that may cause a potential injury to the patient)[20]. The devices that do not inject current are Class A devices, and their validation process is easier. A second drawback of this method is power consumption, due to the utilization of current generators and dedicated circuitry to measure the skin-electrode impedance. The devices that do not inject current to the patient do not need additional current generators, and so they are going to consume less power. This issue is especially relevant given that recent years have witnessed the proliferation of wireless designs for IONM[21,22], which could mark the beginning of battery-powered systems. An additional issue is the abrasion of the skin when measurements are constant and repeated, needed to maintain the signal quality, which requires tedious scalp conditioning that may lead to an increase of infection risk[6] and of skin diseases; being able to monitor the contact impedance often without the need of injecting any current in the tissue will permit to extend the time between electrode repositioning or skin treatments.

On the other hand, the exact value of the impedance is often not interesting for the IONM application; the only information required is an almost binary flag indicating if the connection is *good enough* for a correct measurement, or if the placement of the electrode must be corrected. Several instruments just report if the value is safely lower, more or less around, or clearly higher than a designated threshold–which is typically near 5 kΩ.

This paper presents a novel impedance measurement method that overcomes the problems presented by the injection of current (power consumption, different class of the device for the validation process, skin abrasion) by evaluating the effect of a change in the input resistance of the LNA on the measured signal. A description of the methodology proposed is presented in Section 2. Section 3 shows the experimental arrangement carried out to validate the system and the results obtained. Conclusions of the study are stated in Section 4.

Most of the experiments in our paper were carried out using a prototype instrument, with an "ad-hoc" testing system developed to simulate the EEG signals in shape, value and impedance, and using a synthesized signal. In the last part of Section 3, preliminary results of a new measurement and test campaign on volunteer human subjects is also reported.

Proposed Methodology

The passive method (without the injection of a probe current) proposed here is based in the changes in the measured signal when a purely resistive load is connected in parallel to either the positive or the negative input terminals of the LNA. Altough similar techniques are found in the literature[6], in this proposal the signal analyzed to assess the impedance is the biological input signal and not a signal known *a priori*. The hardware implementation for the system is depicted in Fig. 2.

In this work, the contact between electrode and skin is modeled as a series resistor and a DC voltage source. This simplification with respect to the Webster model[3] presented in Fig. 1 is made possible thanks to the following considerations:

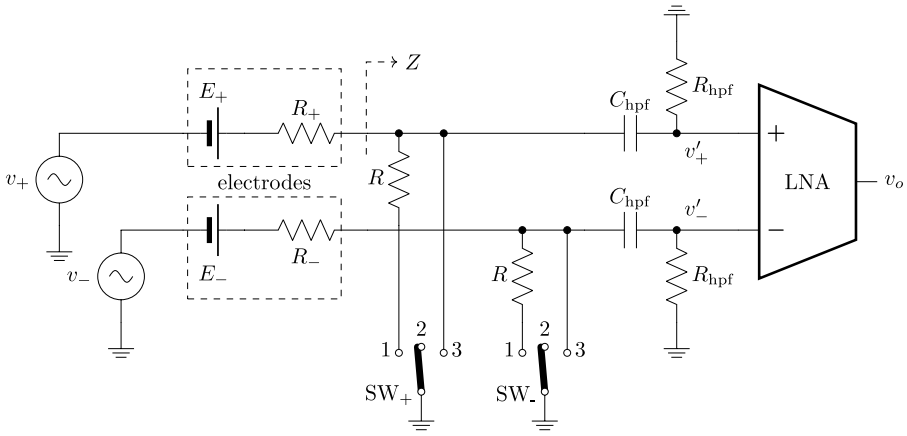

Figure 2. Simplified schematic of system implementing the measurement technique.

- Firstly, the tissue impedance term (R_s in Fig. 1) is neglected since it is generally at least two orders of magnitude smaller than the contact impedance[2].
- Secondly, measuring the value of the reactive elements is important for the frequency-domain analysis of the contact impedance; but in this method the effect of this impedance is assessed with the same signal which is being measured, so that we can consider the contact resistance as an averaged-out equivalent in the band of interest.
- Finally, the intent of the measurement is to just estimate if the contact impedance is *low enough* for a correct measurement, and not a value for the impedance itself.

The half-cell potential due to the interface between each electrode and the tissue in the contact interface is modeled, as shown in Fig. 2, by two batteries E_+ and E_-. These potentials will be similar in all the terminals due to the utilization of the same type of electrodes. The effect of these DC voltage sources is filtered out by the high pass filter at the input terminals of the LNA, composed by the capacitors C_{hpf} and resistors R_{hpf}. R_+ and R_- model the resistive behaviour of the contact between the electrode and the skin of the patient for each electrode. Finally, the signal to be measured is modeled by the pair of generators v_+ and v_- that represent the ideal (unknown) pair of monopolar biopotentials that is to be measured.

If the amplifier is considered ideal, the output of the circuit will follow

$$v_o = G \cdot (v'_+ - v'_-) \tag{1}$$

where G is the gain of the LNA and v'_+ and v'_- are the voltages at each input terminal of the amplifier in the frequency domain.

The position of switches SW_+ and SW_- determine the relationship between v'_+ and v_+ and, in the same way, between v'_- and v_-. Position 1 connects a resistor of known value (R) in parallel to the input, while position 3 grounds the respective input, setting it to zero. When the switches are in position 2, the system is in normal operation.

In normal operation mode, the voltage at the input of the positive terminal of the LNA can be calculated, ignoring the effect of the DC voltage source due to the filter and assuming that the input impedance of the amplifier is large enough:

$$v'_+ = v_+ \cdot \frac{R_{hpf}}{R_{hpf} + \frac{1}{j\omega \cdot C_{hpf}} + R_+} \tag{2}$$

Assuming that the frequency of the signal and the value of the resistor of the filter are large enough with respect to the value of the contact impedance, (2) can be simplified:

$$v'_+ \simeq v_+ \tag{3}$$

The same calculation is carried out when the parallel resistor is connected to the positive input of the LNA (SW_+ in position 1 in Fig. 2):

$$v'_+ = v_+ \cdot \frac{Z}{R_+ + Z} \cdot \frac{R_{hpf}}{R_{hpf} + \frac{1}{j\omega \cdot C_{hpf}}} \tag{4}$$

where Z can be calculated as

$$Z = \frac{\left(R_{hpf} + \frac{1}{j\omega \cdot C_{hpf}}\right) \cdot R}{R_{hpf} + \frac{1}{j\omega \cdot C_{hpf}} + R} \tag{5}$$

Assuming again that the frequency of the signal is large enough with respect to the cutoff frequency of the filter, and considering that the values of R and R_{hpf} are known and $R_{hpf} \gg R$, (5) can be simplified to

$$Z \simeq \frac{R_{hpf} \cdot R}{R_{hpf} + R} \simeq R \tag{6}$$

and therefore, (4) becomes

$$v'_{+} = v_{+} \cdot \frac{R}{R_{+} + R} \tag{7}$$

that corresponds to the equation of a resistive voltage divider, similar to what is calculated in by Ferree *et al.*[6]. The same procedure can be applied to the negative terminal input of the system.

Consequently, a difference in the input signals measured is observed when the parallel resistor R is connected to any of the electrodes. One can define α and β as the attenuation coefficients caused by the relation between the contact impedance R_{+} and R_{-} and the known resistance (R) when the corresponding switches are closed.

$$\alpha = \frac{R}{R + R_{+}} \qquad \beta = \frac{R}{R + R_{-}} \tag{8}$$

These coefficients become useful when defining a set of voltage measurements that can be obtained when combining the different positions of the switches shown in Fig. 2:

$$\begin{aligned} v_a &= G \cdot (v_{+}) && (2,3) \\ v_b &= G \cdot (\alpha \cdot v_{+}) && (1,3) \\ v_c &= G \cdot (-v_{-}) && (3,2) \\ v_d &= G \cdot (-\beta \cdot v_{-}) && (3,1) \end{aligned} \tag{9}$$

where the position of SW_{+} and SW_{-} are indicated, in this order, between brackets.

To apply the method for the assessment of the impedances, the voltages in (9) are measured consecutively. More specifically, v_a is obtained when the negative terminal is connected to the system ground (SW_{-} in position 3) and the positive terminal is in normal operation mode (SW_{+} in position 2). Subsequently, R is connected in parallel to the positive terminal (SW_{+} in position 1) and v_b is measured. Then v_c and v_d are measured in a similar way, with the positive terminal grounded (SW_{+} in position 3) and SW_{-} toggled between positions 2 and 1, respectively.

Thus, α and β can be calculated independently by means of the measurements taken, following

$$\alpha = \frac{v_b}{v_a} \qquad \beta = \frac{v_d}{v_c} \tag{10}$$

In the general case, these voltages are variable in time, and from the perspective of the method, they can be considered almost as they were random, or random-like signals. To obtain a value for α and β, which are needed to assess the values of R_{+} and R_{-}, a statistical value extracted by the measurements is applied to the equations in 9, such as the Root Mean Square (RMS) value. Calling $F(\cdot)$ the function that calculated the designated statistical value from each voltage, we have:

$$\alpha = \frac{F(v_b)}{F(v_a)} \qquad \beta = \frac{F(v_d)}{F(v_c)} \tag{11}$$

Finally, with the help of 8, the skin-electrode contact impedance can be calculated from the measurements taken:

$$R^{+} = R \cdot \frac{1 - \alpha}{\alpha} \qquad R^{-} = R \cdot \frac{1 - \beta}{\beta} \tag{12}$$

Experimental Setup

In order to verify the system, firstly the method has been evaluated mathematically (using ideal, simplified models for the components) and by simulation with the full models of the electronic circuit. Afterward, a laboratory test system that simulates the signal sources has been implemented, and the method has been validated using synthetic signals recorded by real EEG and ECoG. Finally, a preliminary test was carried out with a prototype on human volunteers, with satisfactory results.

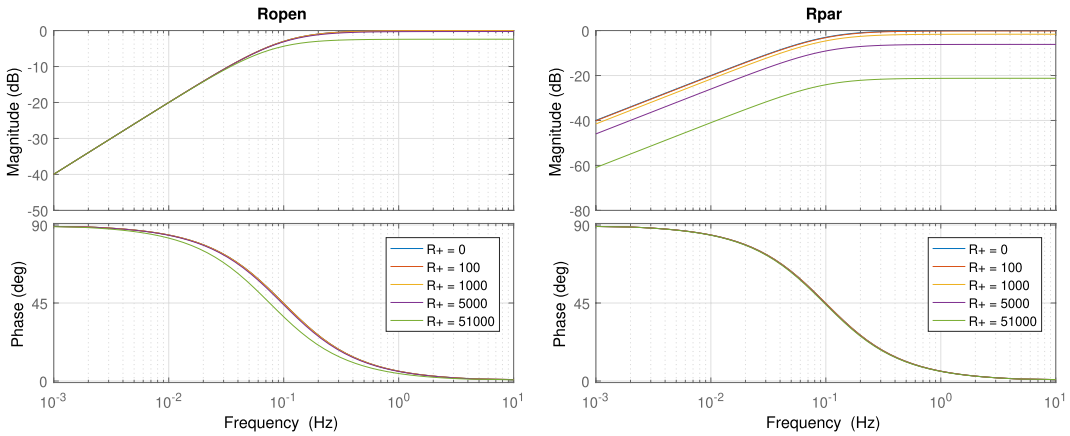

Figure 3. At the left, Bode diagram of v'_+/v_+ with v'_- grounded, in normal operation mode; at the right, with a 5 kΩ parallel resistor connected, for several contact resistance values (values of R_+ in Ω).

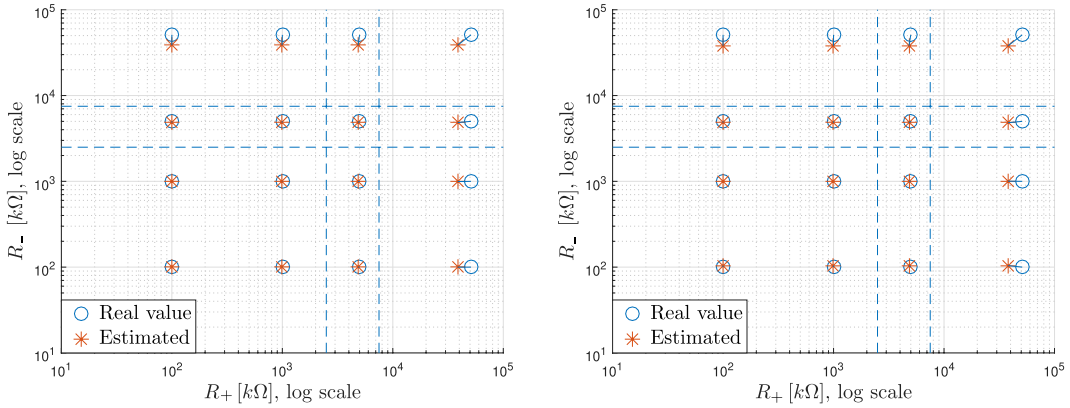

Figure 4. On the left, result of the calculations performed on the simplified model; on the right, result of the simulations with the full circuit model. Value of resistive impedances estimated vs. calculated.

Mathematical model and simulations. As a first step, we checked that the effects of the added resistors R on the frequency response of the system are acceptable. Two different configurations have been studied: in normal operation mode and when the parallel resistor R is placed in the positive input. The Bode diagrams of the frequency response of the system, for several values of the contact resistor R^+, are shown in Fig. 3; the first one represents the transfer function v'_+/v_+ in normal operation, and the second one shows the same transfer function when a resistor $R = 5\text{k}\Omega$ is connected (SW + in position 1).

As can be seen from the figures, the frequency response of the system is almost constant when the contact impedance changes and no resistor is placed in parallel. On the other hand, when the parallel resistor is connected, an increase in the value of the contact resistor leads to a signal attenuation basically constant in the frequencies of interest. Nevertheless, the cut-off frequency of the input high-pass filter is not altered in any scenario.

To test the method, we calculated the output voltage for a sinusoidal voltage with a frequency of 1 kHz as input. The output voltage of the signal is analyzed and the impedance estimated with the help of equations (9), (11) and (12), and then compared with the real value.

The root mean square (RMS) value of the input signal is selected as the statistical property (function $F(\cdot)$ in Eq. 11), because it offers a good trade-off between robustness and computational cost.

Three different cases are possible, depending on the values of the contact resistances of the two inputs. Firstly, if the contact impedance is much lower than 5 kΩ, the voltage drop in R_+ (or R_-) due to the connection of R will be negligible and the coefficients α (or β) will be close to 1. Secondly, a contact impedance around 5 kΩ will give values for α or β close to 0.5. Finally, in the case that R_+ is much greater than R, the voltage drop in the contact impedance will be noticeable, and hence the coefficients will reach a value close to 0.

The results of this estimation are shown in the left diagram in Fig. 4, where the calculated impedance is represented in comparison to the real values of the resistors tested. A total of sixteen cases have been represented, resulting from the combination of the values 100 Ω, 1 kΩ, 5 kΩ and 51 kΩ for R_+ and R_-. This set of values has been chosen because the border between acceptable and non-acceptable contact impedance has been set at 5 kΩ, and to explore the behavior with similar or very different values. In the result, the differences arise basically from rounding errors in the operations, mainly due to the numerical calculation of RMS.

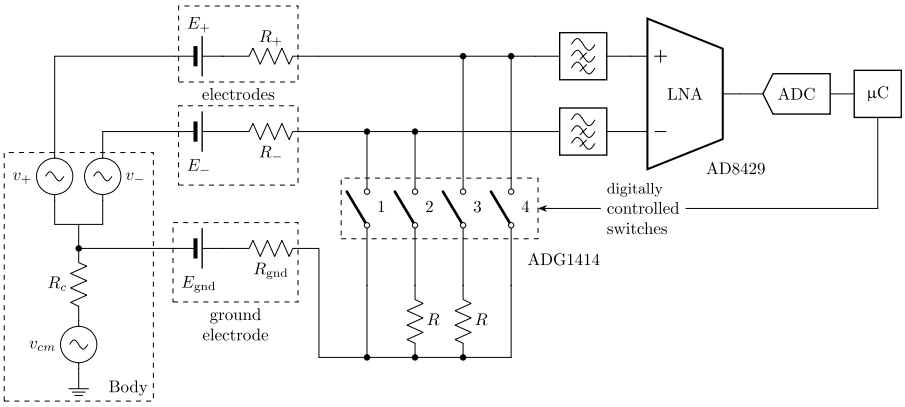

Figure 5. Schematic of the prototype test bench tested.

Since the aim of this methodology is the assessment of the contact impedance between electrode and skin, two thresholds are arranged in order to classify the impedance as good, middling or unacceptable. In the figure, these two thresholds are set to the values of $R = 2.5\ \text{k}\Omega$ and $7.5\,\text{k}\Omega$, providing a separation between nine different scenarios, each one identified by the combination of one of the three possible classes of the real contact impedance and one of the three possible outcomes of the measurement. In other words, the objective of the method is that real and measured impedances share the same scenario, meaning that a good contact impedance is estimated as good, a middling as middling, and so on.

As expected, and as can be seen from Fig. 4, the impedances are correctly estimated in all scenarios, when the model is evaluated mathematically.

Once the methodology has been validated through a mathematical model where the components are represented in ideal conditions, a set of simulations have been carried out in order to confirm the validity of this method taking into account the full model of the active components of the circuit.

The freely available LTSpice simulation software has been utilized to simulate the corresponding circuit. The AD8429 low noise amplifier, which is the one chosen for the prototype, has been simulated using the model made available by the manufacturer. The switches that connect the resistor R in parallel to the inputs are modeled with a voltage-controlled switch, so that the four configurations stated in (9) are simulated sequentially.

A sinusoidal voltage at 1 kHz with a peak to peak value of $15\,\mu\text{v}$ and an offset value of 1 mV is utilized as input. Each configuration switching is followed by a transient period due to the response of the HPF located in both terminal inputs of the LNA. Due to the transient, the RMS value has to be computed after the signal is settled. Considering a trade-off between the duration of the algorithm and the precision, the calculation of the RMS is carried out after 2τ.

Again, sixteen cases are simulated, combining four impedance values ($100\,\text{k}\Omega$, $1\,\text{k}\Omega$, $5\,\text{k}\Omega$ and $51\,\text{k}\Omega$) for both R_+ and R_-. The comparison between the calculated and the real impedance is represented in the right diagram in Fig. 4. In this figure it can be seen that, even though the estimation of the impedances is fairly good, the estimation error has increased slightly with respect to the theoretical analysis. The identification of the working scenario of the system with respect to the impedance condition (good, middling or unacceptable) is correct.

Laboratory tests. In the following phase, an experimental setup was arranged in order to check the validity of the methodology proposed with real electric signals similar to the ones found in real application; for this reason, a system as depicted in Fig. 5 was used. In this circuit, we use a classical configuration of common-mode plus differential signal to simulate the measured waveforms; the measurements are most commonly done using a differential configuration (all the switches open in Fig. 5) to be able to reject the common-mode signal.

A two-channel RIGOL-DG1022 waveform generator is utilized to simulate the input signal of an IONM acquisition system, including v_+, v_- and the common mode voltage v_{cm}. These voltages are generated and combined with the help of a summing amplifier and a differential amplifier arrangement (not shown in the schematic), in order to obtain the desired differential and common mode value at each input. A series resistance is connected to the positive and negative electrodes in order to simulate the tissue-electrode contact impedance, following the simplifications presented in Section 2. Notice that the ground electrode is normally connected to the reference terminal of the instrumentation amplifier, either directly or through a voltage-follower setup. The ground electrode impedance is considered distributed into R_+ and R_-.

As indicated above, the differential voltage between the two electrodes is obtained by means of an AD8429 LNA. The analog output of the LNA is converted by means of a 16 bits digital to analog converter (ADC). Finally, the digital signal is registered by a microcontroller that is in charge of recording the signals and controlling the digital switches that configure the different connections required by the algorithm. For this purpose, an ADG1414 SPI-controlled array of switches is connected in parallel to the terminal inputs of the amplifier, in such a way that closing the corresponding switch allows either the parallel connection of the known resistance R (switches 2, 3 in Fig. 5) or grounding (switches 1, 4 in Fig. 5) independently for each input.

The circuit utilized in the experiments was configured with the following features (voltages are peak-to-peak values):

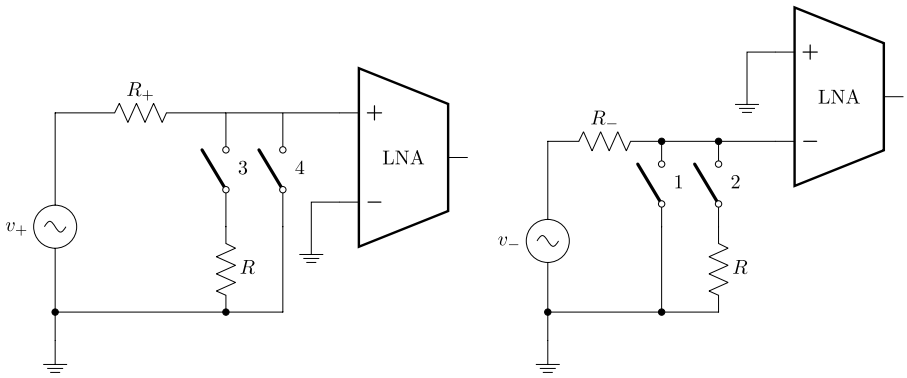

Figure 6. Schematic connection when measuring α (left) and β (right) in monopolar configuration.

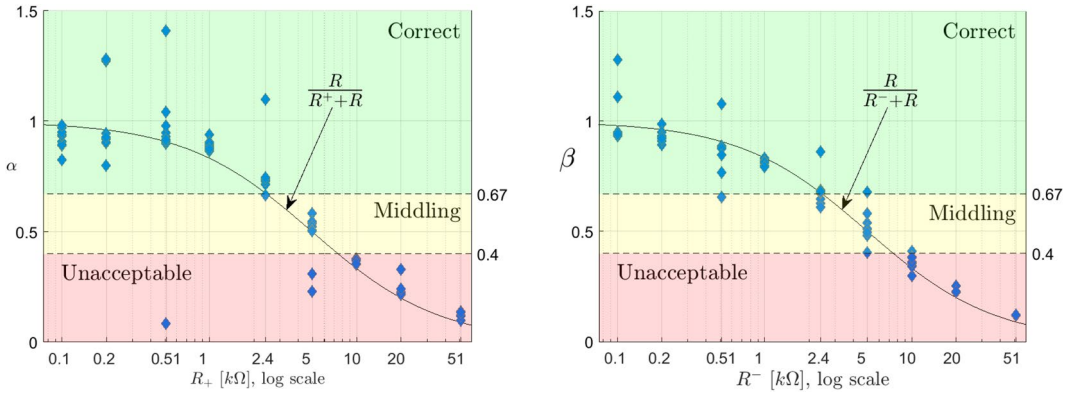

Figure 7. Value of α (left) and β (right), obtained respectively with the inverting and non-inverting input grounded. Measured vs. calculated.

- $v_{cm} = 1$ mV, sinusoidal at 50 Hz.
- $v_+ = -\ v_- = 15\,\mu$V, from a previously recorded and digitalized neurological signal.
- R_c is considered negligible. Given the high CMRR of the amplifier and the floating ground arrangement, it should not influence greatly the measurement.
- $R = 5\,$kΩ.
- R_+, R_- varied among {100 Ω, 200 Ω, 500 Ω, 1 kΩ, 2.4 kΩ, 5 kΩ, 10 kΩ, 20 kΩ, 51 kΩ}.
- $G = 50$V/V.
- The contact potential E_+, E_-, E_{gnd} were included in the voltage generated by the waveform generator.

The experiments were carried out with two different configurations of the amplifier: monopolar (where just one channel of the amplifier is used) and bipolar (with the amplifier connected in full differential mode). In the following, monopolar and bipolar refers to the amplifier configuration, and not on the type of pulse applied to v_+ or v_-; the latter is obtained from real-life registered signals that are reproduced by the arbitrary generators. The system itself does not apply any voltage, barring the unavoidable noise; bias current voltages leakage from the amplifier are cut by the high-pass filter capacitors. In the system we tested, the maximum amplitude that the system is able to accept is ±32 mV, but this is just related to the front-end used and the method can be applied with other, different designs.

In the first set of tests, the value of α and β were calculated by means of monopolar measurements. For this, one terminal input is grounded directly (without the help of the digital switch), while the opposite terminal receives the signal from the generator while the parallel load is switched. This configuration is depicted in Fig. 6.

From the voltages recorded during these experiments, (9) and (11) are applied to obtain the values of α and β.

Figure 7 contain the results obtained after 10 measurements for different values of R_+ and R_-. The black line represents the theoretical value of α and β, calculated following (8) and provided that R_+ and R_- are known. Consistency between experimental and theoretical results can be observed.

Afterward R_+ and R_- can be calculated once that α and β are obtained, by way of Eq. (12). The results are shown in Fig. 8. The similarity between the resistor located for the tests and the calculated impedance can be observed. The thresholds for 2.5 kΩ and 7.5 kΩ are also shown in the figures.

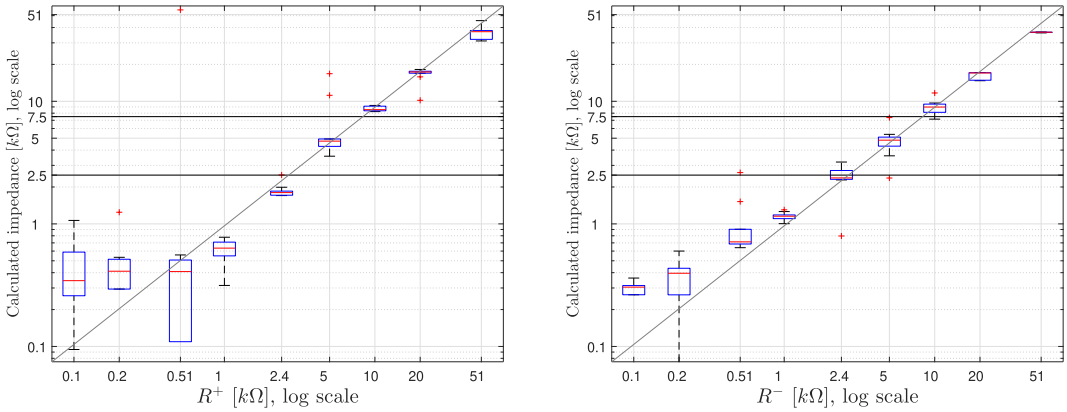

Figure 8. Boxplot of R^+ (left) and R^- (right) calculated (ordinate), vs. resistor value located for the tests (abscissa).

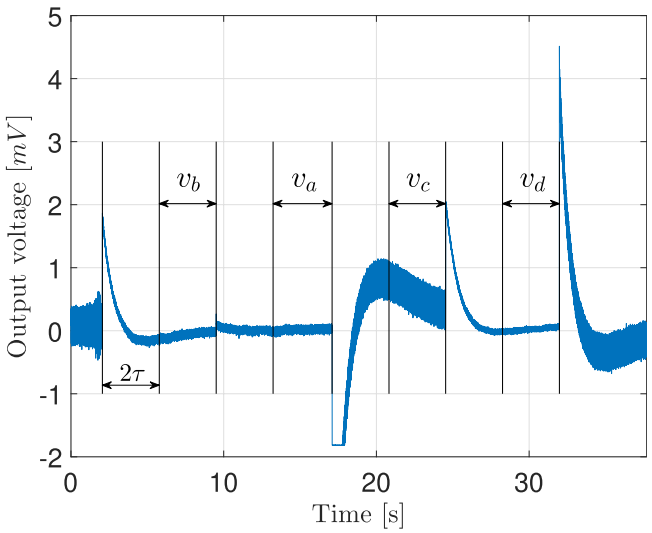

Figure 9. Gain corrected output voltage of one realization. Variation depending on the switch configuration.

Secondly, we carried out the assessment of both impedances in a bipolar and sequential fashion. In this case, no terminal is grounded and both electrodes are connected to the emulated biopotential sources. The digitally controlled switch is activated in order to obtain v_b, v_a, v_c and v_d, so that the value of α and β are computed in this order. A total of nine cases have been tested, resulting from the combination of three different resistor values for each terminal. Three significantly different impedance values have been utilized: 100 Ω, 5 kΩ and 51 kΩ.

Figure 9 shows the output voltage (without filtering) of the LNA for a realization of one of the experiments, where $R_+ = 100\ \Omega$ and $R_- = 51$ kΩ. During the contact impedance evaluation, the switches are toggled to measure the voltages for the four configurations. In the figure, the variation of the signal amplitude and the transient phenomenon due to the high pass filtering is clearly visible. The period 2τ, also indicated, is the chosen compromise between the steady-state condition and the overall speed of the measurement.

The realization of these experiments in a real device implies an additional challenge: the calculation of the RMS in real time. Computation of the RMS of each period requires a cumulative sum of the square of the samples obtained, followed by a division by the number of samples in the interval and the square root of the resulting value. This process has to be repeated four times, in order to compute all the values stated in (9). Because of its simplicity, the algorithm proposed can be implemented in a conventional 32-bits microcontroller. Following this procedure, the values obtained in the case shown in Fig. 9 are $\alpha = 0.987$ and $\beta = 0.124$.

In order to establish an analogy with the figures containing the results for the mathematical model and the simulation, the values obtained for α and β have been arranged in Fig. 10 (left-side diagram). Note that the thresholds are now placed in coefficient values 0.4 (corresponding to $R = 7.5$ kΩ) and 0.67 ($R = 2.5$ kΩ).

From these results, it can be seen that the estimation error has increased with respect to the mathematical calculations and simulation, and moreover, there are two cases where the value of α overpasses the threshold separating the nine scenarios. In both cases, a middling value of impedance was assessed as bad, resulting in a

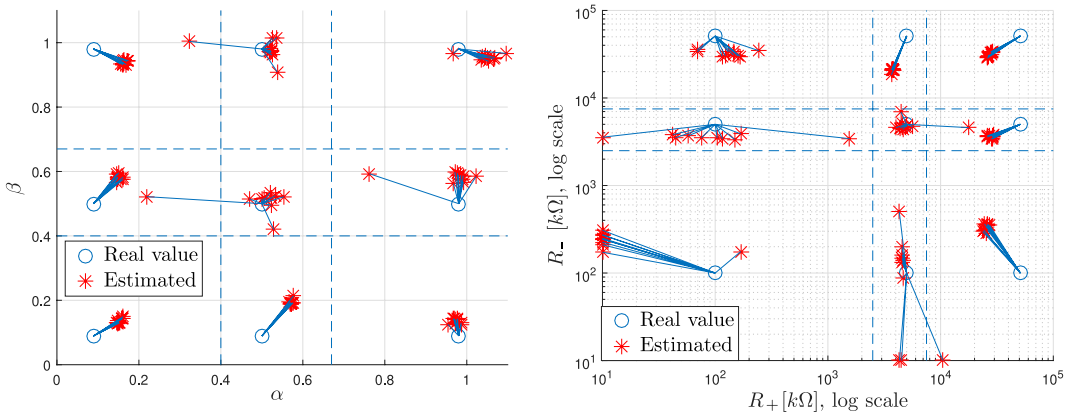

Figure 10. In the left side, value of α and β coefficients obtained with sequential experiments. On the right side, the same results mapped to the resulting values of contact resistance.

false negative. These discrepancies are probably due to the effect of impulsive noise that may affect only to one part of the measurement, distorting the calculations.

The right-side diagram of Fig. 10 summarizes the results obtained for the calculation of the impedances and compares them with the theoretical calculations. For simplification and ease of representation, coefficient values larger than 1, which would indicate impossible negative contact resistances have been equated to 10 Ω. In a real implementation, these values will be considered as an equivalent input impedance of 0 Ω.

Considering the thresholds that divide the working cases of the system into the nine possible scenarios, a few realizations are classified as false negatives, corresponding to the cases where $R_+, R_- = 5$ kΩ, which is the threshold set between middling or unacceptable impedance, leading to a conservative algorithm. In a practical application, the three possible states of the impedance for each input terminal are indicated by a multicolour LED (red to mean a defective connection, yellow to indicate a connection in the limit of validity, and green for a good one). The false negatives are a minor defect and will lead to a recalculation of the impedance or, in the worst case, to a reconnection of the electrode.

***In-vivo* tests.** A series of tests has been performed on human volunteers (several of the authors) in the laboratories of the IIT and of the University Hospital "La Princesa", in Madrid, respecting the internal protocols of the Institute; the experimental protocols were approved by the Ethical Committee of Clinical Research of Hospital de la Princesa (number of register PI-843, approved Dec. 21, 2015). The test has been duly authorized, and performed in accordance with the approved protocols, on two of the authors of the paper, whose have been informed and agreed to conduct the experiments, providing specific informed consent, and being fully aware of the risks and methodology of the experiment.

The experimental prototype used was battery-powered (with d.c. voltage never in excess of 10 V, and power dissipation well under 10 W), completely floating so that there were no possible leakage current towards main, and passive, not injecting any current. The experiment consisted on contact impedance measurements with the standard hospital equipment and the prototype system.

The contact impedances for four channels where previously measured by the standard IONM apparatus of the hospital, measuring values between 0.6 kΩ and 1.8 kΩ using the classical injected current methodology. Immediately after, the standard device was disconnected and the experimental device[23] implementing the new method was connected, and the contact resistances assessed in five consecutive trials.

Figure 11 report the obtained results. As it can be seen, apart for the expected noisy nature of each of the consecutive trial, the averaged value is well in accordance with the measurement performed by the traditional instrument and, more important, is assessing the same scenario of "good" contact impedances.

Discussion

A novel methodology for estimating the skin-electrode contact impedance is presented in this paper. This technique is based in the variation experienced by the measured voltage caused by the controlled connection of a parallel resistor to the input stage of the measurement device. Thus, injection of current to the patient is avoided and, by contrast, the signal utilized to carry out the assessment is the same random signal recorded from the patient. Problems such as skin abrasion, power consumption and complexity of the certification process are then reduced.

The capabilities of the new method have been evaluated and assessed by means of a mathematical model, a simulation, a prototype test bench analysis and several *in vivo* measurements. In the last two cases, the data is registered by a microcontroller that computes the algorithm proposed and gives back an estimation of the contact impedance of both positive and negative electrodes. It has been proved that computing the root mean square value of the output voltage and comparing the different measurements obtained allows the system to identify the correctness of the contact impedance for each electrode. This permits warning the user whether the measurements taken can be considered acceptable, doubtful or unacceptable.

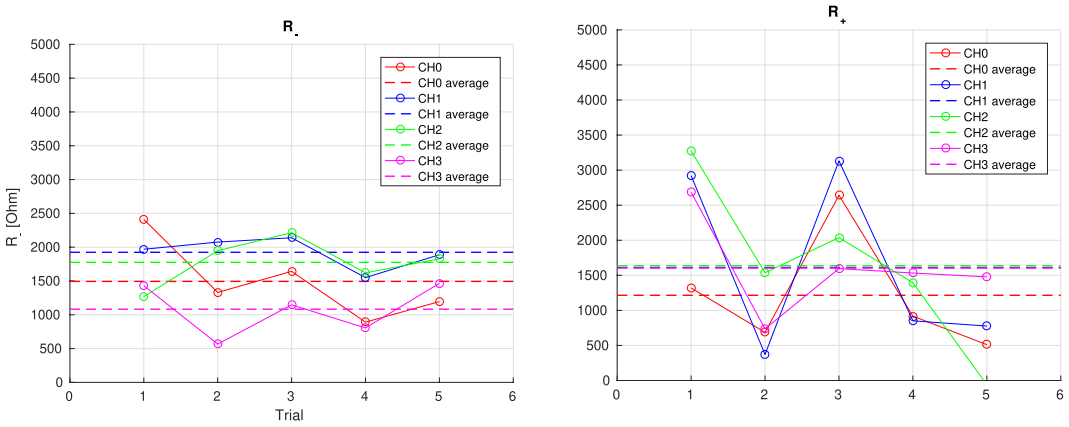

Figure 11. Result of the *in-vivo* measurements.

The proposed method is found to be an improvement in current IONM technologies, and may imply a significant gain, particularly in battery powered autonomous systems, by omitting the circuitry needed to inject the probe current. The simplification of the certification procedure represents a substantial cost-cutting feature with respect to the same procedure for a device injecting current into the patient.

This method has been implemented in a wireless IONM system (WIONM) that is currently under field validation. The design has been patented[23] and is currently in certification phase.

Data availability

Data has been gathered by experimental measurements directly on the several prototypes of the system. The author will share all the data available upon request.

Received: 6 June 2019; Accepted: 24 January 2020;
Published online: 18 February 2020

References

1. Vega-Zelaya, L., Sola, R. G. & Pastor, J. Intraoperative Neurophysiological Monitoring in Neuro-oncology. In Agrawal, A. (ed.) *Neurooncology - Newer Developments*, July, chap. 9, https://doi.org/10.5772/63241 (IntechOpen, 2016).
2. Guermandi, M., Cardu, R., Scarselli, E. F. & Guerrieri, R. Active Electrode IC for EEG and Electrical Impedance Tomography With Continuous Monitoring of Contact Impedance. *IEEE Transactions on Biomed. Circuits Syst.* **9**, 21–33 (2015).
3. Webster, J. G. *Medical Instrumentation Application and Design*, 4th edn. (Wiley, Hoboken, NJ, 2009).
4. Patki, S. *et al.* Wireless EEG system with real time impedance monitoring and active electrodes. In *2012 IEEE Biomedical Circuits and Systems Conference (BioCAS)*, 108–111, https://doi.org/10.1109/BioCAS.2012.6418408 (IEEE, 2012).
5. Buxi, D. *et al.* Correlation between electrode-tissue impedance and motion artifact in biopotential recordings. *IEEE Sensors J.* **12**, 3373–3383, https://doi.org/10.1109/JSEN.2012.2221163 (2012).
6. Ferree, T. C., Luu, P., Russell, G. S. & Tucker, D. M. Scalp electrode impedance, infection risk, and EEG data quality. *Clin. Neurophysiol.* **112**, 536–544 (2001).
7. Kappenman, E. S. & Luck, S. J. The effects of electrode impedance on data quality and statistical significance in ERP recordings. *Psychophysiol.* **47**, 888–904, https://doi.org/10.1111/j.1469-8986.2010.01009.x (2010).
8. Sagha, H., Perdikis, S. & Chavarriaga, R. Quantifying Electrode Reliability During Brain – Computer Interface Operation. *IEEE Transactions on Biomed. Eng.* **62**, 858–864 (2015).
9. Tautan, A.-M. *et al.* Signal Quality in Dry Electrode EEG and the Relation to Skin-electrode Contact Impedance Magnitude. In *Proceedings of the International Conference on Biomedical Electronics and Devices (BIOSTEC 2014)*, 12–22, https://doi.org/10.5220/0004738700120022 (2014).
10. Nuwer, M. R. *et al.* IFCN standards for digital recording of clinical EEG. The International Federation of Clinical Neurophysiology. *Electroencephalogr. clinical neurophysiology. Suppl.* **52**, 11–4 (1999).
11. Chi, Y. M., Jung, T.-P. & Cauwenberghs, G. Dry-Contact and Noncontact Biopotential Electrodes:. *IEEE Rev. Biomed. Eng.* **3**, 106–119 (2010).
12. Teplan, M. Fundamentals of EEG Measurement. *Meas. Sci. Rev.* **2**, 1–11 (2002).
13. Taji, B., Shirmohammadi, S., Groza, V. & Batkin, I. Impact of skin-electrode interface on electrocardiogram measurements using conductive textile electrodes. *IEEE Transactions on Instrumentation Meas.* **63**, 1412–1422, https://doi.org/10.1109/TIM.2013.2289072 (2014).
14. Langlois, P. J., Neshatvar, N. & Demosthenous, A. A Sinusoidal Current Driver With an Extended Frequency Range and Multifrequency Operation for Bioimpedance Applications. *IEEE Transactions on Biomed. Circuits Syst.* **9**, 401–411 (2015).
15. Xu, J. *et al.* A wearable 8-channel active-electrode EEG/ETI acquisition system for body area networks. *IEEE J. Solid-State Circuits* **49**, 2005–2016, https://doi.org/10.1109/JSSC.2014.2325557 (2014).
16. Zamani, M., Rezaeiyan, Y., Shoaei, O. & Serdijn, W. A. A 1.55 μw Bio-Impedance Measurement System for Implantable Cardiac Pacemakers in 0.18 μm CMOS. *IEEE Transactions on Biomed. Circuits Syst.* **12**, 211–221, https://doi.org/10.1109/TBCAS.2017.2776528 (2018).
17. Rodriguez, S., Ollmar, S., Waqar, M. & Rusu, A. A Batteryless Sensor ASIC for Implantable Bio-Impedance Applications. *IEEE Transactions on Biomed. Circuits Syst.* **10**, 533–544, https://doi.org/10.1109/TBCAS.2015.2456242 (2016).
18. Sanchez, B., Schoukens, J. & Bragos, R. Novel Estimation of the Electrical Bioimpedance Using the Local Polynomial Method. Application to *In Vivo* Real-Time Myocardium Tissue Impedance Characterization During the Cardiac Cycle. *IEEE Transactions on Biomed. Eng.* **58**, 3376–3385 (2011).

19. Kubendran, R., Lee, S., Mitra, S. & Yazicioglu, R. F. Error Correction Algorithm for High Accuracy Bio-Impedance Measurement in Wearable Healthcare Applications. *IEEE Transactions on Biomed. Circuits Syst.* **8**, 196–205 (2014).
20. ISO. ISO 62304:2006. Medical device software - Software life cycle processes. Tech. Rep. (2006).
21. Mays, J., Rampy, P., Sucato, D., Sparagana, S. & Chiao, J. C. A wireless system improves reliability of intraoperative monitoring recordings. *BioWireleSS 2016 - Proceedings, 2016 IEEE Top. Conf. on Biomed. Wirel. Technol. Networks, Sens. Syst*. 5–7, https://doi.org/10.1109/BIOWIRELESS.2016.7445546 (2016).
22. Farajidavar, A. *et al*. A wireless system for monitoring transcranial motor evoked potentials. *Annals biomedical engineering* **39**, 517–23, https://doi.org/10.1007/s10439-010-0152-x (2011).
23. Jimenez-Carles Gil-Delgado, E. Intraoperative Monitoring System: Patent application WO 2018/011439 Al (2018).

Acknowledgements
This work has been supported by SOINDE S.L. and developed in collaboration with Hospital Universitario de La Princesa (Madrid, Spain). The authors would like to thanks Prof. Chris Turner for proofreading the article.

Author contributions
The five authors of this Work have been contributing in roughly the same way to the research that lead to this article, and all of them have contributed to writing, proofing and correcting the paper and the associated figures. In detail, E.A. contributed all over the map, building the prototype, debugging it, planning the measurements and analyzing them. R.G. was more involved in the analog design; C.R.-M., J.M. and J.D.M.-F. were more involved in the digital design (hardware and software) and PCB optimization. All the authors participated in the debugging of the system, its deployment and the measurement campaigns, as well as in revising the manuscript.

Competing interests
The authors declare no competing interests.

Additional information
Correspondence and requests for materials should be addressed to R.G.

Reprints and permissions information is available at www.nature.com/reprints.

Publisher's note Springer Nature remains neutral with regard to jurisdictional claims in published maps and institutional affiliations.

2.2 A Novel Approach for the Design of Fast-Settling Amplifiers for Biosignal Detection

electronics

MDPI

Article

A Novel Approach for the Design of Fast-Settling Amplifiers for Biosignal Detection

Eduardo Alonso Rivas [1,†,‡], Graziella Scandurra [2,‡], Carmine Ciofi [2], Carlos Rodríguez-Morcillo García [1] and Romano Giannetti [1,*]

[1] Instituto de Investigación Tecnológica, Universidad Pontificia Comillas, 28015 Madrid, Spain; eduardo.alonso@comillas.edu (E.A.R.); carlosrg@comillas.edu (C.R.-M.G.)
[2] Dipartimento di Ingegneria, Università degli Studi di Messina, I-98166 Messina, Italy; graziella.scandurra@unime.it (G.S.); carmine.ciofi@unime.it (C.C.)
* Correspondence: romano@comillas.edu; Tel.: +34-915406283
† Currently at SOINDE, 28692 Madrid, Spain; ealonso@soinde.com.
‡ These authors contributed equally to this work.

Abstract: The most common method used to pick up biomedical signals is through metallic electrodes coupled to the input of high-gain, low-noise amplifiers. Unfortunately, electrodes, amongst other effects, introduce an undesired contact resistance and a contact potential. The contact potential needs to be rejected since it would otherwise cause the saturation of the input stage of the amplifiers, and this is almost always obtained by inserting a simple RC high-pass filter in the input signal path. The contact resistance needs to be estimated to ensure that it does not impair correct measurements. Methods exist for estimating the contact resistance by dynamically modifying the input network configuration, but because of the presence of the input RC filter, long transients are induced any time a switch occurs between different input configurations, so that the measurement time may become unacceptably long. In this paper, we propose a new topology for a DC removal network at the input of the differential signal amplifier that results in an AC filter whose time constant can be continuously changed by means of a control voltage. As such, we can speed up the recovery from transients by setting very short time constants (during the input resistance estimation process) while maintaining the ability to obtain very low cut-in frequencies by setting a much larger time constant during actual measurements. A prototype of the system was built and tested in order to demonstrate the advantage of the approach we propose in terms of reduced measurement time.

Keywords: differential amplifier; DC removal; biological signals; electrode potential

Citation: Alonso Rivas, E.; Scandurra, G.; Ciofi, C.; Rodríguez-Morcillo García, C.; Giannetti, R. A Novel Approach for the Design of Fast-Settling Amplifiers for Biosignal Detection. *Electronics* **2021**, *10*, 2631. https://doi.org/10.3390/electronics10212631

Academic Editor: Maysam Abbod

Received: 30 September 2021
Accepted: 22 October 2021
Published: 28 October 2021

1. Introduction

Biological acquisition systems are commonly designed with a low-noise voltage amplifier (LNA) as a front-end [1]; recent research shows, for example, low-power and low-noise configurations [2,3] and differential and high-CMRR circuits for EEG acquisition [4,5]. These amplifiers are almost always differential and with a band that extends from DC, as reported in [6,7]; even when the electrode is of the capacitive type, the amplifier is designed as a directly coupled one [8].

The electrical behavior of the contact between the patient and the amplifier is complex [9,10]; it is often nonlinear and, even when linear models are used, frequency-dependent. However, with the exception of capacitive electrodes, two elements are always present: a series resistance and a series DC potential, called the half-cell potential. The series resistance is detrimental to the quality of the measured signal [11–13], both because of the added noise and the attenuation that results when considering the input resistance of the amplifier; it is paramount to monitor its value when performing measurements. The half-cell potential is often much bigger than the signals of interest. As the amplifier designs usually present a high gain, they may saturate if the input signal is not properly conditioned.

As a consequence, removing the DC component of the input signal is a necessary stage when low-voltage signals are acquired. Especially in the case of neurophysiological monitoring, adhesive or needle electrodes are connected to the subject being monitored [14–16]; the half cell potential of the two electrodes between which the measurement is carried out are never exactly the same, causing an inherent differential voltage in the contact circuit. This results in a DC offset in the input signal that has to be removed [17,18].

A common solution is to use a high-pass (HP) RC (resistance-capacitor) filter. The corner frequency of the high-pass filter must be quite low, in the order of tenths of Hertz, to account for the band of several physiological signals. This results in very slow settling times (in the order of tens of seconds) for the whole system. In other words, the low corner frequency allows a constant response in the band of interest, but increases the time response when the input voltage is affected by a steep change due to the large RC value.

A long settling time is not only a problem when connecting and disconnecting the system to the subject: changing the input configuration with the subject connected to the amplifier also causes transients. In addition to the filtering and amplifier stages, monitoring systems are usually fitted with the circuitry necessary to measure contact impedance; a too high contact impedance is a sign of a poor or deteriorating contact and can strongly affect the quality of the measurement. Generally, the impedance assessment circuit consists of a generator that injects a current into the patient [19–21], usually by means of a square or sinusoidal signal. This methodology also implies stopping and resuming the acquisition process for a period of time. In [22,23], a novel passive method is presented, consisting of analyzing the voltage variation when parallel loads are connected to the input of the system, thus preventing the injection of current.

The approach in [22] consists of continuously monitoring the biopotential source. When an impedance measurement is needed, several electronic switches are acted upon so that several known resistors are connected in parallel to the input signal path. If the sources are ideal (zero connection impedance), no voltage change would be expected; conversely, the presence of a contact impedance will degrade the input signal [20]. Assessing the contact impedance is, however, not trivial as the source signal is essentially unpredictable. In most cases, the exact value of the impedance is not needed: assessing whether it is low enough to guarantee a correct measurement is sufficient in many cases. Literature and current clinical practice set an approximate value of 5 kΩ as the limit for most common monitoring techniques such as EEG or evoked potentials [24–26]. Several statistical characteristics and estimation methods have been used to predict the impedance value from the registered signal [19]. In [22], observing and computing the changes in the input signal during the impedance measurement cycle enabled us to detect if the impedance was within an acceptable range.

The main problem with the procedure of connection and disconnection of the additional loads is that it causes changes in the DC values of the equivalent input sources, thus triggering long transients that need to be extinguished before actual measurements can be obtained. Therefore, the lower the cut-in frequency, the longer the time needed to complete the measurements required for the characterization of the contact impedance.

Ideally, we would like to be able to speed up the transients during the changes in the input circuit configuration and return to the low cut-in frequency configuration as soon as the transients are extinguished. Of course, such an approach would be effective only if we are able to avoid the introduction of further transients when switching back from a higher cut-in frequency (resulting in faster transients) to a lower cut-in frequency (required for extending the measurements in the low frequency range).

In [27], a new method is proposed to address a similar issue that consists of the integration of an active loopback to compensate for the DC offset of the signal. This is obtained due to a current generator that charges and discharges a capacitor in series with the input of the amplifier. This capacitor acts as a floating voltage source that cancels the variation in the DC voltage at the input much faster than a common RC filter. An intrinsic nonlinearity is exploited in order to obtain fast transients upon large and abrupt

changes in the input while retaining a very low cut-in frequency when such transients are extinguished. However, in [27], there is no direct control on the input filter cut-in frequency, as would be desirable for our application.

The aim of this study is to extend and adapt the method presented in [27] to the case of a differential amplifier for bio-potential measurements by introducing the ability to employ a control voltage for setting the cut-in frequency. This approach, as will be shown in the experimental section, allowed us to dramatically reduce the time required to perform impedance measurements with the method outlined in [22]. This time reduction is significant, since it allows us to effectively address and solve the most important drawback of the approach in [22].

In Section 2, we explain the process that leads to the proposed circuit topology. In Section 3, we detail the circuit of the prototype and apply it to the problem of measuring contact resistances in a passive way. Finally, we discuss the results in Sections 4 and 5.

2. Proposed Approach

In this section, we describe how we propose to solve the problem of having an AC-coupled amplifier that can be smoothly switched from a configuration where it has a very low cut-in frequency (and therefore very long time constant that generates slow transients) to one where the cut-in frequency is higher but with faster transients. Firstly, we summarize the case for a single-ended amplifier based on the active filter presented in [27] and adding the proper circuitry to allow the active filter to be controllable with an external voltage; finally, we extend the principle to a fully differential amplifier topology.

2.1. Single-Ended Amplifier

As outlined in the Introduction, the main problem with performing the estimation of the contact impedance using a purely passive approach is that it requires repeated measurements while changing the input circuit configuration by means of switches. Any time a switch is moved to short the input or connect and disconnect resistances in the signal path, long transients are induced because of the very low input cut-in frequency of the system. This translates into quite long measurement times that might not be acceptable in a number of situations.

While a low cut-in frequency is required in order to not lose information during actual measurements on the patient, higher cut-in frequencies could be tolerated during the contact impedance estimation process.

A simple method to obtain an AC-coupled amplifier with an adjustable cut-in frequency would be to resort to a number of electronic-controlled switches to change the blocking capacitor in the input path, as shown in the simplified diagram in Figure 1a. With a larger capacitance (switches closed), we obtain a lower cut-in frequency; by disconnecting some of the capacitors, we increase the cut-in frequency. During transients, we may open all or some of the switches to obtain a high cut-in frequency, thus speeding up the transients, and when the transients are extinguished, we can close all switches to obtain the largest equivalent capacitance and, hence, the lowest cut-in frequency.

The obvious problem with this approach is that the capacitors connected to open switches would be charged to voltage levels that are, in general, different from those of the capacitors still connected in the circuit. Therefore, when the previously disconnected capacitors are switched back in, to obtain the lowest cut-in frequency, an almost instantaneous charge redistribution occurs. This results in a voltage step whose amplitude depends on the previous history and that, in turn, results in a transient that will evolve with the time constant corresponding to the lowest cut-in frequency, thus making the approach just described completely useless.

If we want to effectively reduce the set-up time, a system must be devised for switching from a high cut-in frequency to a low cut-in frequency, minimizing the transient time. The approach we developed to address this issue relies on the design of an auxiliary system that acts upon the main circuit in so that the lower cut-in frequency can be continuously

adjusted by a voltage signal, thus allowing for gradual transitions from one configuration to another. Moreover, when the steady state is reached with the lowest cut-in frequency, the auxiliary system is essentially deactivated and does not contribute in any way to the actual measurements on the patient.

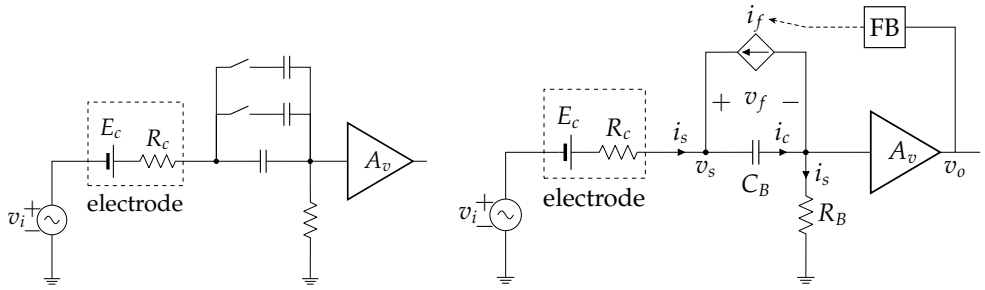

(**a**) (**b**)

Figure 1. Simple (**a**) and proposed (**b**) amplifier topology for obtaining a variable bandwidth. The current generator is controlled by the output voltage $i_f = G_m v_o$, where G_m is the transconductance gain.

It is interesting to reflect on the fact that the presence of a capacitor in series with the signal path in a voltage amplifier merely blocks the DC component across the source. We can look at the transients as the time required for the capacitor to change to a DC voltage that subtracts from the input DC component so that the high gain stages of the amplifier do not saturate. From this view, in order to reduce the transient time, we need to find a method to speed up the charging of the input capacitor at the correct value without interfering, if at all possible, in the overall response of the system during actual measurements. This approach was followed in [27] in the case of a single-ended amplifier for low-frequency noise measurements in a situation in which the maximum peak-to-peak voltage of the input signal was not expected to exceed a few tens of microvolts, and the availability of a control voltage for directly controlling the cut-in frequency was not necessary.

In this paper, we exploit the basic concept developed in [27] and show how we can obtain a voltage-controlled cut-in frequency and how this can be extended to the case of a differential amplifier with adjustable bandwidth. In order to simplify the discussion, let us start with the case of a single-ended amplifier, as in the schematic diagram in Figure 1b. We essentially add an auxiliary system to what would otherwise be a conventional AC-coupled amplifier. Such an auxiliary system reduces to the feedback block (FB) controlling the value of the current i_f charging the capacitor C_B. The entire auxiliary system can be regarded as a voltage controlled floating current source and can be easily implemented using integrated photovoltaic couplers, as in [27].

A key observation is that, if the FB sets the current i_f to a constant 0, the auxiliary circuit would have no effect on the circuit response, and we might as well remove the auxiliary system from the amplifier. In general, however, the FB operates according to the following equation:

$$i_f = G_m v_o \tag{1}$$

Since we are interested in the behavior of the system at low frequencies, we can assume the gain A_v of the amplifier is constant (i.e., independent of the frequency). Moreover, assuming, as is often the case, $R_c \ll R_B$, we can easily obtain the overall response of the system in the Laplace domain as follows (we use capital letters for quantities in the Laplace domain):

$$V_o = A_v V_i = A_v(V_s - V_f) \tag{2}$$

Since:

$$V_f = \frac{I_c}{sC_B} = \frac{I_f + I_s}{sC_B} = \frac{G_m V_o}{sC_B} + \frac{V_i}{sC_B R_B} \tag{3}$$

when combining Equation (2) with Equation (3), we have:

$$A_{vF} = \frac{V_o}{V_i} = A_v \frac{s\tau_F}{1 + s\tau_F} \qquad \tau_F = \frac{R_B C_B}{1 + G_m A_v R} \tag{4}$$

The result in Equation (4) shows that that we obtain a high pass response with a cut-in frequency f_{LF} given by:

$$f_{LF} = \frac{1}{2\pi\tau_F} = \frac{1 + G_m A_v R_B}{2\pi R_B C_B} \tag{5}$$

As we anticipated, if $G_m = 0$, the cut-in frequency corresponds to the one set by the passive AC filter R_B-C_B in the input path. Moreover, from Equation (5), it is apparent that we can change the value of the cut-in frequency by changing the gain G_m. Since we want to be able to control the value of the cut-in frequency by means of a control voltage, we modified the approach followed in [27] by adding an analog multiplier in the path from the output of the amplifier to the input of the FB block, as shown in Figure 2a. Assuming a constant control voltage v_{ctrl}, we have:

$$V_{om} = (k_v v_{ctrl}) V_o \tag{6}$$

where k_v is the multiplier scaling factor. Now A_{vF} has the same form as in Equation (4), except that we have, for τ_F and f_{LF}:

$$\tau_F = \frac{R_B C_B}{1 + G_m A_v R_B k_v v_{ctrl}} \qquad f_{LF} = \frac{1 + G_m A_v R_B k_v v_{ctrl}}{2\pi R_B C_B}, \tag{7}$$

from which it is clear that we can change the cut-in frequency by adjusting the control voltage v_{ctrl}. Note that whatever value of f_{LF} is set with the circuit discussed so far, in the pass-band (i.e., for $f \gg f_{LF}$), the input impedance of the amplifier remains unchanged and equal to R_B. As an example of the results that could be obtained in term of frequency response, Figure 2b shows the result of SPICE simulations performed with typical values of the circuit parameters that can be experienced when implementing the FB, as in [27].

2.2. Extension to a Differential Amplifier

Extending the approach we discussed above to the case of a differential amplifier requires some caution. In a single-ended amplifier, the error signal at the input of the FB is proportional to the output voltage, which is directly proportional, as in Equation (2), to the difference between the input signal and the voltage across the coupling capacitor C_B. In a differential configuration, we have two blocking capacitors, C_{B1} and C_{B2}, as in Figure 3. If we indicate with V_{S1} and V_{S2} the input voltages and with V_{f1} and V_{f2} the voltages at which C_{B1} and C_{B2} are charged, respectively, we have:

$$V_o = A_v V_d = A_v[V_{s1} - V_{f1} - (V_{s2} - V_{f2})] \tag{8}$$

We must therefore devise a strategy in order to use the output voltage for inducing a change in the voltages V_{f1} and V_{f2} across the blocking capacitors. The decision taken in

this study was to induce equal and opposite changes in the voltages V_{f1} and V_{f2} , i.e., to ensure that it is $i_{f1} = -i_{f2}$ at all times.

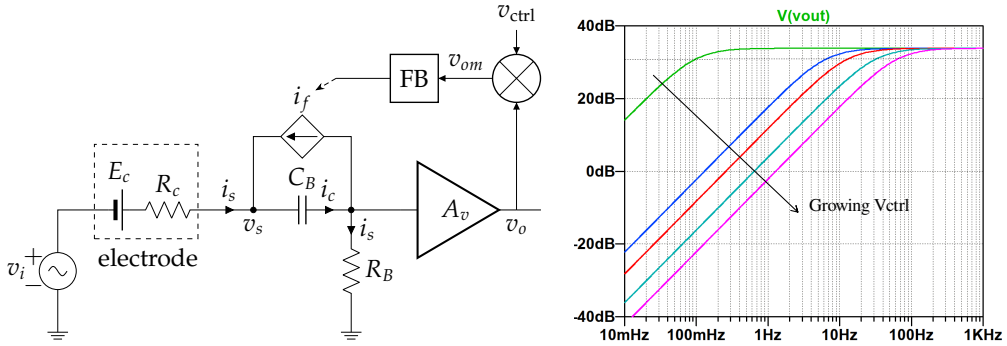

(**a**) (**b**)

Figure 2. Controlling the feedback loop (with a variable-gain amplifier or a multiplier) enables an external controlling voltage: (**a**) the basic circuit; (**b**) the results of the LT-SPICE simulation with $G_m = 80\,\mu\Omega^{-1}$, $k_v = 1\,V^{-1}$, $A_v = 50\,V/V$, $C_B = 10\,\mu F$, $R_B = 160\,k\Omega$, $E_c = 0\,V$, $R_c = 5\,k\Omega$, over several values of the controlling voltage.

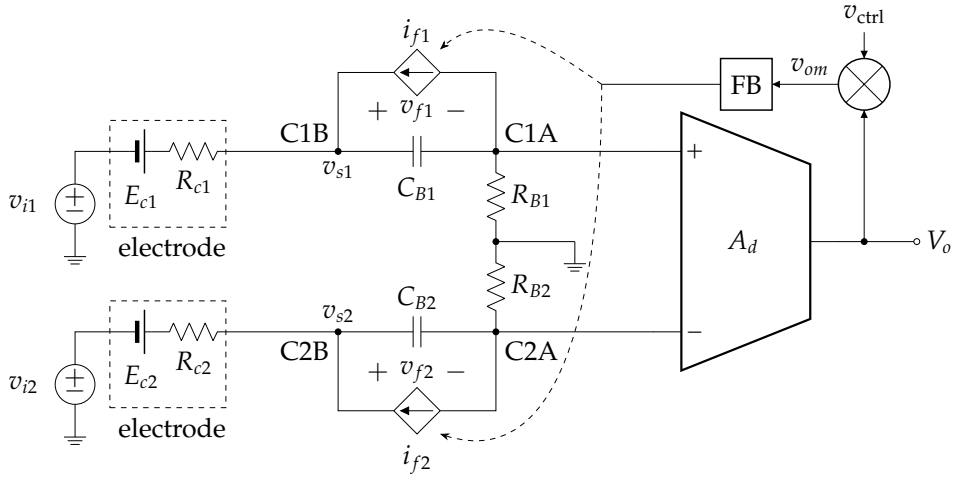

Figure 3. Simplified schematic diagram of the differential case.

With this choice, the FB block only acts on the dynamics of the differential signal: if a step occurs at the inputs, resulting in a step in the common mode voltage V_C together with a step in the differential voltage V_D, the FB will only react to the change in V_D, with the dynamics of V_C evolving as if the FB was not present.

To be more precise, if a pure common mode step is presented at the input, this will not be sensed by the FB, since the instantaneous voltages at the inverting and noninverting inputs of the instrumentation amplifier would be ideally the same during the transient. In this case, and in the absence of any other signal following the common mode input step, the inputs of the instrumentation amplifier evolve toward zero with a time constant $R_{B1}C_{B1} = R_{B2}C_{B2}$, regardless of the setting of the FB.

Up to this point, we assumed ideal behavior for the instrumentation amplifier and, in particular, we assumed no offset to be present. The presence of the offset, however, needs to be carefully discussed in view of how we plan to employ the FB.

If both the input offset voltage and the input offset current are null (i.e., if the bias currents are the same on each input), the steady state corresponding to a constant common mode voltage at the inputs of the system is $i_{f1} = i_{f2} = 0$. The input bias currents of the

instrumentation amplifier flows through the resistances R_{B1} and R_{B2} and produces a purely common mode voltage at the inputs (resulting in $V_o = 0$). In this situation, switching on and off the FB produces no transient on the system.

However, if an offset is present, when the FB loop is active, it tends to compensate for such an offset by forcing opposite currents $i_{f1} = -i_{f2}$ at steady state in order to produce a differential input, compensating the intrinsic offset of the instrumentation amplifier. In this situation, when we switch off the FB, we necessarily introduce a transient, which, since the FB is disconnected, evolves with the smallest time constant of the circuit. The amplitude of the transient and the time required for its effect to become negligible depend on the magnitude of the offset. This effect is likely to be small in most situations. However, in order to ensure that it is negligible and that we take full advantage of the proposed approach, we need to guarantee that we can act on the system in order to compensate for the offset of the instrumentation amplifier. Adding a circuit for offset compensation and making it automatic so that the final user need not worry about it would be quite simple. As we show in the next section, in order to minimize the complexity of the prototype, we opted for a manual compensation approach. However, the compensation setting does not depend on the source impedance, which means that it needs to be performed only once and checked from time to time.

3. Results

To showcase the new amplifier design, we built a fully functional prototype. We then applied it to replace the front-end amplifier of the system in [22], tackling the problem of the passive measurement of contact resistances. In this section, we first introduce the details of the implementation, providing a complete prototype schema. Then, we show that the new circuit topology can markedly reduce the time needed to perform contact resistance estimation.

3.1. Prototype

A prototype was built and tested to demonstrate the effectiveness of the proposed approach. A low-noise AD8429 amplifier was chosen for the differential measurement, and configured for a gain of 50 V/V, similar to the system in [22].

The main difference with respect to [22] is the presence of the two floating current sources i_{f1} and i_{f2} across the capacitors C_{B1} and C_{B2} in the top portion in Figure 4, which represent the action of the FB whose detailed implementation is reported in the bottom portion of the figure.

Switches from 1 to 4 were used to change the configuration of the input section of the system. Following [22], these were operated to perform a series of measurements from which the contact resistances were estimated. As noted above, the task of the FB is to speed up the recovery of the system from the transients induced by repeated changes in the configuration of the switches.

The operation of the differential amplifier in the absence of the floating current sources is discussed in [22]. A circuit was built around the operational amplifier OA3 to enable the fine adjustment of the offset of the system (when the FB was inactive), avoiding transients when the FB was deactivated following a change in the switch configuration.

The implementation of the FB was based on two integrated dual photo-voltaic MOSFET drivers (VO1263). Each VO1263 essentially contains two miniaturized solar cells, each with its own light emitter source in the form of an integrated LED. As discussed in [27], a single VO1263 can be used to obtain a current-controlled floating current source capable of delivering positive and negative currents in the order of a few microamperes with a voltage compliance in excess of 10 V. In our prototype, two VO1263 were combined to form a dual floating current source, with nominally opposite currents, controlled by the current at the output of OA2 in Figure 4.

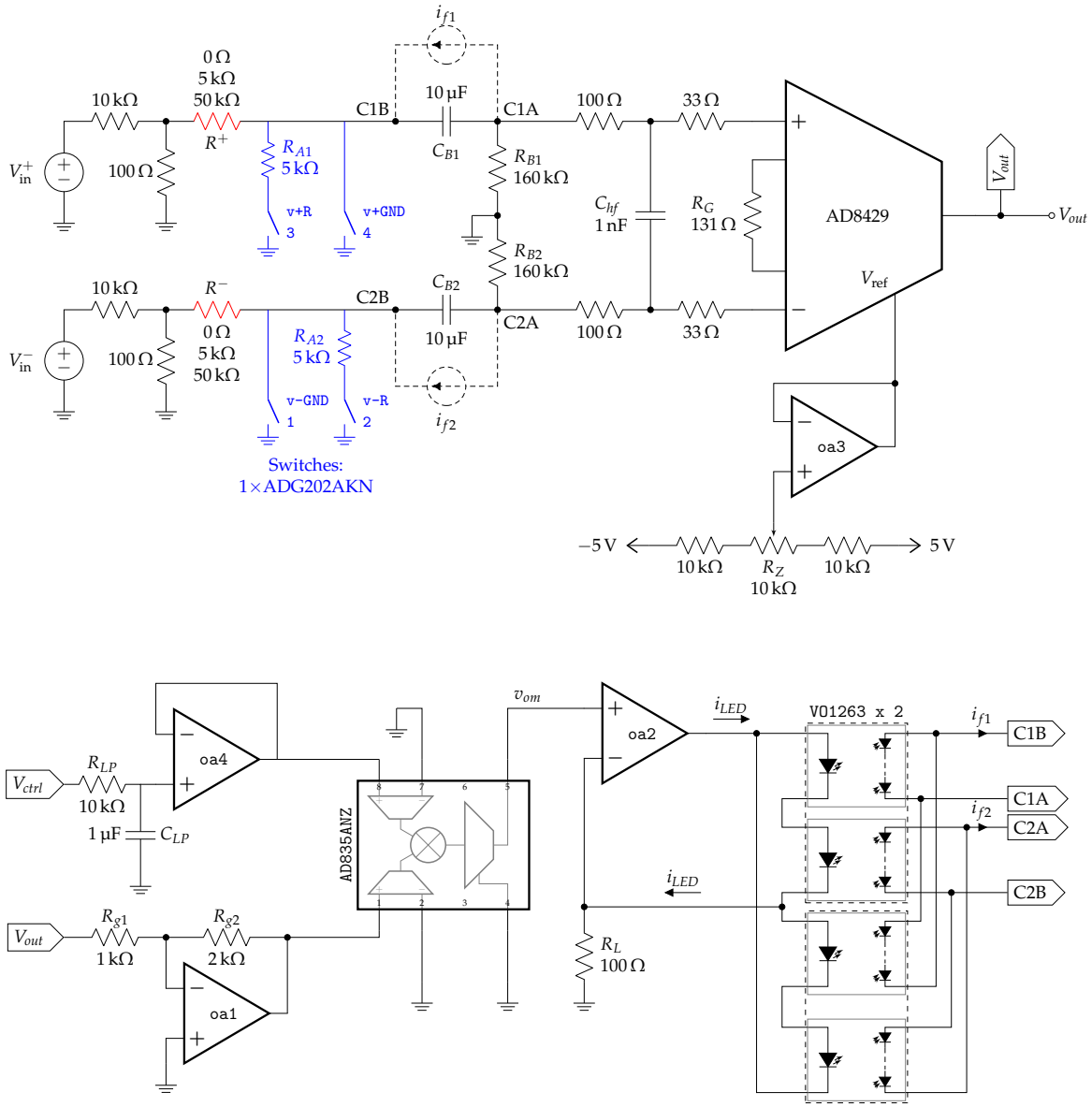

Figure 4. Full circuit used in the tests. The components without labels were added following the suggestions of the respective data sheets, so they are not substantial for the discussion of the behavior. The upper circuit is the main amplifier with the switches used to check the contact impedance, simulated by the R^+ and R^- resistors (together with the equivalent output resistance of the divisor used to reduce the input voltage range). The lower circuit is the FB, consisting of a multiplier, G_m, and current injection stage. All the components were supplied with a symmetric ±5 V source.

The transfer coefficient α from the driving current toward the output current is typically in the order of 2×10^{-3} A/A for driving currents above a few tens of microamperes, as illustrated in Figure 5. This plot also shows that the behavior is not linear for low output currents. This is not a limitation in our case since the FB is used merely to speed up the transients after the switch configuration changes.

In ideal conditions, toward the end of the transients, we should be approaching $i_{f1} = 0$ and $i_{f2} = 0$. The decrease in the slope of the input-output curve in Figure 5 for low currents means that the effectiveness of the feedback decreases as well. Consequently, we obtain a disengaging effect of the FB close to the steady state, which helps to smooth the the transition from active to inactive FB at the end of the transients.

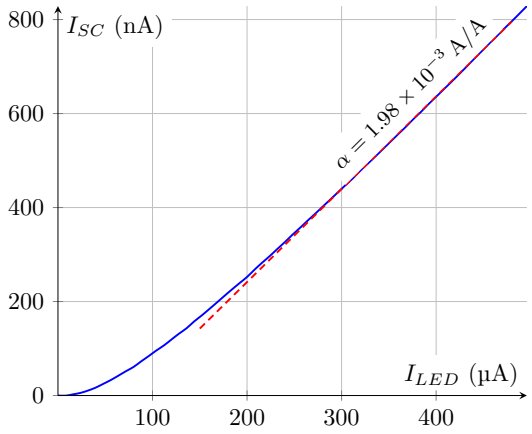

Figure 5. Input-output characterization of the optocoupler. I_{LED} is the input current and I_{SC} is the short-circuit output current.

The voltage multiplier AD835 was used to change the feedback gain from the voltage v_{out} toward the currents i_{f1} and i_{f2}, by means of the voltage v_{ctrl}. If we neglect, for the moment, the effect of the low pass filter R_{LP}-C_{LP}, the voltage v_{om} at the output of the multiplier is:

$$V_{om} = -\frac{R_{g2}}{R_{g2}} k_V v_{ctrl} V_{out} \tag{9}$$

with $k_V = 1\,\mathrm{V}^{-1}$ in the case of the AD835.

The voltage at the output of the multiplier drives a voltage-to-current converter implemented with the operational amplifier OA2, so that the current through the LEDs inside the VO1263 devices is:

$$I_{LED} = \frac{v_{om}}{R_L} \tag{10}$$

Note that when $I_{LED} > 0$, the two upper LEDs in Figure 4 are "on" and the two bottom LEDs are "off"; when $I_{LED} < 0$, the two upper LEDs are "off" and the two bottom LEDs are "on".

Finally, including the transfer coefficient α, the gains G_{m1} and G_{m2} from the output voltage to the currents i_{f1} and i_{f2} are:

$$G_{m1} = \frac{i_{f1}}{v_{out}} = -\frac{i_{f2}}{v_{out}} = G_{m2} = -\alpha \frac{R_{g2}}{R_L R_{g2}} k_V v_{ctrl} V_{out} \tag{11}$$

with the values of the parameters in Figure 4. When v_{ctrl} is at the maximum value of 1 V, the gains amount to:

$$G_{m2} = -G_{m1} \simeq 20\,\mu\mathrm{A/V} \tag{12}$$

Extending the results in Equation (7) to the case of the differential configuration, when the FB is active with $v_{ctrl} = 1\,\mathrm{V}$, we obtain a low-pass limit that is 160 times larger than the low-frequency corner corresponding to the time constant $C_B R_B$, i.e., about 16 Hz instead of 100 mHz. When v_{ctrl} is 0, the FB is inactive and the low-frequency corner is set by R_B and C_B, which is 100 mHz.

Finally, a low-pass filter R_{LP}-C_{LP}, with a time constant of 10 ms, was added to the control signal in the input of the multiplier control voltage and used to smooth the gain change in the feedback loop.

The remaining differences in the full circuit in Figure 4 with respect to that in Figure 3 were implementation details, applied following the recommendations in the component's data sheets.

A separate microcontroller board provided the v_{ctrl} output in a 0 V to 1 V range and was also used to control the switches when performing the source resistance assessment.

3.2. Measurements on the Prototype

Although the system is, strictly, nonlinear for small values of feedback loop signal (due to the aforementioned nonlinearity in the coupling devices, which makes the loop inactive for very small signals), we tested the frequency response with relatively large signals, keeping the output voltage as high as possible, around 2 V peak-to-peak. The result (measured in the range 1 Hz to 1000 Hz) is provided in Figure 6a; the behavior is basically the same as that shown in Figure 2b.

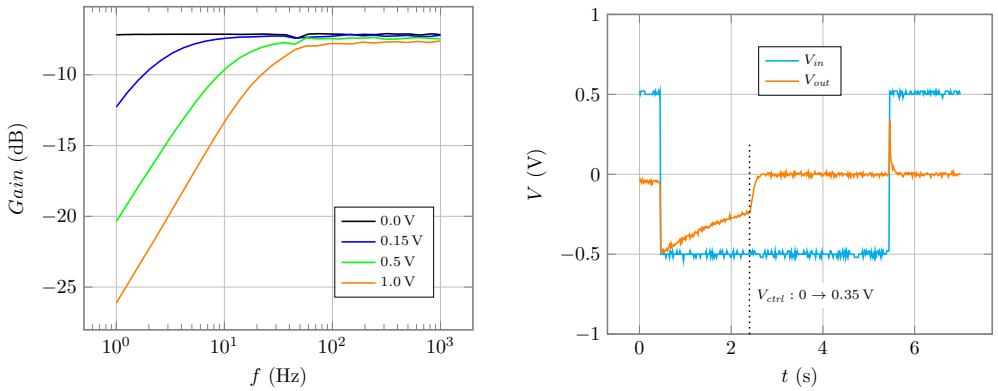

(**a**) Frequency response. (**b**) Transient response.

Figure 6. (**a**) The measured frequency response (please see the main text) for different values of v_{ctrl}; (**b**) transient response when v_{ctrl} is changed abruptly from 0 to 0.35 V at $t = 2.5$ s.

In the time domain, the behavior of the amplifier was checked by applying a pure differential square voltage to the amplifier input (cyan line in Figure 6b) with the feedback loop disabled ($v_{ctrl} = 0$); at a certain point in time, v_{ctrl} is abruptly raised to a value of 0.35 V (not shown in the diagram; the switching instant is marked with a dotted vertical line).

The exponential transient of the output (orange line) before the change shows the natural hard response of the circuit, with a time constant in the order of ten seconds. As soon as the feedback loop is enabled, the system smoothly switches to a much faster response, as can be easily deduced from the shape of the following transient. In conclusion, we can speed up the circuit when we expect large transients due to the switching of the input configuration during the resistance measurement phase, and switch back to the normal behavior for the measurement phase.

3.3. Application to Resistance Estimation

Similar to the procedure in [22], the parallel connection circuit is managed with a digitally-controlled switch and a microcontroller that activates and deactivates the corresponding connections within the four configurations necessary to complete the impedance measurement. To summarize the procedure, the RMS of the signal is first estimated over a selectable period T_S, and then measured again over the same T_s for each switch configuration reported in Figure 7b. From this information, we can calculate the approximate values or the contact resistance. The mathematical details can be found in [22].

In the original system, the switching phase lasted at least 30 s due to the time needed to wait for the end of the transient. One example sequence of measurement, for the four different switch configurations, is shown in Figure 7a.

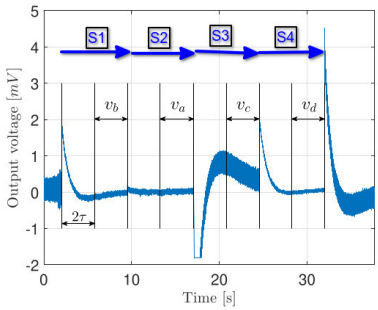

(**a**) Time response during the resistance measurement.

State	switches			
	v-gnd	v+gnd	v-R	v+R
S1	ON	OFF	OFF	OFF
S2	ON	OFF	OFF	ON
S3	OFF	ON	OFF	OFF
S4	OFF	ON	ON	OFF

(**b**) Switch position for each phase (ON, closed; OFF, open).

Figure 7. Example of the output of the amplifier during the resistance measurement in the system described in [22]. S1 to S4 are the four configurations of the input switches for each stage; normal operation is with all switches off. The table in (**b**) specifies the switch position for each stage.

Since this kind of system is intended for input voltages in the range of microvolts or millivolts, the waveform generator that emulated the input signal in our tests was followed by a resistor attenuator. The differential signal was obtained by a linear circuit with adders and a difference amplifier circuit (not shown) so that we generated two signals with known common and differential mode components. The differential input signal used as a test signal was a sinusoidal waveform with a frequency of 100 Hz and an amplitude around 20 mV peak-to-peak. The common mode was a similar sinusoidal signal, at the same frequency, with a 20 mV amplitude as well.

During the switching phases, the v_{ctrl} signal was set high, and then re-set to zero after the output amplitude and RMS were measured.

To test the system, we set R^+ and R^- to known values: in this case 100 Ω, 5 kΩ, and 50 kΩ, which correspond to a good, middling, and poor contact, respectively. The resistance values obtained with the procedure outlined above were then compared with the known value of contact resistance.

Figure 8 contains the output voltage (v_{out} in Figure 4) of one of the impedance measurements corresponding to the impedance values $R_+ = 5\,\text{k}\Omega$ and $R_- = 51\,\text{k}\Omega$. The transients are much more subdued than those in [22], and the measurement can be carried out in a shorter time.

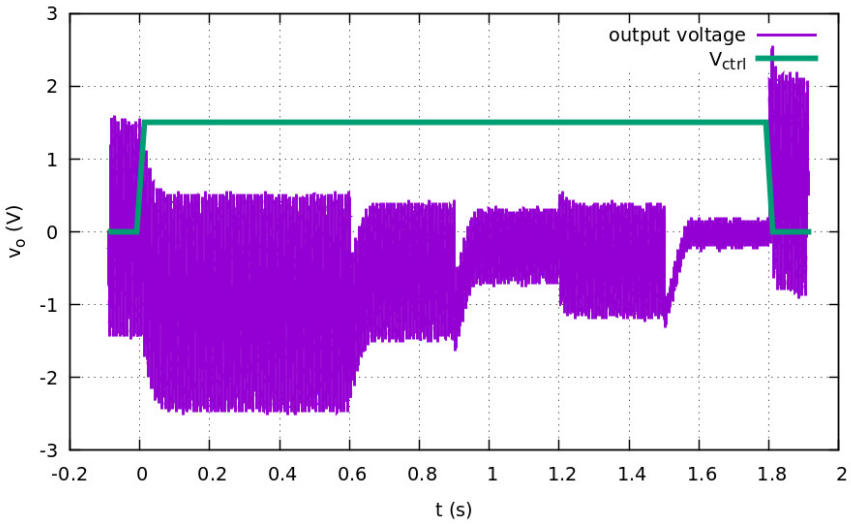

Figure 8. Example of the output voltage from the prototype for $R_+ = 5\,\text{k}\Omega$ and $R_- = 51\,\text{k}\Omega$, switching every 400 ms. The base signal is a 100 Hz sinusoidal one; it is evident that the transients are fast when the control voltage is high.

Finally, Figure 9 shows the result of the passive resistance measurement performed across all possible combinations of the three chosen values of contact resistance, comparing the results obtained with the approach in [22] (RC filter) with the methodology proposed in this paper (active filter) considering the enhanced, shorter measurement time. The active filter enables a better global resistance assessment and avoids false positives (detecting poor contact resistance as good or middling) which is the main objective of the system.

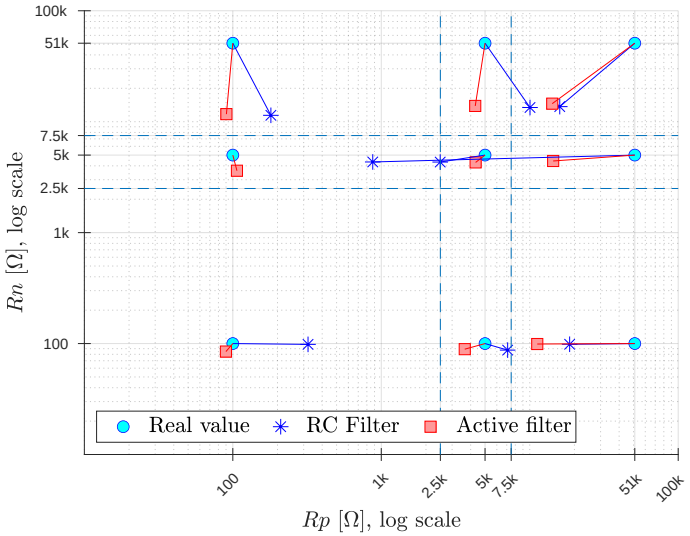

Figure 9. Resistance assessment result, with a switching period of 1 s. The cyan dots are the real values of the contact resistance, the red squares are those estimated using the active filter, and the blue stars are the values estimated with the RC filter.

4. Discussion

As previously stated, one of the main drawbacks of the original impedance measurement methodology proposed in [22] is the time needed for the completion of the contact resistance estimation process, due principally to the transient responses triggered by the steep changes in the input voltage. In the case of the original RC filter circuit, and considering a balance between accuracy and latency, a safety period proportional to the time constant of the high pass filter is required before starting the RMS calculation (chosen as representative statistical measurement) in order to avoid the transient effect. A typical measurement with that system is shown in Figure 7a; the time spent performing the contact resistance measurement is in the order of a minute (around 30 s in the case of the measurement shown).

The time constant with the active filter is much shorter, which means that the safety period can also be shortened in the same order of magnitude. The new system settles much faster than the older system, as can be seen by comparing Figures 7a and 8.

The results of the resistance detection, as shown in Figure 9, are slightly worse in absolute value than those obtained in [22]. However, the time spent in the resistance measurement is at least one order of magnitude less than that needed without the active filter topology. In the end, the only relevant information for the monitoring devices is if the contact is good enough. In Figure 9, note that no contact resistance configuration lying outside the quadrant where both contact resistances are low (the lower left one) is mis-detected as good. The absence of such a case shows that there are no false positives in the detection, which confirms the suitability of the approach.

In addition to the application shown here, a similar topology can be applied to all the cases where a differential amplifier needs to be designed with a high-pass filter with very low cut-in frequency, while a fast settling time is advantageous during the phases of connection and re-connection of the system to the signal sources.

5. Conclusions

In this paper, a new topology was proposed to design AC-coupled differential amplifiers with a cut-in frequency that can be continuously changed through a control voltage. This feature allows us to speed up the recovery from transients by setting very short time constants (when large transients occur at the input) while maintaining the ability, by setting a much larger time constant during actual measurements, to obtain a flat response down to very low frequencies. A prototype of an amplifier employing the proposed topology was built, tested, and used to speed up a recently proposed measurement procedure to determine the contact resistance due to electrodes in bio-signal measurement experiments. This procedure, based on measurements performed after provoking controlled changes in the input network configuration, while effective, was limited by the presence of long transients after each change occurs. With the prototype we built, comprising an adjustable AC input filter with a time constant ranging from 8 ms up to 1.6 s, it was possible to reduce the overall measurement time for the determination of the parasitic resistances from about 30 s to about 5 s. The new circuit shows no degradation in sensitivity and in the lowest frequency that can be explored during signal acquisition.

Author Contributions: Conceptualization, R.G., C.C. and G.S.; methodology, E.A.R., C.R.-M.G.; software, E.A.R., C.R.-M.G. and R.G.; validation, R.G. and E.A.R.; formal analysis, C.C. and G.S.; investigation, E.A.R., G.S., C.C., C.R.-M.G. and R.G.; resources, C.R.-M.G.; writing—original draft preparation, E.A.R., C.C., G.S. and R.G.; writing—review and editing, G.S., C.C., C.R.-M.G. and R.G.; visualization, R.G.; project administration, C.R.-M.G. All authors have read and agreed to the published version of the manuscript.

Funding: This research received no external funding.

Data Availability Statement: Measurement and simulation data are fully available upon request.

Acknowledgments: The authors would like to acknowledge the support from the technical personnel at the Universidad Pontificia Comillas laboratories, namely José María Bautista and Antonio Martínez. They would like to acknowledge the collaboration with Analog Devices, for providing a ADALM-2000 system that was partially used for the building of the prototype. Finally, they would like to thank Christopher Michael Turner for the English language help and review.

Conflicts of Interest: The authors declare no conflict of interest.

Abbreviations

The following abbreviations are used in this manuscript:

LNA	Low-noise amplifier
RMS	Root mean square
HP, HPF	High pass (filter)
RC filter	Resistance-capacitor filter
FB	Feedback block
DC	Direct current (used for continuous signals)
AC	Alternating current (used for variable signals)

References

1. Webster, J.G. *Medical Instrumentation Application and Design*, 4th ed.; Wiley: Hoboken, NJ, USA, 2009.
2. Simmich, S.; Bahr, A.; Rieger, R. Noise Efficient Integrated Amplifier Designs for Biomedical Applications. *Electronics* **2021**, *10*, 1522. [CrossRef]
3. Kim, J.; Ko, H. A Dynamic Instrumentation Amplifier for Low-Power and Low-Noise Biopotential Acquisition. *Sensors* **2016**, *16*, 354. [CrossRef]
4. Chebli, R.; Ali, M.; Sawan, M. High-CMRR Low-Noise Fully Integrated Front-End for EEG Acquisition Systems. *Electronics* **2019**, *8*, 1157. [CrossRef]
5. Ruiz-Amaya, J.; Rodriguez-Perez, A.; Delgado-Restituto, M. A Low Noise Amplifier for Neural Spike Recording Interfaces. *Sensors* **2015**, *15*, 25313–25335. [CrossRef] [PubMed]

6. Bansal, M.; Srivastava, G. Design and Implementation of LNA for Biomedical Applications. In *Intelligent Computing, Information and Control Systems*; Pandian, A.P., Ntalianis, K., Palanisamy, R., Eds.; Springer International Publishing: Cham, Switzerland, 2020; pp. 154–167.
7. Ruiz-Amaya, J.; Rodríguez-Pérez, A.; Delgado-Restituto, M. A review of low-noise amplifiers for neural applications. In Proceedings of the 2010 2nd Circuits and Systems for Medical and Environmental Applications Workshop (CASME), Merida, Mexico, 13–15 December 2010; pp. 1–4. [CrossRef]
8. Portelli, A.J.; Nasuto, S.J. Design and Development of Non-Contact Bio-Potential Electrodes for Pervasive Health Monitoring Applications. *Biosensors* **2017**, *7*, 2. [CrossRef] [PubMed]
9. Alimisis, V.; Dimas, C.; Pappas, G.; Sotiriadis, P.P. Analog Realization of Fractional-Order Skin-Electrode Model for Tetrapolar Bio-Impedance Measurements. *Technologies* **2020**, *8*, 61. [CrossRef]
10. Chi, Y.M.; Jung, T.p.; Cauwenberghs, G. Dry-Contact and Noncontact Biopotential Electrodes. *IEEE Rev. Biomed. Eng.* **2010**, *3*, 106–119. [CrossRef] [PubMed]
11. Kappenman, E.S.; Luck, S.J. The effects of electrode impedance on data quality and statistical significance in ERP recordings. *Psychophysiology* **2010**, *47*, 888–904. [CrossRef] [PubMed]
12. Buxi, D.; Kim, S.; Van Helleputte, N.; Altini, M.; Wijsman, J.; Yazicioglu, R.F.; Penders, J.; Van Hoof, C. Correlation between electrode-tissue impedance and motion artifact in biopotential recordings. *IEEE Sens. J.* **2012**, *12*, 3373–3383. [CrossRef]
13. Taji, B.; Shirmohammadi, S.; Groza, V.; Batkin, I. Impact of skin-electrode interface on electrocardiogram measurements using conductive textile electrodes. *IEEE Trans. Instrum. Meas.* **2014**, *63*, 1412–1422. [CrossRef]
14. Musteata, M.; Borcea, D.G.; Ștefănescu, R.; Solcan, G.; Lăcătuș, R. Influence of Stainless Needle Electrodes and Silver Disk Electrodes over the Interhemispheric Cerebral Coherence Value in Vigil Dogs. *Sensors* **2018**, *18*, 3990. [CrossRef]
15. Fu, Y.; Zhao, J.; Dong, Y.; Wang, X. Dry Electrodes for Human Bioelectrical Signal Monitoring. *Sensors* **2020**, *20*, 3651. [CrossRef]
16. Acar, G.; Ozturk, O.; Golparvar, A.J.; Elboshra, T.A.; Böhringer, K.; Yapici, M.K. Wearable and Flexible Textile Electrodes for Biopotential Signal Monitoring: A review. *Electronics* **2019**, *8*, 479. [CrossRef]
17. Sundarasaradula, Y.; Thanachayanont, A. A Low-Noise, Low-Power, Wide Dynamic Range Logarithmic Amplifier for Biomedical Applications. *J. Circuits Syst. Comput.* **2018**, *27*, 1850104. [CrossRef]
18. Zhao, W.; Li, H.; Zhang, Y. A low-noise integrated bioamplifier with active DC offset suppression. In Proceedings of the 2009 IEEE Biomedical Circuits and Systems Conference, Beijing, China, 26–28 November 2009; pp. 5–8. [CrossRef]
19. Sanchez, B.; Schoukens, J.; Bragos, R. Novel Estimation of the Electrical Bioimpedance Using the Local Polynomial Method. Application to In Vivo Real-Time Myocardium Tissue Impedance Characterization During the Cardiac Cycle. *IEEE Trans. Biomed. Eng.* **2011**, *58*, 3376–3385. [CrossRef] [PubMed]
20. Guermandi, M.; Cardu, R.; Scarselli, E.F.; Guerrieri, R. Active Electrode IC for EEG and Electrical Impedance Tomography with Continuous Monitoring of Contact Impedance. *IEEE Trans. Biomed. Circuits Syst.* **2015**, *9*, 21–33. [CrossRef] [PubMed]
21. Dardé, J.; Hyvönen, N.; Kuutela, T.; Valkonen, T. Electrodeless electrode model for electrical impedance tomography. *arXiv* **2021**, arXiv:2102.01926.
22. Alonso, E.; Giannetti, R.; Rodríguez-Morcillo, C.; Matanza, J.; Muñoz-Frías, J.D. A Novel Passive Method for the Assessment of Skin-Electrode Contact Impedance in Intraoperative Neurophysiological Monitoring Systems. *Sci. Rep.* **2020**, *10*, 1–11. [CrossRef] [PubMed]
23. Jimenez-Carles Gil-Delgado, E. Intraoperative Monitoring System. Patent Application WO 2018/011439 Al, 18 January 2018.
24. Ferree, T.C.; Luu, P.; Russell, G.S.; Tucker, D.M. Scalp electrode impedance , infection risk, and EEG data quality. *Clin. Neurophysiol.* **2001**, *112*, 536–544. [CrossRef]
25. Tautan, A.M.; Mihajlovic, V.; Chen, Y.H.; Grundlehner, B.; Penders, J.; Serdijn, W. Signal Quality in Dry Electrode EEG and the Relation to Skin-electrode Contact Impedance Magnitude. In Proceedings of the International Conference on Biomedical Electronics and Devices (BIOSTEC 2014),Loire Valley, France, 3–6 March 2014; pp. 12–22. [CrossRef]
26. Teplan, M. Fundamentals of EEG Measurement. *Meas. Sci. Rev.* **2002**, *2*, 1–11.
27. Scandurra, G.; Cannatà, G.; Giusi, G.; Ciofi, C. A new approach to DC removal in high gain, low noise voltage amplifiers. In Proceedings of the 2017 International Conference on Noise and Fluctuations (ICNF), Vilnius, Lithuania, 20–23 June 2017; pp. 1–4. [CrossRef]

2.3 A Quasi-Wireless Intraoperatory Neurophysiological Monitoring System

electronics

MDPI

Article

A Quasi-Wireless Intraoperatory Neurophysiological Monitoring System

Eduardo Alonso Rivas [1,†,‡], Romano Giannetti [1,‡], Carlos Rodríguez-Morcillo García [1,‡], Javier Matanza Domingo [1,‡], José Daniel Muñoz Frías [1,‡], Graziella Scandurra [2,*,‡], Carmine Ciofi [2,‡], Lorena Vega-Zelaya [3,‡] and Jesús Pastor [3,‡]

[1] Instituto de Investigación Tecnológica, Universidad Pontificia Comillas, 28015 Madrid, Spain
[2] Dipartimento di Ingegneria, Università degli Studi di Messina, 98166 Messina, Italy
[3] Clinical Neurophysiology and Instituto de Investigación Biomédica, Hospital Universitario La Princesa, 28006 Madrid, Spain
* Correspondence: gscandurra@unime.it
† Current address: Soinde s.l., Calle Burdeos 12B, Las Rozas de Madrid, 28232 Madrid, Spain.
‡ These authors contributed equally to this work.

Abstract: Intraoperative Neurophysiological Monitoring is a set of monitoring techniques that reads electrical activity generated by the nervous system structures during surgeries. In non-trivial surgeries, neurophysiologists require a significant number of electrical signals to be picked up to check the effects of the surgeon's actions in real time or to confirm that the correct nerves are selected. As a result, cabling the patient in the operating room can become cumbersome. The proposed WIONM module solves part of the problem by converting a good part of those cables into a wireless connection that is substantially transparent to the human operator and the existing medical instrumentation.

Keywords: intraoperative monitoring; ECG; EMG; EEG; MEP; SSEP; AEP; wireless

Citation: Alonso Rivas, E.; Giannetti, R.; Rodríguez-Morcillo García, C.; Matanza Domingo, J.; Muñoz Frías, J.D.; Scandurra, G.; Ciofi, C.; Vega-Zelaya, L.; Pastor, J. A Quasi-Wireless Intraoperatory Neurophysiological Monitoring System. *Electronics* **2022**, *11*, 3918. https://doi.org/10.3390/electronics11233918

Academic Editor: Enzo Pasquale Scilingo

Received: 28 October 2022
Accepted: 24 November 2022
Published: 27 November 2022

1. Introduction

Intraoperative Neurophysiological Monitoring (IONM) [1] is a set of techniques that provide increased functional knowledge of the nervous system structures during a surgical operation. This denomination includes both stimulus-based techniques, such as evoked potentials (EP), that measure the response to a previous stimulation, as well as free running techniques, in which signals are acquired continuously without any stimulus, such as Electroencephalography (EEG), Electromyography (EMG) and Electrocorticography (ECoG).

These tools are routinely used by the surgeon and the assisting neurophysiologist to identify and prevent possible injuries during the medical procedure [2]. Several tens of signals are often needed for the average process; the burden of cabling and connections around the operating table is a common cause of uneasiness for the medical and technical staff. Figure 1 shows an example of this situation. The picture was taken during the preparation of a surgery. All the cabling remains below the sterile drapes with the connection adapters below or hanging from the operating table, making it uneasy not only the preparation, but the access to the cables during the surgery in case it is needed. Eliminating or at least reducing the cabling complexity is seen as a big step towards a more efficient clinical practice during intraoperative monitoring. Reducing this cabling using a wireless system is the main objective of the work presented here.

The characteristics of the signals to be measured are also wildly different, running from relatively low-band and high-level ones (like ECG) to very low-level and relatively high-band ones, like EMG or EP. The analog front-ends must be configurable to pick and amplify all those kind of signals. The back-end systems used for the IONM are quite complex, too, running complex software which is often highly expensive and proprietary;

the medical staff is familiar with these systems and substituting them on a short or medium time scale is not really feasible for most medical centers.

Figure 1. Example of cabling during a surgery preparation with IONM. Note the bundle of coloured cables (electrodes) and the number of adapters of the monitoring system.

The designed system presented here is capable of substituting most of the cabling with a wireless system in an almost completely transparen way; the existing electrodes, electrode connectors, and integrated instrumentation can be used without major changes in the medical procedure (the only exception is the contact impedance evaluation procedure, as will be explained later). This focus makes the system quite different from other wireless physiological monitoring systems oriented to brain-computer interfaces ([3,4]), long term monitoring ([5–7]), or completely independent systems ([8,9]).

In brief, the system described here is intended to sense and register analog biological neurophysiological signals coming from neural activity, transmit and reproduce them with the same analog characteristics. Input of the system will be the sensing electrodes connected to the patient, whereas the output will be connected to a conventional IOM system. Additionally, the system must adapt automatically and transparently to the amplitude range of the signal sensed on each channel.

Moreover, the system presents a minimal user interface with two purposes: on the one hand, a set of switches is utilized to configure each channel in referential (single-ended) or differential mode, as well as change the input reference between ground or any other channel. An additional switch permits selecting between normal acquisition mode or impedance measurement mode, needed to insure that excessive contact impedance does not compromise the signal quality [10–12]. Incorrect value of contact resistance and configuration status of the analog front-end is indicated visually by means of an array of multicolor LEDs.

In broad terms, as depicted in Figure 2, the system can be divided in Transmitter, communication link (also referred to as RF link) and Receiver. Each of these system components will be discussed in the following sections.

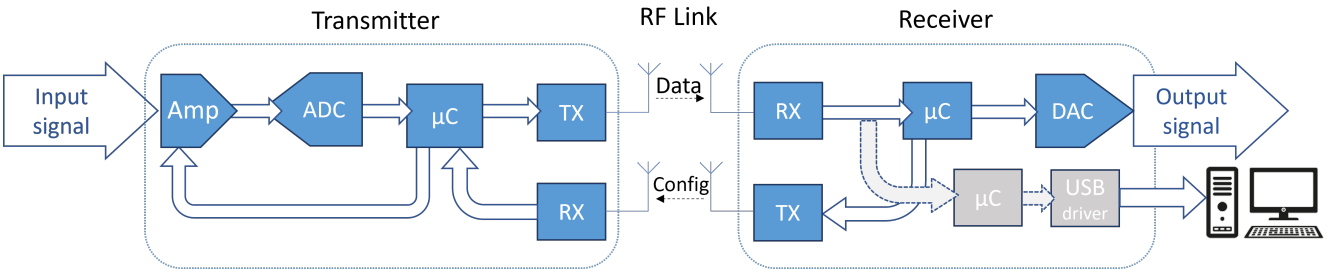

Figure 2. Schematic of the system. The input signal is delivered through standard surface or needle electrodes; the output system is normally the existing IONM setup of the medical facility.

In Section 2 the theoretical framework for the system is summarized. In Section 3, the hardware of the system is described, with subsection dedicated to explain the design of the transmitter, receiver and the debugging/tracking system used during verification. Next, in Section 4, the experimental results are reported, both from laboratory tests with reconstructed signals and in the field with human volunteers; finally, in Section 5, we discuss the measurements obtained and the effectiveness of the system.

2. Theoretical Framework

The fundamental idea of the system is to sample the input signals, transmit them in digital form, and then re-build the original signal at the end point, as shown in Figure 3. The measured signal is band-limited by the antialiasing filter, which removes all the signal components above band B (which in the presented system has been chosen to be 5 kHz). After the digitalization by the analog-to-digital converter (ADC), the signal is transmitted to the receiver. In the receiver device, it is transformed again into an analog signal by a digital-to-analog converter (DAC) and an anti-imaging filter. It is well know that when using the correct sample rate, antialiasing filter, and anti-imaging (reconstruction) filter, in absence of noise, and with a perfect analog to digital conversion, the output signal is guaranteed by the Shannon theorem [13] to be the same in band B.

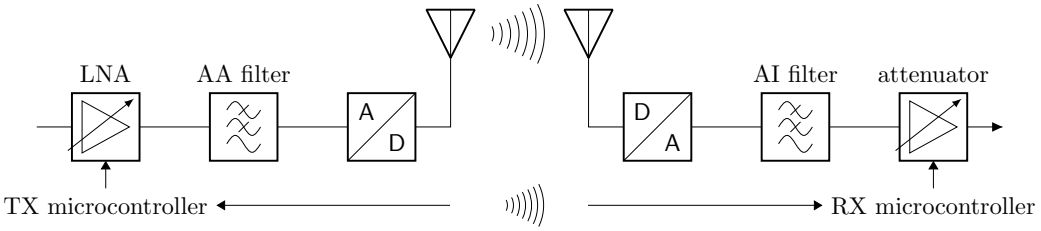

Figure 3. Theoretical operation of the system. The Low Noise Amplifier (LNA) and the programmable attenuator are coordinated by the two microcontrollers (in the transmitter and in the receiver) that cooperate to reconstruct the measured signal. The blocks in the figure represent, from left to right, the LNA, the anti-aliasing filter, the analog-to-digital converter, the digital-to-analog converter, the anti-imaging filter, and the programmable attenuator.

In the presence of noise, and due to the limited resolution of the ADC and DAC converters, there is a limit to the accuracy with which the input signal can be reproduced at the output; for this reason it is paramount to add the variable amplification and attenuation circuits, so that the full range of the ADC system is used all the time. In the proposed system, the adjustment of the two stages is made on-the-fly and in a transparent way, without the need for any intervention by the operator.

With the aforementioned conditions, the link is practically invisible to the instrumentation connected at its output, which acts as if the signal is arriving directly from the electrodes. The only exception is when there is the need to check the electrodes' connection impedance; this is resolved by performing that task in the transmitter and informing the operator of the results, as will be explained later.

3. WIONM Prototype

The prototype, called WIONM (Wireless IONM) from now on, is composed by a Transmitter, which is a compact module of about 15 cm × 10 cm × 2 cm (Figure 4, right), battery-powered, thought to be positioned near the site where the signals are connected—for example, fastened to the operating table head; and a line-powered Receiver (left), whose size is less important, located near the analyzing instrumentation. The receiver has no wires connected to the patient, so its positioning is easy and it can be located outside of the operation table.

Figure 4. Photo of the complete prototype; **left** side, the receiver, which will rebuild the original signals; **right** side, the transmitter, to which the electrodes will be connected.

3.1. Transmitter

Biological signals are sensed with the help of electrodes (surface or needle-ended) that are connected to the acquisition system through standard medical-safe DIN connectors (touch-proof). The prototype here described uses said connectors, followed by a differential amplifier with its corresponding filtering and conditioning circuitry. Due to the nature of the biological signals of interest, that range from µV to mV, and with wildly different bandwidth requirements [14], this is the most delicate and important part of the system. Accordingly, very high amplification and noise rejection is required. An in-house design based around very low noise instrumentation amplifiers (AD8429 [15]), digitally-controlled variable-gain amplifiers, passive contact impedance assessment, and aggressive anti-aliasing and high-pass filtering has been adopted [16–19], with a bandwidth ranging from 0.1 Hz to 5 kHz. In parallel to the acquisition hardware, as part of any of the commercial systems of this kind, an impedance measurement system is present in the analog part of the designed hardware. A detailed description of this section can be found in [16]. Although it is out of the scope of this paper, the noise of the analog front-end of the Transmitter was analyzed. Figure 5 shows the minimum noise obtained for the minimum possible input impedance.

Scalp measurements, useful for EEG and evoked potentials such as somato-sensory (SSEP) and auditory (AEP), as well as for brain-computer interfaces [20], are commonly registered referentially. This means that the input channels are acquired in single-ended fashion, and all the channels registered are referenced to the same electrode (whose positioning depend on the specific measurement required). On the other hand, muscle responses (EMG or motor evoked potentials (MEP)) are registered in differential mode, with a pair of electrodes per channel, plus a reference ground. Although the system is designed mainly

for differential inputs, a set of switches in the input are arranged in order to modify the input reference. This permits varying between single-ended and fully differential acquisition, providing high flexibility for any kind of signals. We opted for a modular system with a base unit hosting 8 differential channels in order to match industry standard.

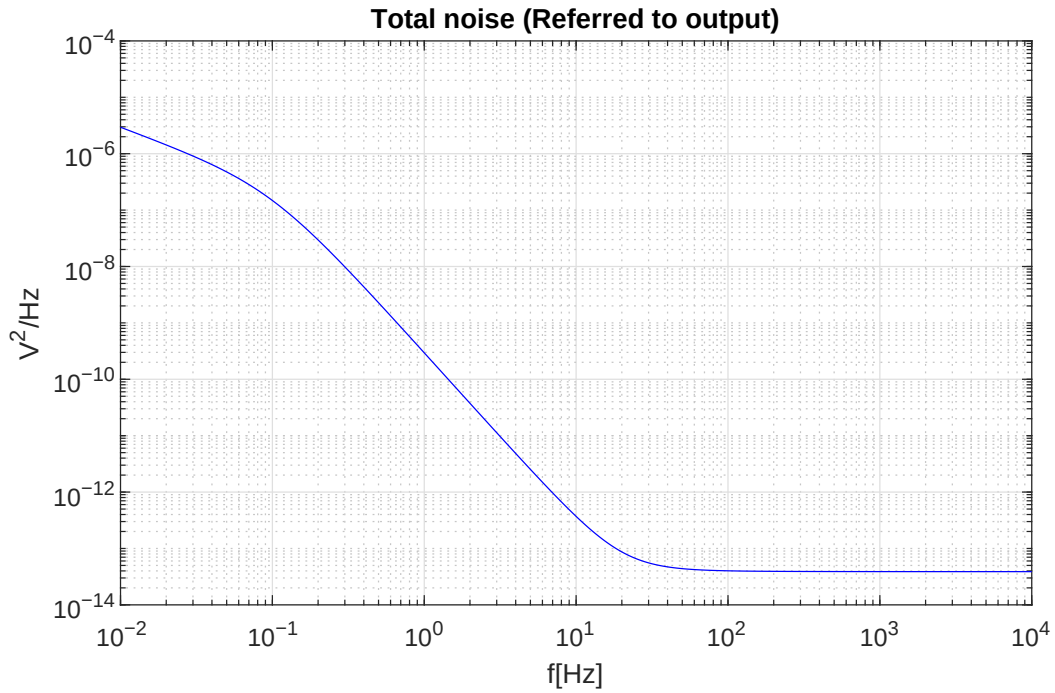

Figure 5. Minimum noise obtained for the analog front-end of the Transmitter device, measured at the output of the amplifier, with gain set to 50 V/V. The flat noise level corresponds to the expected input-referred noise for the AD8429, which is stated at around $3\,\mathrm{nV}/\sqrt{\mathrm{Hz}}$ [15].

Since signals of different amplitude ranges are to be utilized, it is important to have a set of variable gain amplifiers available. Commonly, the amplification gain is set by software by means of the user interface of the IOM system, but in this case the system modifies it automatically, through an amplitude evaluation algorithm that detects the voltage span of the signal. The dynamic range of the analog input design spans from $\pm 180\,\mu\mathrm{V}$ to $\pm 36\,\mathrm{mV}$, depending on the variable gain selected for each channel. The analog signal is then sampled and digitized by means of a dedicated multichannel Analog to Digital Converter (ADC). Digital information is passed through a microcontroller that is in charge of managing the rest of the components via SPI protocol. Timing and synchronization are of paramount importance in order to comply with specific sampling frequency. The maximum delay between the sampling and processing of the analog signal is 112 µs. Nevertheless, the total delay between the acquisition of the signal and the reconstruction is mainly affected by the communication process between Transmitter and Receiver, as it will be shown below. There are four processes managed by the microcontroller: sampling, modifying programmable amplification, handling data packaging and transmission as well as attending the interrupt request from incoming communications.

Moreover, the transmission device relies on a rechargeable battery pack that provides for an uninterrupted operation lasting 8 h. Battery level is also monitored by the controller and an acoustic signal is sent out with an integrated beeper when it reaches a low-level threshold. This battery provides high flexibility for the system, increasing ergonomics and allowing for shorter electrode wires, which is one of the main objectives of the design we propose.

The design and development of this device has been carried out taking into account medical regulation and ISO 60601 requirements. For this reason, the applied part (the part that is in contact with human tissue) is physically isolated from powering part via

multichannel digital insulators located downstream the ADC conversion, and the front-end amplifier stage is insulated up to 5 kV from external voltages.

3.2. Receiver

As stated before, this system is intended to create a wireless bridge between the signal sensed from the patient and a conventional monitoring system (Figure 2). The receiver device is in charge of reproducing such signal. This part is composed of a transmitter/receiver module, a microcontroller, an 8-channels parallel Digital to Analog Converter (DAC) with suitable anti-imaging filtering and an analog variable gain stage that adjusts the signal voltage range. The output of the system is available via touchproof standard connectors. The receiver also hosts the user interface consisting in a series of switches to configure the analog front end, and a set of LEDs that provide visual information regarding the state of the system (for example, the result of the impedance measurement process).

In normal operation mode, the Receiver device is in a passive state, waiting for the reception of data frames from the Transmitter. When a transmission frame is received by the corresponding transceiver, an interrupt request is generated and the microcontroller starts the extraction of the information received. This frame is then parsed and decoded and the data, channel per channel, is sent to the multichannel DAC modules, where analog signals are regenerated. Depending on the voltage range of the signal received, an analog gain selector modifies its amplitude.

The usual data flow goes from Transmitter to Receiver. This normal operation mode is abandoned when a configuration change is requested by the user via the user interface of the device. If one of the switches is activated, the Receiver device interrupts the reception of the frames and swaps to transmission state. Then, a configuration frame is sent from the receiver to the transmitter instructing the latter that a configuration change or an impedance measurement is requested. These changes are managed by a state machine programmed in the Receiver microcontroller so that data can be correctly interpreted. If a change in the input configuration is requested, the receiver will wait for a confirmation frame from the transmitter and if it is correct, a LED signal will indicate that the specific channel is configured in the requested mode. On the other hand, if an impedance measurement is started, a calculation period begins and all data is collected and analyzed and the result of the measurement is shown with a color coded LED visual flag, along with an acoustic signal indicating the end of the measurement. Further details on these methodology can be found in [16].

3.3. USB Tracker

Besides intermediate digital and analog signals debugging, the development process of the prototype required the implementation of a mechanism to assess the correctness of the information sent and received as part of the configuration protocol. To this end, and as shown in Figure 2, an additional microcontroller is added to the Receiver device in order to gather the messages exchanged between the master microcontroller and the receiving transceiver. This microcontroller essentially acts as a "sniffer".

The information read is buffered, encapsulated and, taking advantage of the USB controllers and libraries available for the microcontroller, sent out to a PC via USB port. Micro-USB port and conditioning circuitry is arranged in the PCB of the prototype, permitting both programming of the micro-controllers and extracting the information. A common PC is utilized to get the data, acting as USB master.

With the help of open source software `USBPcap`, raw data from selected USB port is captured in a *.pcap* file. Matlab software is utilized to parse and check the information at bit level, verifying data integrity and consistency with data sent. Additionally, visual representation of the signals is carried out. It is worth mentioning that the system does not require the integration of an internal physical memory, since the sampling, processing, transmission, reception and reconstruction of the information is made in real time. Note that, if the the specifications on data format for the standard visualization system

were available, there would be no need to convert the received digital data into analog form. The sniffer could be used, in this case, to send digital acquired data directly to the visualization software.

3.4. Transmission Wireless Link

The main goal of the work we have done was to obtain a wireless system that enables the transmission of neurophysilogical signals without the utilization of cables. To do so, several technologies were considered ([5,21,22]). Power consumption, simplicity, and especially latency (delay between recording and reconstruction of the signal) were the factors taken into account. Intra-operative monitoring involves analysing evoked potential responses with stimulus-response times in the order of milliseconds. Hence, communication protocols requiring data compression or buffering were discarded. Therefore, it was required the utilization of a technology with a bandwidth large enough to support the transmission of the registered data at the specific sampling frequency rate.

All these aspects led to the implementation of an ad-hoc radio-frequency communication link. A Nordic Semiconductor `nRF24L01` transceiver chip and the corresponding conditioning circuit is utilized. This component permits the operation on the industrial, scientific and medical (ISM) band with a bandwidth of 2.4 GHz to 2.5 GHz. This component is SPI-controlled, as are all the other complex devices in the system. The peculiarity of the application oriented the choice toward a custom protocol instead of adopting a standard one (such as, for example, Bluetooth or WiFi).

Although, as discussed above, the usual data flow goes from Transmitter to Receiver, configuration commands need to be transmitted in the opposite direction. Since the Transmitter is intended to be close to the patient and the access to it will be limited due to ergonomic reasons during surgical procedures, the configuration control panel is located in the Receiver, which is out of the operating table and accessible to the staff. The control panel contains configuration switches as well as tri-color LEDs to inform the user about the configuration state. When the position of at least one of the switches of the control panel is modified, a configuration frame is sent from the Receiver to the Transmitter. The RF transceiver selected permits power down, standby, reception (RX) and transmission (TX) modes (not simultaneously). Time division duplexing was considered in the design process, but a settling time of 130 µs for each mode switching made it unfeasible due to the bandwidth and transmission speed required for the application time constraints. Because of that, a second radio link is added, with one additional transceiver added to each device (Receiver and Transmitter), thus obtaining separate and independent channels for data and command exchange. Taking advantage of the flexibility of the transceivers, each link is configured to occupy a different band and use a different address.

3.4.1. Data Transmission

Digital data is encapsulated in a dedicated frame that consists, broadly speaking, in an identification header, timestamp and for each channel, digital data information (without compression) and a code indicating the gain utilized for the amplification of the sample sent. This frame is buffered in the transceiver of the Transmitter device byte per byte via SPI, alternating with sample extraction. The RF transceiver is configured to add two CRC bytes in order to add robustness to the transmission. Calculations were carried out to ensure that the combination of frame size, number of channels, bit resolution and sampling rate do not overpass maximum bandwidth of the transceiver (2 Mbps), according to (1).

$$\begin{aligned} BitRate =& ((Data\ bits/measurement + Scale\ bits/measurement) \cdot 8\ channels \\ &+ address\ bytes + CRC\ bytes) \cdot sampling\ rate \\ =& ((16\ bits/measurement + 8\ bits/measurement) \cdot 8\ channels \\ &+ 4\ bytes + 2\ bytes) \cdot 8.93\ kHz = 1.923\ Mbps. \end{aligned} \tag{1}$$

The 8 channels do indeed fill the available bandwidth of the link. However, several 8-channel modules can be used at the same time. Clearly, each pair is going to employ different channels (two channels for each pair of devices); the specific radio devices used allow for up to a theoretical maximum of 30 pairs to be deployed, covering up to 240 channels without need to change the hardware.

The timestamp and identification header of the frames received are analyzed. If the samples are received in a sequential order, the communication link is considered to be stable. On the other hand, if some frames are missing, the link is considered below optimum or inadequate, depending on the number of samples lost. This verification is carried out continuously, and the status of the connection is shown through a LED in the control panel that can be activated in green, yellow or red, based on the degree of reliability of the link, so that the user can move or rearrange the devices of the system to provide a better line of sight between radios. Additionally, the system implements a safety feature that prevents that loss of several consecutive samples results in a blank or flat response in the output.

Because of the application for which our design is intended, the latency between recording and regeneration of the signal at the output of the Receiver has to be as short as possible. Nevertheless, an unavoidable delay has to be expected, due to the several processes involved in the data chain: sampling, digitizing, data buffering, SPI transmission to sending transceiver, data transmission, buffering at the receiver, data extraction via SPI, parsing and, finally, DAC conversion to reconstruct the analog signals. The time delay introduced by a few of these processes can be known and predicted because of the sequence programmed in the microcontroller, and is basically constant if the error rate of the RF link is low. In other cases, and especially as far as the time elapsed between transmission and reception of each single frame is concerned, there is a degree of uncertainty. In order to estimate the maximum delay in a worst case scenario, systematic measurements are performed under laboratory conditions monitoring the activity of the SPI buses in the Receiver and the Transmitted during data exchange.

Figure 6 shows logic-analyzer measurements of SPI bus activity in the Transmitter (TX) and in the Receiver (RX) during data exchange. The portion of the data highlighted by the left-most blue square corresponds to the insertion of a known sequence of data in the transmitting buffer of the radio, while the portion of the data highlighted by the blue square at close to the bottom/right end of the figure in the right corresponds to the extraction of said data from the receiver radio FIFO. As the time marker shows, the delay between transmission and reception is lower than 500 µs, acceptable for the required performance, as it will be discussed later on in the paper.

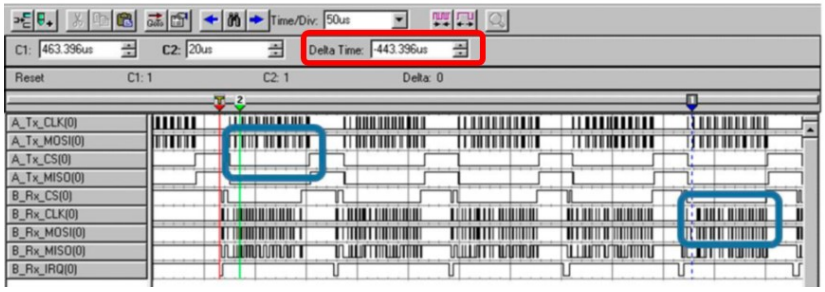

Figure 6. Capture of the transmission and reception between Transmitter and Receiver devices. Blue boxes show correspondent frames in transmission and reception, and the red box highlights the delay between them.

3.4.2. Configuration Frame Transmission

As stated before, the Transmitter device relies on a set of programmable devices that allow to modify the analog input configuration. Each channel can be set in differential or single-ended mode. In the latter case, the reference can also be modified between ground and any of the channels. Additionally, impedance measurement demands controlled

changes in the front-end. Due to ergonomics and utilization convenience, the control panel is located in the Receiver device. This means that the configuration information has to be sent from Receiver to Transmitter, in upstream direction.

It is worth mentioning that during normal utilization of an IOM system, i.e., during a surgical procedure, changes in configuration are scarce and most commonly only carried out at the beginning of the setup of the system. Also, impedance measurement takes place before recording the first signals in order to check that the connections of the electrodes to the patient are good enough. Once the procedure is ongoing, changes are only done if any of the responses monitored is lost or shows a sudden weird behaviour. That being the case, impedance is re-checked to confirm whether the electrodes are well placed or have suffered a disconnection. When this happens, the recording of the signal is interrupted, so a more prolonged transmission delay can be acceptable. These kind of feature is also present in commercial systems, where the impedance measurement procedure interrupts the recording of data.

A state machine implemented in the system we developed manages the communication protocol, as follows. Whenever one of the switches of the control panel is moved, reception state is halted in the Receiver device, and a configuration frame is sent via the transmitting radio towards Transmitter device. This frame comprises a specific header to indicate the type of configuration, and a configuration word, that contains the information required by the Transmitter to vary the corresponding parameters in the analog front-end. The frame is captured by the receiver radio in the Transmitter, issuing an interrupt request to the microcontroller of the device. The recording and transmission of samples is then halted and the system initiates reception state. The microcontroller starts a dialog with the transceiver to extract the received configuration frame out of the FIFO, parsing it and configuring the corresponding programmable switches in the analog front-end. After this, the registering and transmission of samples is resumed, and the whole system returns to normal operation mode.

Assessing a correct configuration is of paramount importance for the reliance on the accuracy of subsequent measurements. Hence, a confirmation protocol is implemented into the dialog between both devices of the system. The flow chart of said protocol is depicted in Figure 7. The starting point is the configuration frame sent by the Receiver (*Config Frame Sent* in Figure 7). In a favourable case, the Transmitter device will receive this frame, and configure the corresponding switches in the analog front-end accordingly to the received information (*Config Dev. A*). The header of the data frame is modified in the subsequent samples, and it will contain a coded value corresponding to the response to the received configuration frame header (*Modify frame Header*). When this configuration is completed (*Succesful configuration*), the sampling and sending process is resumed (*Resume sampling*).

After sending the configuration frame, the Receiver falls into a waiting state. If no response is received after a period of time (*Dev. B Reception?*), a timeout is triggered and the configuration frame is re-sent. In case the reception is not successful, the process is repeated several times until a maximum number of trials (M in Figure 7) is reached. If this is the case, the configuration is considered unsuccessful and the user is warned by means of a visual signal in the LEDs (*Incorrect Configuration signal*). On the other hand, if an incoming new data frame is received, its header is extracted and analyzed (*Header correct?*). The configuration is also considered incomplete when the header received by the Receiver is not equal to the one corresponding to the configuration state initially selected and, again, M trials are carried out. If the maximum number of trials is reached (*Error counter* > M), the configuration process is considered incorrect and terminated, although it can be started again by activating any of the switches.

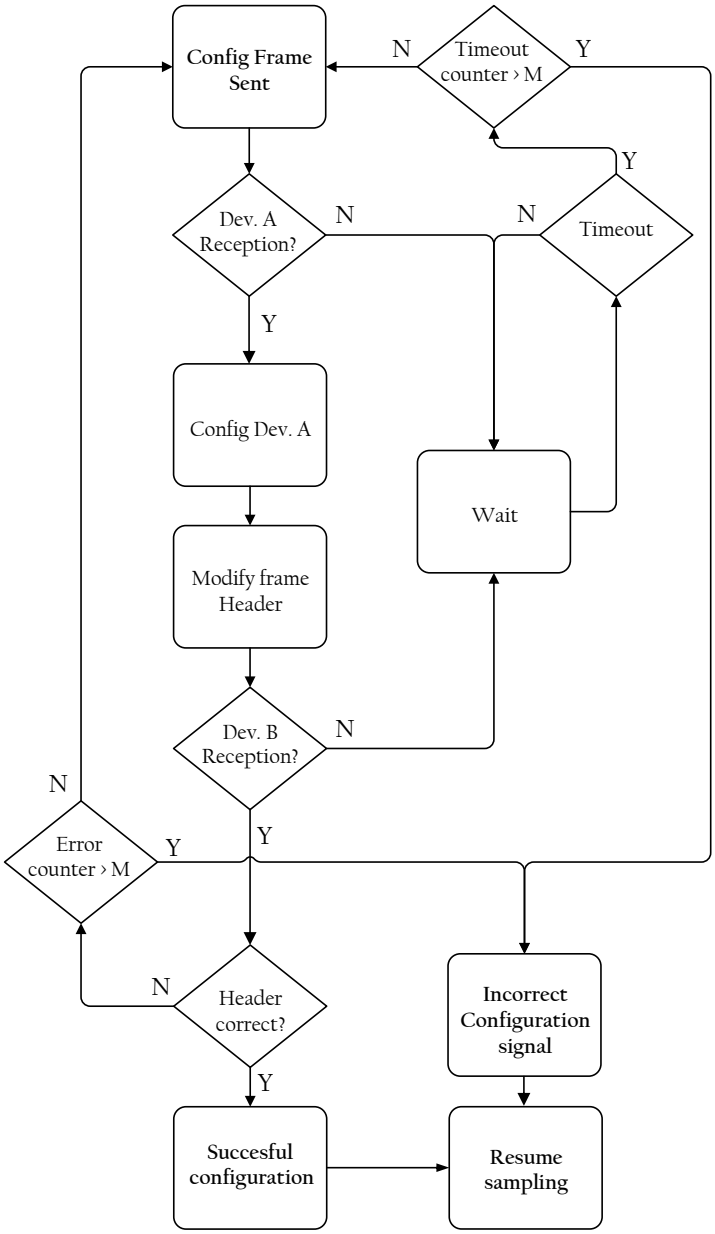

Figure 7. Flowchart of the configuration assessment protocol. Device A is the Transmitter, and Device B is the Receiver. Frame header is utilized to check if the configuration is correct. Two criteria shall be met to obtain a successful configuration: Frame received by Dev. B before a established timeout (*Dev. B Reception?*), and consistent frame header from Dev. A (*Header correct?*). If any of these conditions is not fulfilled, the process is repeated *M* times before considering the configuration incorrect.

The impedance measurement process is also started by a dedicated switch in the control panel of the Receiver device that allows the selection between normal mode or impedance measurement mode. Though automatic, in terms of configuration this technique utilizes the same tools described before, with the only difference that 4 different configurations are needed [16]. If any of these four configurations fails, the measurement is considered unsuccessful and the user will be warned. If the measurement is obtained successfully, the result of the impedance assessment will be shown in the LEDs for each input, indicating a good (green), middling (yellow) or too high (red) contact impedance. The whole algorithm is repeated until the user selects normal operation mode with the

corresponding switch of the control panel. Then, data sampling is resumed and the LEDs go back to their previous state.

4. Results

The prototype was tested in two different setups. Firstly, it was tested in laboratory conditions where recorded signals from real measurements are utilized. Secondly, a set of field tests was carried out, under the same conditions that are expected for the normal operation of the system. Results of the measurements are discussed below.

In both environment, the connectivity has been excellent to very good when transmitter and receiver were located in the same room, or in contiguous rooms like for example the operating room and the preparation/analysis room. Unfortunately, the quality of farther connections depends on too many factors (like type of walls, building geometry, and so on) to be easily quantified. As commented further below, the system has a self-check method to assess if the quality of the connection is acceptable, and will warn the user if not, as well as an algorithm to cope with sample losses. Once the connection is correct, the system proved very robust, with a very low number of lost frames.

4.1. Laboratory Results

Taking into account that the system is composed of several stages both in the Transmitter and the Receiver device, a laboratory setup is arranged in order to assess the correctness and consistency of the signal at all stages of the acquisition and elaboration path.

It is worth noting that the signals commonly recorded by neurophysiological monitoring systems are in the range of micro to millivolts and such low amplitudes are too small for direct monitoring with a standard oscilloscope. In order to tackle this difficulty, the oscilloscope probe is connected at the output of the first stage of amplification, that provides for a gain of at least 50 V/V. This solves the problem of monitoring the input signal, but the same problem arises at the output of the reconstructed waveform at the Receiver side. In this case, we utilized an unused channel of the transmission device as a preamplifier, and the output signal of the Receiver is monitored at the output of the low-noise amplifier of that channel (the configuration is shown using CH2 in Figure 8).

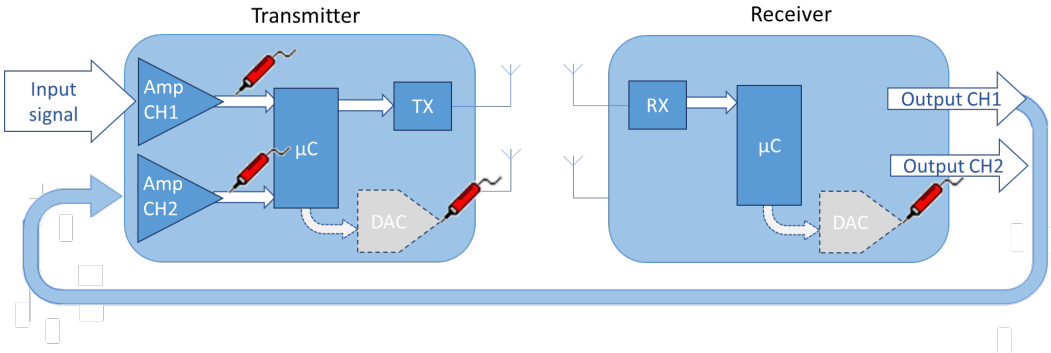

Figure 8. Configuration of the laboratory setup. Given that the noise performances of the first stage amplifier are much better than the oscilloscope's ones, the internal amplifier is used for both the original and the received signal, using different channels in loopback.

Moreover, the microcontroller utilized in both devices of the system includes an integrated DAC, whose output can be wired to the oscilloscope. This allows monitoring also the processes of digitization and sampling, frame construction and transmission. The information corresponding to the channels to be assessed is passed to the internal DAC. Scale factor and different resolutions have to be taken into account, since this internal DAC presents a lower resolution (only 12 bit), in a span of 0 to 3.3 V.

This test arrangement is outlined in Figure 8, where it can be seen that the reconstructed signal, corresponding to the channel 1 input in the Transmitter is wired back to Channel 2 of the same device. A probe symbol indicates where the oscilloscope is connected,

including the output of the first analog amplification stage, as well as the output of the microcontroller-integrated DAC. The rest of the elements of the system have been omitted for the sake of clarity.

Some results of the tests are shown in the oscilloscope captures shown in Figures 9–11. In all the cases, the used input is a response to a MEP that was previously recorded from a volunteer and reproduced by means of a waveform generator. Figure 10 shows a comparison between input analog signal and the result of the digital conversion evaluated through the DAC of the microcontroller. Notice the different scale of the curves. Figure 11 shows a comparison between the analog input signal and the digital signal received and extracted by the Transmitter, again with the help of the internal DAC. Latency between both waveforms is measured with a value close to 800 µs. Finally, Figure 10 contains a comparison between analog input signal, digital signal in the Receiver, and the output signal, recorded in the output of the first LNA stage in channel 2 of the Transmitter. Because of the duration of the evoked response, latency between original and reconstructed signals is not evident in this case. Nevertheless, correspondence between waveforms can be observed.

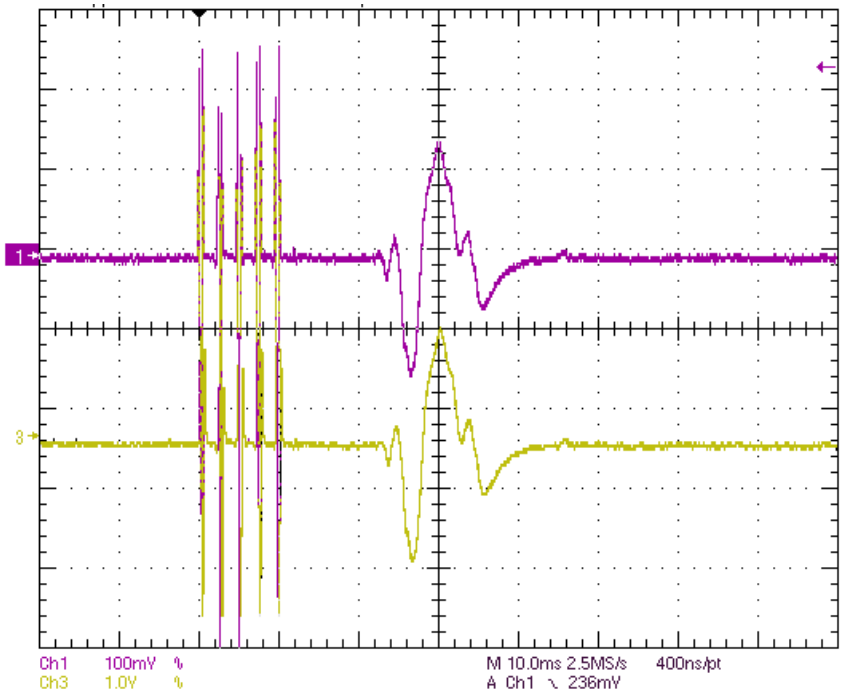

Figure 9. Amplification and ADC stage in Transmitter. Purple track: input signal; Yellowish track: embedded DAC output signal. Horizontal scale is 10 ms/div.

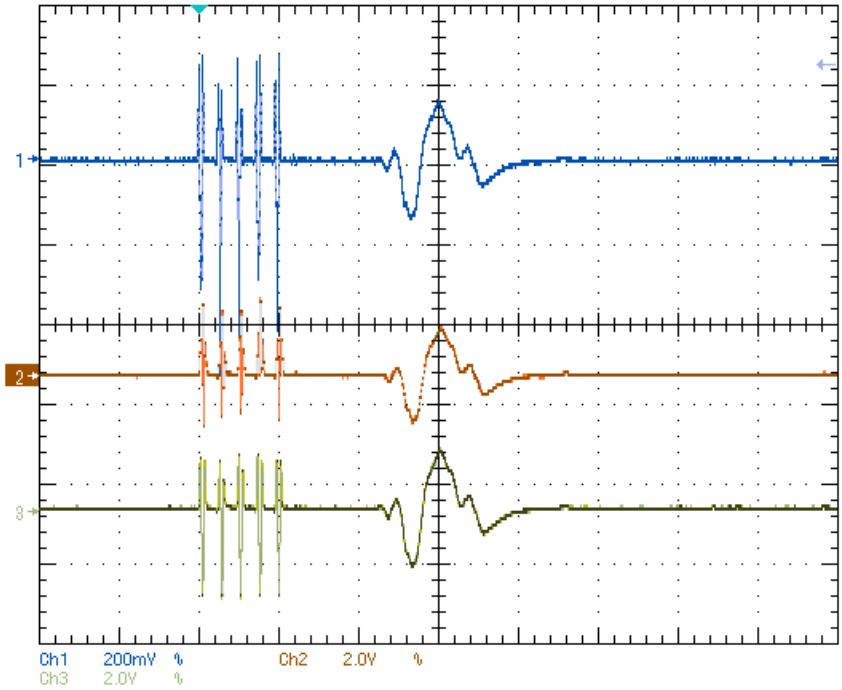

Figure 10. Blue curve: Transmitter input signal; purple curve: Receiver embedded DAC output signal; Olive green track: Receiver analog output signal. Horizontal scale is 10 ms/div.

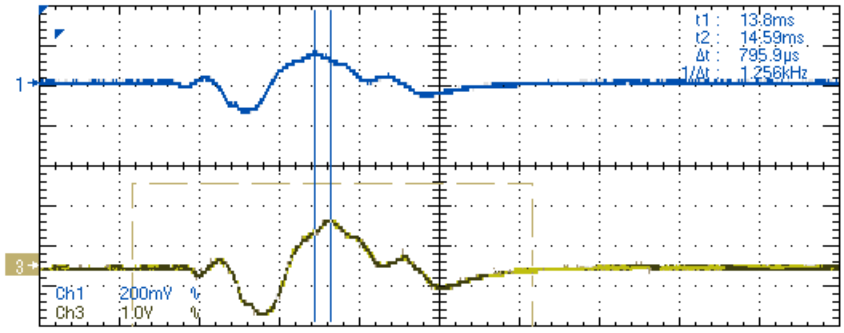

Figure 11. Delay between Transmitter input signal (blue curve), and Receiver embedded DAC output signal (olive green curve). Horizontal scale is 5 ms/div.

4.2. Medical Site Results

In the previous sections, intermediate signals in laboratory tests have been shown in order to check that all the stages of the system work properly. Once this validation phase was completed, several field tests were carried out in order to assess the performance under working conditions with signals coming from a healthy volunteer.

In this case, the experiments take advantage of the utilization of a commercial IONM system that was available in a medical environment. The test setup is sketched in Figure 12. The intraoperative monitoring system that is available is made of three main parts. Firstly, it includes a set of extension adapters with touchproof standard connector inputs, where the electrodes are connected. These adapters are located close to the patient during the surgical procedures. Secondly, the amplifier headbox, where the adapters are connected, is in charge of conditioning and transferring the signals to the visualization section. Lastly, a dedicated PC is connected to the headbox, containing the monitoring software, which is in charge of the plotting and recording of the signals and of the overall configuration. Additionally, the monitoring system has an independent stimulator whose outputs are connected to the patient, but is out of the interest of this test arrangement.

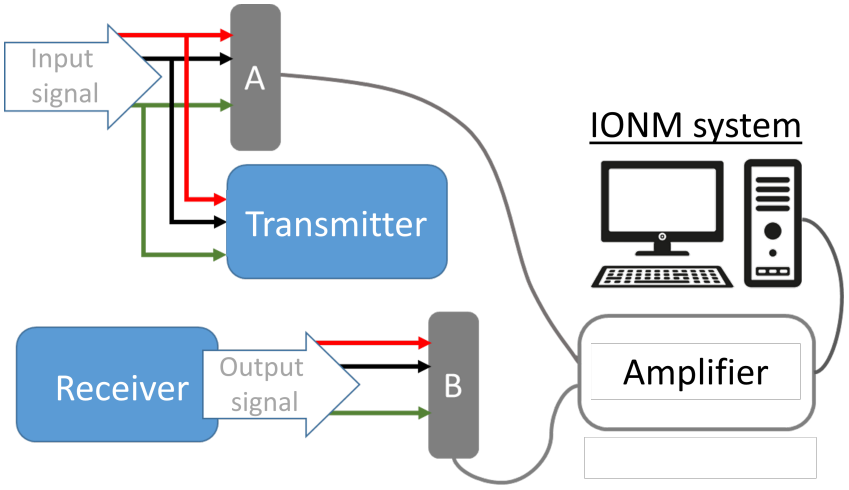

Figure 12. Schematic of the configuration of the performed test.

The input signal coming from the *patient* (in this case, a healthy volunteer) is connected to one of the multichannel input extension adapters of the monitoring system (A). With the help of touch-proof Y connectors, this signal is inserted in parallel in the Transmitter device of the system to be tested. The output of the system, coming out from the Receiver, is then connected to available inputs in a different multichannel adapter (B). Under this arrangement, one can configure the software in order to have a duplicated register of the same biological response, one recorded through A and the other one through B and compare them in the same display window.

Although the system developed is multichannel and allows several signals to be represented at the same time, for the sake of clarity only individual signals are shown in order to carry out the comparison between different signal ranges.

It is important to highlight that the evaluation of this type of signals during a surgery is made visually, with special interest in the changes of each curve registered during the surgery, taking into account the history of the signals and the reference baselines. Latency and changes in amplitude (with respect to the past plots of the same curve) are considered in order to evaluate the neurophysiological status of the patient. This entails that the adequacy of the signal representation can be assessed with a naked-eye comparison, and as so they were evaluated in the medical environment. The figures containing the results are obtained directly as screenshots from the IONM software utilized for the tests.

The first signal shown is Electrocardiography. This monitors the electrical activity of the heart by means of surface electrodes. This is the largest signal tested, with amplitudes of up to 4 mV. The period of the signal is in the range of seconds. Figure 13 shows the result of the measurements taken. The grey curve is the one originally taken from the patient (through A in Figure 12), and the blue curve represents the output of the system under test (through B in Figure 12). A close correspondence between signals can be observed.

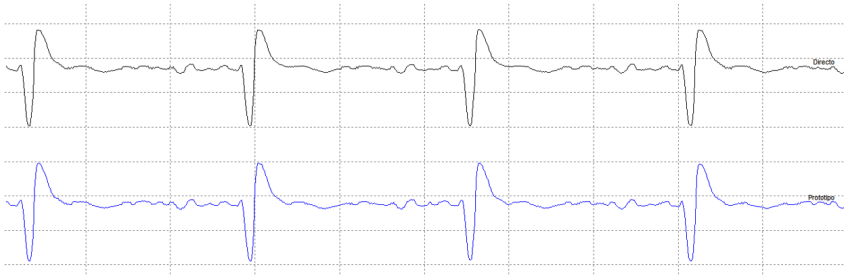

Figure 13. ECG of a healthy volunteer. Grey curve, originally obtained from the system. Blue curve, obtained from the proposed system. Voltage scale is 20 µV/div, time scale is 300 ms/div.

The next type of signals tested are Motor Evoked Potentials (MEP). These are the response of one or more muscles to a stimulation in motor structures of the brain, typically carried out by scalp electrodes. Figure 14 shows a comparison between two consecutive signals recorded from the test subject directly (left) and through the system developed (right). The timescale is 5 mV/div, and a slight (expected) delay is observed. The small alternate response at the beginning on the curves of the right corresponds to the stimulation artifact. This kind of response is always present in the recorded curves, but the monitoring software usually relies on specific algorithms in order to filter it out or to place just before the origin of the time scale, like in the original pictures on the left. Nevertheless, the representation of this artifact does not pose a problem, since the specialist analyzing the curves will pay attention to the latency between the muscle response and the stimulation, which can be measured easily with the help of screen cursors. Again, a close correspondence between original and reproduced signals is obtained.

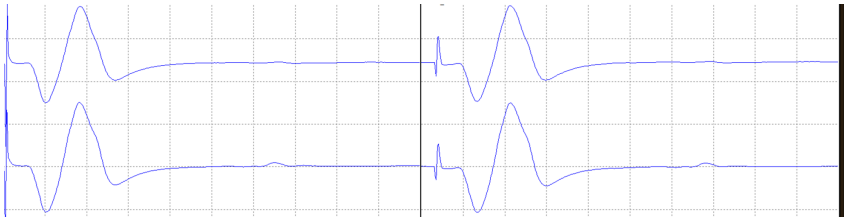

Figure 14. MEP of a healthy volunteer. Curves on the left originally obtained from the system. Curves on the right, obtained from the proposed system. Voltage scale is 2 mV/div, time scale is 5 ms/div.

Another example of the delay of the signal reconstructed is represented in Figure 15, where another pair of MEPs is set against. The blue curve on the top is the original one, and the green curve on the bottom is the reconstructed one. The latter shows a constant delay lower than 2 ms.

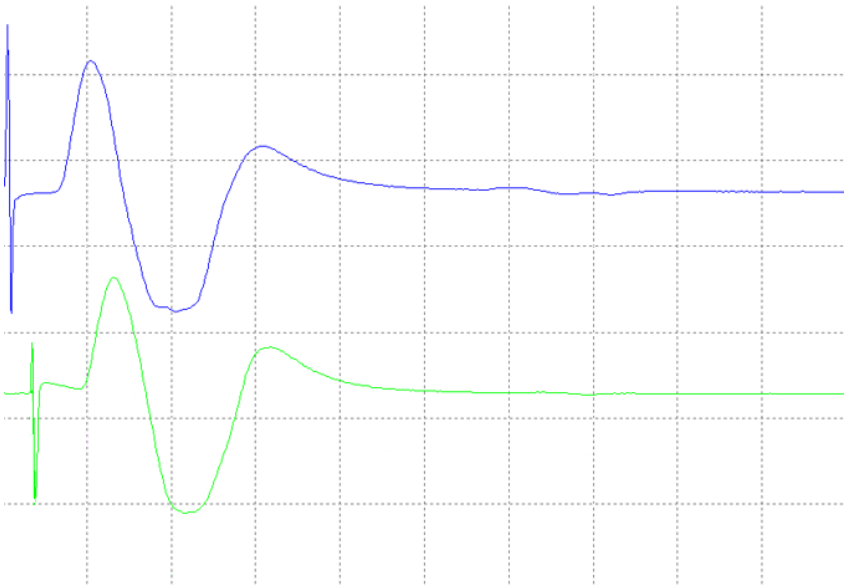

Figure 15. MEP of a healthy volunteer. The blue curve is the one originally obtained from the system. The green curve is obtained with the proposed system. Voltage scale is 5 mV/div, time scale is 5 ms/div.

Because of noise and resolution in analog-to-digital and digital-to-analog conversions, the errors in signal regeneration increase as the amplitude and signal time scale decrease. Because of this, the next type of measurement to be assessed were Somato-Sensory Evoked Potentials (SSEP). These are the record of electrical potentials generated by the somato-sensory pathway in central and peripheral portions of the nervous system, in response

to a stimulus. Typically, stimulation is done in median and tibial nerves (hands and feet), and detection is carried out in the scalp. Because of their small amplitude (in the range of µV), the monitoring software implements special algorithms to average the responses recorded for noise removal, so that the potential can be recognizable after a number of averages, normally between 50 and 150. Figure 16 shows the result of the comparative measurement after 100 averages. Grey and blue curves represent, respectively, the original and reconstructed signals. This case confirms the constant latency in the curve reconstruction, derived for the constant frame rate of the transmission algorithm.

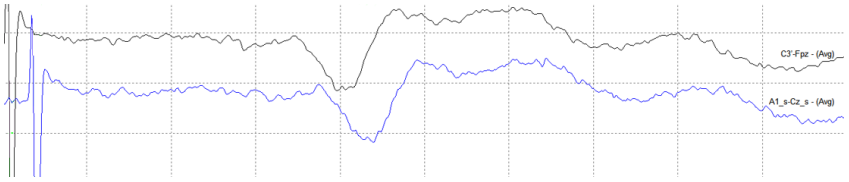

Figure 16. SSEP of a healthy volunteer. Grey curve originally obtained from the system. Blue curve, obtained from the proposed system. Voltage scale is 1 µV/div., time scale is 5 ms/div.

The measurements shown so far serve as a representative example of different amplification ranges. As described before, the acquisition front-end included in Transmitter device is equipped with a set of programmable gain amplifiers that adapt the amplification range to the voltage level of the signal. This adaptation is made automatically by the algorithm programmed in the microcontroller of the device; notice that the amplitude of the signals shown in Figures 13–16 vary from the millivolt range (MEP and ECG) to the microvolt range (SSEP).

Finally, Auditory Evoked Potential (AEP) signals are tested. These signals are obtained as a response of the auditory system structures to an acoustic stimulus that is produced by means of pads inserted in the patient's inner ear. Correct acquisition and reproduction of these signals is quite challenging in common medical practice and, due to their low amplitudes, the number of required averages is in the range of several hundreds. Besides equivalence between original (grey) and reconstructed (blue) signals, Figure 17 shows a measurement of the constant delay introduced by the system tested. The cursors show a time difference between the peaks of the signal of 1.5 ms. In this case, due to the short time scale of the neural response, the latency caused by acquisition, sampling, transmission, reception and reproduction of the information, the delay is quite pronounced. Given that this can be considered a worst-case scenario, the conclusion is that the delay is still acceptable; the important information here is the presence of the neural response, and the normal window used is, as shown in the diagram, of about 15 ms.

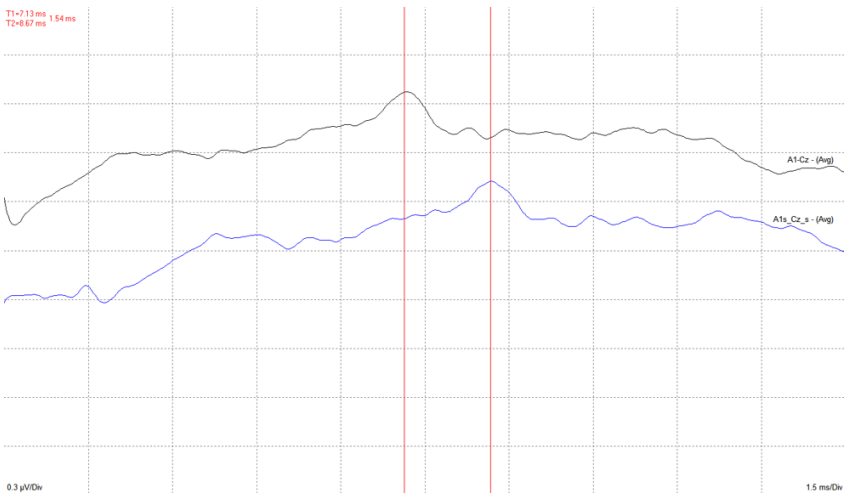

Figure 17. AEP of a healthy volunteer. Grey curve, originally obtained from the system. Blue curve, obtained from the proposed system. Voltage scale is 0.3 µV/div, time scale is 1.5 ms/div.

5. Discussion

The aim of this article was the discussion of a prototype of a wireless device that can be utilized along with already available intraoperative monitoring devices, that represents, in itself, substantial step toward the definition of a new monitoring paradigm. Tests performed on the prototype that has been designed have demonstrated the ability of the system to satisfactorily address the problems that prompted this investigation. In particular:

- Due to all the stages of the system from signal acquisition to reconstruction, a latency time is introduced. Although this feature is critical in the medical evaluation of the recorded signals , test measurements show that this delay is constant and acceptably low for the intended application.
- Several wireless technologies and protocols were considered, and an ISM RF radio module was selected as the most adequate one. A custom protocol was developed in order to comply with the sampling frequency and low latency requested, including data transmission/reception and configuration commands dialog.
- The system developed is versatile, and input channels can be configured to work as single-ended (referential) or differential inputs. The user has the possibility to change the configuration as well as the channel utilized as the reference for the measurements.
- The system includes a novel impedance measurement method, necessary to assess the correct connection of the electrodes, similarly to what is installed in current commercial monitoring devices. This method is implemented in the analog front end of the system and has been thoroughly described in [16].
- Currently available commercial monitoring systems present a software interface that allows the user to adjust the amplification gain depending on the voltage range of the signal. In our system an algorithm is implemented that analyzes the amplitude of the signal recorded on each channel and automatically changes the setting of the programmable gain amplifiers in the analog front-end.
- The validation of the system has been carried out through laboratory and field tests. The results of the experiments demonstrate sufficient accuracy in signal regeneration across the full range of the expected input signals, as well as an acceptable delay between actual and regenerated signal.

Finally, the market for the IONM devices and systems has been estimated [23] to be around USD 1.6 billions in 2020, and to soar up to about USD 9 billions by 2028; in this scenario the proposed device can fit as a valuable step towards a fully wireless implementation of the monitoring system, offering a cost-effective intermediate solution to the reduction of the cumbersome wiring of the patient to the analysis machines. In addition, the approach of the solution proposed permits the utilization of this technology regardless of the monitoring system used, entailing a substantial advantage in the market.

6. Patents

Part of the described system has been submitted to the European Patent Office as WO 2018/011439 [24] and is in course of evaluation. More in detail, the patent cover the system for analog measurement, transmission and reconstruction of bio-potentials with a fully passive detection of the quality of the electrode-tissue contact. This correspond basically to the structure of Figure 2, the procedure indicated in the flowchart of Figure 7, and the contact impedance assessment procedure described in [16].

Author Contributions: The authors of this Work have been contributing in roughly the same way to the research that lead to this article, and all of them have contributed to writing, proofing and correcting the paper and the associated figures. In detail, E.A.R. contributed all over the map, building the prototype, debugging it, planning the measurements and analyzing them. R.G., G.S. and C.C. were more involved in the analog design; C.R.-M.G., J.M.D. and J.D.M.F. were more involved in the digital design (hardware and software) and PCB optimization; L.V.-Z. and J.P. have supervised and assisted in the field tests. All the authors participated in the debugging of the system, its deployment

and the measurement campaigns, as well as in revising the manuscript. All authors have read and agreed to the published version of the manuscript.

Funding: This research was partially funded by Soinde, S.L.

Institutional Review Board Statement: A series of tests has been performed on human volunteers in the laboratories of the IIT and of the University Hospital "La Princesa", in Madrid, respecting the internal protocols of the Institute; the experimental protocols were approved by the Ethical Committee of Clinical Research of Hospital de la Princesa (number of register PI-843, approved 21 December 2015).

Informed Consent Statement: The test has been duly authorized, and performed in accordance with the approved protocols, on volunteers whose have been informed and agreed to conduct the experiments, providing specific informed consent, and being fully aware of the risks and methodology of the experiment.

Data Availability Statement: Data is available upon request.

Conflicts of Interest: The authors declare no conflict of interest. Additionally, the funders had no role in the design of the study; in the collection, analyses, or interpretation of data; in the writing of the manuscript; or in the decision to publish the results.

Abbreviations

The following abbreviations are used in this manuscript:

WIONM	Wireless Intraoperative Neurophysiological Monitoring
IONM	Intraoperative Neurophysiological Monitoring
EEG	Electroencephalography
EMG	Electromyography
ECoG	Electrocorticography
ADC	Analog-to-Digital Converter
DAC	Digital-to-Analog Converter
RF	Radio-Frequency
CRC	Cyclic Redundancy Check
SSEP	Somato-Sensory Evoked Potentials
EP	Evoked Potential
MEP	Motor Evoked Potential
AEP	Auditory Evoked Potential

References

1. Howick, J.; Cohen, B.A.; McCulloch, P.; Thompson, M.; Skinner, S.A. Foundations for evidence-based intraoperative neurophysiological monitoring. *Clin. Neurophysiol.* **2016**, *127*, 81–90. [CrossRef] [PubMed]
2. Vega-Zelaya, L.; Sola, R.G.; Pastor, J. Intraoperative Neurophysiological Monitoring in Neuro-oncology. In *Neurooncology—Newer Developments*; Agrawal, A., Ed.; IntechOpen: Rijeka, Croatia, 2016; Chapter 9.
3. Liao, L.D.; Chen, C.Y.; Wang, I.J.; Chen, S.F.; Li, S.Y.; Chen, B.w.; Chang, J.Y.; Lin, C.T. Gaming control using a wearable and wireless EEG-based brain-computer interface device with novel dry foam-based sensors. *J. Neuroeng. Rehabil.* **2012**, *9*, 5. [CrossRef] [PubMed]
4. Lin, C.-T.; Ko, L.-W.; Chang, M.-H.; Duann, J.-R.; Chen, J.-Y.; Su, T.-P.; Jung, T.-P. Review of Wireless and Wearable Electroencephalogram Systems and Brain-Computer Interfaces—A Mini-Review. *Gerontology* **2010**, *56*, 112–119. [CrossRef] [PubMed]
5. Chi, Y.M.; Cauwenberghs, G. Wireless Non-contact EEG/ECG Electrodes for Body Sensor Networks. In Proceedings of the 2010 International Conference on Body Sensor Networks, Singapore, 7–9 June 2010; pp. 297–301.
6. Sodagar, A.M.; Wise, K.D.; Najafi, K. A Wireless Implantable Microsystem for Multichannel Neural Recording. *IEEE Trans. Microw. Theroy Tech.* **2009**, *57*, 2565–2573. [CrossRef]
7. Vetter, R.J.; Williams, J.C.; Hetke, J.F.; Nunamaker, E.A.; Kipke, D.R. Chronic Neural Recording Using Silicon-Substrate Microelectrode Arrays Implanted in Cerebral Cortex. *IEEE Trans. Biomed. Eng.* **2004**, *51*, 896–904. [CrossRef] [PubMed]
8. Casson, A.J.; Yates, D.C.; Smith, S.J.; Duncan, J.S.; Rodriguez-villegas, E. Weareable Electroenchepalography. *IEEE Eng. Med. Biol. Mag.* **2010**, *29*, 44–56. [CrossRef] [PubMed]
9. Patki, S.; Grundlehner, B.; Verwegen, A.; Mitra, S.; Xu, J.; Matsumoto, A.; Yazicioglu, R.F.; Penders, J. Wireless EEG system with real time impedance monitoring and active electrodes. In Proceedings of the 2012 IEEE Biomedical Circuits and Systems Conference (BioCAS), Hsinchu, Taiwan, 28–30 November 2012; pp. 108–111.

10. Sagha, H.; Perdikis, S.; Chavarriaga, R. Quantifying Electrode Reliability during Brain—Computer Interface Operation. *IEEE Trans. Biomed. Eng.* **2015**, *62*, 858–864. [CrossRef] [PubMed]
11. Buxi, D.; Kim, S.; Van Helleputte, N.; Altini, M.; Wijsman, J.; Yazicioglu, R.F.; Penders, J.; Van Hoof, C. Correlation between electrode-tissue impedance and motion artifact in biopotential recordings. *IEEE Sens. J.* **2012**, *12*, 3373–3383. [CrossRef]
12. Ferree, T.C.; Luu, P.; Russell, G.S.; Tucker, D.M. Scalp electrode impedance, infection risk, and EEG data quality. *Clin. Neurophysiol.* **2001**, *112*, 536–544. [CrossRef] [PubMed]
13. Shannon, C. Communication in the Presence of Noise. *Proc. IRE* **1949**, *37*, 10–21. [CrossRef]
14. Webster, J. *Medical Instrumentation Application and Design*, 4th ed.; John Wiley & Sons: Hoboken, NJ, USA, 2009. Available online: https://books.google.es/books?id=CQ4cAAAAQBAJ (accessed on 15 October 2022).
15. AD8429 1nV/$\sqrt{Hz}$ Low Noise Instrumentation Amplifier. 2017. Available online: https://www.analog.com/media/en/technical-documentation/data-sheets/ad8429.pdf (accessed on 15 October 2022).
16. Alonso, E.; Giannetti, R.; Rodríguez-Morcillo, C.; Matanza, J.; Muñoz-Frías, J.D. A Novel Passive Method for the Assessment of Skin-Electrode Contact Impedance in Intraoperative Neurophysiological Monitoring Systems. *Sci. Rep.* **2020**, *10*, 2819. [CrossRef] [PubMed]
17. Scandurra, G.; Cannatà, G.; Giusi, G.; Ciofi, C. A new approach to DC removal in high gain , low noise voltage amplifiers. In Proceedings of the 2017 International Conference on Noise and Fluctuations (ICNF), Vilnius, Lithuania, 20–23 June 2017; pp. 1–4.
18. Huang, C.c.; Hung, S.h.; Chung, J.f.; Van, L.D.; Lin, C.t. Front-End Amplifier of Low-Noise and Tunable BW/Gain for Portable Biomedical Signal Acquisition. In Proceedings of the 2008 IEEE International Symposium on Circuits and Systems (ISCAS), Seattle, WA, USA, 18–21 May 2008; pp. 2717–2720.
19. Harrison, R.R.; Charles, C. A Low-Power Low-Noise CMOS Amplifier for Neural Recording Applications. *IEEE J. Solid-State Circuits* **2003**, *38*, 958–965. [CrossRef]
20. Müller-Putz, G.R.; Scherer, R.; Neuper, C.; Pfurtscheller, G. Steady-State Somatosensory Evoked Potentials: Suitable Brain Signals for Brain—Computer Interfaces? *IEEE Trans. Neural Syst. Rehabil. Eng.* **2006**, *14*, 30–37. [CrossRef] [PubMed]
21. Chestek, C.A.; Gilja, V.; Nuyujukian, P.; Kier, R.J.; Solzbacher, F.; Ryu, S.I.; Harrison, R.R.; Shenoy, K.V. HermesC : Low-Power Wireless Neural Recording System for Freely Moving Primates. *IEEE Trans. Neural Syst. Rehabil. Eng.* **2009**, *17*, 330–338. [CrossRef] [PubMed]
22. Farajidavar, A.; Seifert, J.L.; Bell, J.E.S.; Seo, Y.S.; Delgado, M.R.; Sparagana, S.; Romero, M.I.; Chiao, J.C. A wireless system for monitoring transcranial motor evoked potentials. *Ann. Biomed. Eng.* **2011**, *39*, 517–523. [CrossRef] [PubMed]
23. IGlobal Intraoperative Neuromonitoring (IONM) Market to Reach USD 9.03 Billion by 2028: Vantage Market Research. 2021. Available online: https://www.globenewswire.com/en/news-release/2021/11/18/2337755/0/en/Global-Intraoperative-Neuromonitoring-IONM-Market-to-Reach-USD-9-03-Billion-by-2028-Vantage-Market-Research.html (accessed on 15 October 2022).
24. Jiménez-Carles Gil-Delgado, E. Intraoperative Monitoring System. Patent Application WO 2018/011439 Al, 18 January 2018. Available online: https://patentscope.wipo.int/search/es/detail.jsf?docId=WO2018011439 (accessed on 15 October 2022).

Chapter 3

Conclusion

In short, the aim of the work reported here was the development of a wireless solution to improve the ergonomics of current intraoperative neurophysiological monitoring technology and facilitate its deployment by medical staff. This broad goal was divided in objectives, already addresses in the document and listed below:

- Designing and prototyping an analog front-end compliant with the current commercial standard of IONM systems and embed it in a transmitter device.
- Developing a wireless communication link for the biological signals monitored.
- Designing and prototyping a device to receive and reconstruct the sensed signal capable of connecting to current commercial systems.
- Developing and testing a functional prototype of the whole system designed.
- Including a novel and passive impedance measurement method in the system, more adequate for wireless applications than those in place today.
- Proposing a new approach for the fast-settling of amplifiers in biosignal acquisition systems.

3.1 Contributions

The three papers that give shape to this thesis contain the main outcomes resulting from the work carried out towards the fulfilment of the initial objectives.

To begin with, [84] depicts a novel methodology for estimating the skin-electrode contact impedance for biosignal acquisition. This technique assesses the variation experienced by a measured signal when a parallel load is connected and disconnected in a software-controlled process. Changes in the signals are registered and computed, and as a result, an estimated assessment of the impedance can be provided. This method arose as an alternative to prevailing current injection approaches, present in most acquisition devices, and is seen as a better alternative for wireless systems, since it reduces power consumption and can facilitate certification processes according to medical devices regulation. The PhD candidate, as first author of this paper, has been in charge of developing the mathematical procedure, carrying out the simulations, hardware and software deployment, laboratory and field tests and result analysis. The results show the capabilities of this new method to compare the registered values, identify the correctness of the contact impedance, and warn the user of the system about it.

Nevertheless, duration of the measurement was identified as a weakness of this new methodology, since the connection of a parallel resistor in the input stage of the acquisition system creates a steep voltage difference that combined with the time constant of the input HP filter creates a slow transient in the signal registered that delays the contact impedance measurement. As a result, a new set-up is proposed in [85], including a voltage control that permits a faster recovery from transients in the input as well as a low cut-in frequency during signal measurement. In this case, the PhD candidate developed the simulations, initial design of the prototype, hardware and software deployment, laboratory testing and result analysis. The prototype utilized for the measurements included the impedance measurement method in [84] and results demonstrated the possibility of reducing drastically the time required to carry out such measurements, while maintaining sensitivity and bandwidth in biosignal acquisition. Details of the analog front-end designed were also provided.

Though innovative, the solutions described only respond to two of the objectives of this work. The rest of them are addressed in [7], where the wireless solution intended is presented as a complete system. The design comprises a custom-protocol RF link, the novel methodology for contact impedance measurement mentioned above and several algorithms to cope with lost samples and to automatically adjust the gain of the amplifiers depending on signal voltage level. In this work, the PhD candidate collaborated with the design of the prototype, took care of hardware and software implementation and was in charge of the laboratory and field tests, as well as the result analysis. The principal findings of the paper presented are the results obtained in laboratory and under field tests conditions, compared to a commercial IONM system. As a main conclusion, the signal reconstructed by the system designed matches the original biosignal in a wide range of techniques of diverse voltage and frequency range, with the difference of a constant and acceptable slight delay. The results shown overpass the ones shown in [6], [11], [12] and [13] for a wireless system, validating the research work aimed at obtaining a solution with commercial potential. Moreover, the patent WO 2018/011439 [86] currently under evaluation covers some of the aspects of this design, like the wireless data transmission and the analog reconstruction of the biosignal in the receiver. Additionally, the development presented here was part of the project *WIONM Novel medical wireless data link for Intraoperative Neurophysiological Monitoring*, that was presented by Soinde SL to the European Commission and was awarded with the seal of excellence within the Horizon 2020 initiative in 2019.

3.2 Future Work

Since this work has led to the development of a functional prototype, there is room for future works with the aim of obtaining a fully wireless solution.

Since the methodology for the fast-settling amplifier solution has been developed and tested in an stand alone way under laboratory conditions, it would be desirable to develop an enhanced prototype including this solution in order to undertake field test measurements to validate this technology in the realm it was designed for.

Although the application of this approach was the response to a problem in the embedded impedance measurement method, it may also prevent saturation due to steep voltage changes in the input during monitoring.

Current impedance measurement methods imply halting monitoring while undertaking the impedance measurements (that lasts for seconds). The utilization of this fast-settling approach may lead to the measurement of this impedance without interrupting the acquisition of signals.

As shown in [7], the prototype developed is equipped with a RF link between the acquisition unit and the receiver connected to the recording device. Even though the prototype has been tested during on-site measurements, and the system itself has an algorithm both to secure communication and cope with sample loss, it is desirable to obtain a formal analysis of this link with respect to robustness, coverage and transmission distance.

Current commercial IONM systems consist of a central PC unit and a specific software to parse, process, display and analyse the biosignals obtained in real time. Although the system has been designed with a high flexibility and can be combined with current IONM systems (even other kind of systems like EEG or EMG specific systems) through standard analog connections, this development is seen as one step towards a complete wireless solution. For this, and taking advantage of the USB tracker interface developed to check the signals [7], a receiver-PC interface can be developed, so that one can get rid of the connection between the receiver device and the acquisition amplifier of current systems, replacing the analog connection with a digital one,

more stable and less susceptible to noise. This solution may have two main possible approaches. The first one would be collaborating with current technology manufacturers, so that the signals can be parsed directly to their solution. The second one would be developing a software solution that matches the current functionalities of commercial systems.

Bibliography

[1] J. G. Webster, *Medical Instrumentation Application and Design*, 4th ed. Hoboken, NJ: Wiley, 2009.

[2] M. Teplan, "Fundamentals of EEG measurement," *Measurement Science Review*, vol. 2, pp. 1–11, 2002.

[3] R. M. Dondelinger, "Electromyography—an overview," *Biomedical Instrumentation & Technology*, vol. 44, no. 2, pp. 128–131, mar 2010.

[4] L. Vega-Zelaya, R. G. Sola, and J. Pastor, "Intraoperative neurophysiological monitoring in neuro-oncology," in *Neurooncology - Newer Developments*, A. Agrawal, Ed. Rijeka: IntechOpen, 2016, no. July, ch. 9. [Online]. Available: http://www.intechopen.com/books/neurooncology-newer-developments/intraoperative-neurophysiological-monitoring-in-neuro-oncologyhttps://doi.org/10.5772/63241

[5] M. R. Nuwer, "Overview and history," in *Intraoperative Monitoring of Neural Function*, ser. Handbook of Clinical Neurophysiology. Elsevier, 2008, vol. 8, pp. 2–6.

[6] A. Farajidavar, J. L. Seifert, M. R. Delgado, S. Sparagana, M. I. Romero-Ortega, and J. C. Chiao, "Electromagnetic interference in intraoperative monitoring of motor evoked potentials and a wireless solution," *Medical Engineering and Physics*, vol. 38, pp. 87–96, 2016.

[7] E. Alonso Rivas, R. Giannetti, C. Rodríguez-Morcillo García, J. Matanza Domingo, J. D. Muñoz Frías, G. Scandurra, C. Ciofi, L. Vega-Zelaya, and J. Pastor, "A quasi-wireless

intraoperatory neurophysiological monitoring system," *Electronics (Switzerland)*, vol. 11, no. 23, pp. 1–19, 2022. [Online]. Available: https://doi.org/10.3390/electronics11233918

[8] "Iglobal intraoperative neuromonitoring (ionm) market to reach usd 9.03 billion by 2028: Vantage market research," https://www.globenewswire.com/en/news-release/2021/11/18/2337755/0/en/Global-Intraoperative-Neuromonitoring-IONM-Market-to-Reach-USD-9-03-Billion-by-2028-Vantage-Market-Research.html, 11 2021, accessed: 2022-11-15.

[9] "Intraoperative neuromonitoring (ionm) market - growth, trends, covid-19 impact, and forecasts (2023 - 2028)," https://www.mordorintelligence.com/industry-reports/intraoperative-neuromonitoring-market, accessed: 2023-01-01.

[10] "Intraoperative neuromonitoring: Global strategic business report," https://www.researchandmarkets.com/reports/5139886/intraoperative-neuromonitoring-global-strategic#product--adaptive, 10 2022, accessed: 2023-01-01.

[11] J. Mays, P. Rampy, D. Sucato, S. Sparagana, and J. Chiao, "A wireless solution for intraoperative monitoring," in *RF and Wireless Technologies for Biomedical and Healthcare Applications (IMWS-BIO), 2015 IEEE MTT-S 2015 International Microwave Workshop Series on*, 2015, pp. 244–245.

[12] J. Mays, P. Rampy, D. Sucato, S. Sparagana, and J. C. Chiao, "A wireless system improves reliability of intraoperative monitoring recordings," *BioWireleSS 2016 - Proceedings, 2016 IEEE Topical Conference on Biomedical Wireless Technologies, Networks, and Sensing Systems*, pp. 5–7, 2016.

[13] J. Chiao, D. Sucato, S. Sparagana, J. Mays, and P. Rampy, "Report of clinical results in intraoperative wireless recording," in *Radio-Frequency Integration Technology (RFIT), 2016 IEEE International Symposium on*, 2016.

[14] L.-D. Liao, C.-Y. Chen, I.-J. Wang, S.-F. Chen, S.-Y. Li, B.-w. Chen, J.-Y. Chang, and C.-T. Lin, "Gaming control using a wearable and wireless EEG-based brain-computer interface

device with novel dry foam-based sensors," *Journal of Neuroengineering and Rehabilitation*, vol. 9, no. January, 2012.

[15] B. S. Makeig, C. Kothe, T. Mullen, N. Bigdely-shamlo, Z. Zhang, and K. Kreutz-Delgado, "Evolving signal processing for Brain–Computer Interfaces," *Proceedings of the IEEE*, vol. 100, no. Special Centennial Issue, pp. 1567–1584, 2012.

[16] E. Chua and W.-c. Fang, "Mixed bio-signal lossless data compressor for portable brain-heart monitoring systems," *IEEE Transactions on Consumer Electronics*, vol. 57, no. 1, pp. 267–273, 2011.

[17] Y. Fu, J. Zhao, Y. Dong, and X. Wang, "Dry electrodes for human bioelectrical signal monitoring," *Sensors (Switzerland)*, vol. 20, no. 13, pp. 1–30, 2020.

[18] A. J. Portelli and S. J. Nasuto, "Design and development of non-contact bio-potential electrodes for pervasive health monitoring applications," *Biosensors*, vol. 7, no. 2, 2017.

[19] B. Taji, S. Shirmohammadi, V. Groza, and I. Batkin, "Impact of skin-electrode interface on electrocardiogram measurements using conductive textile electrodes," *IEEE Transactions on Instrumentation and Measurement*, vol. 63, no. 6, pp. 1412–1422, 2014.

[20] G. Acar, O. Ozturk, A. J. Golparvar, T. A. Elboshra, K. Böhringer, and M. Kaya Yapici, "Wearable and flexible textile electrodes for biopotential signal monitoring: A review," *Electronics*, vol. 8, no. 5, pp. 1–25, 2019.

[21] R. a. Andersen, S. Musallam, and B. Pesaran, "Selecting the signals for a brain-machine interface," *Current opinion in neurobiology*, vol. 14, no. 6, pp. 720–726, dec 2004.

[22] A. J. Casson, D. C. Yates, S. J. Smith, J. S. Duncan, and E. Rodriguez-villegas, "Weareable electroenchepalography," *IEEE Engineering in Medicine and Biology Magazine*, vol. 29, no. 3, pp. 44–56, 2010.

[23] T. C. Ferree, P. Luu, G. S. Russell, and D. M. Tucker, "Scalp electrode impedance , infection risk , and EEG data quality," *Clinical Neurophysiology*, vol. 112, pp. 536–544, 2001.

[24] R. R. Harrison and C. Charles, "A low-power low-noise CMOS amplifier for neural recording applications," *IEEE Journal of Solid-State Circuits*, vol. 38, no. 6, pp. 958–965, 2003.

[25] C.-c. Huang, S.-h. Hung, J.-f. Chung, L.-D. Van, and C.-t. Lin, "Front-end amplifier of low-noise and tunable BW / gain for portable biomedical signal acquisition," in *Circuits and Systems, IEEE International Symposium on*, 2008, pp. 2717–2720.

[26] R. F. Yazicioglu, P. Merken, R. Puers, and C. V. Hoof, "A 60µW 60nV/$\sqrt{Hz}$ readout front-end for portable biopotential acquisition systems," *IEEE Journal on Solid-State Circuits*, vol. 42, no. 5, pp. 1100–1110, 2007.

[27] J. Xu, B. Büsze, C. Van Hoof, K. A. Makinwa, and R. F. Yazicioglu, "A 15-channel digital active electrode system for multi-parameter biopotential measurement," *IEEE Journal of Solid-State Circuits*, vol. 50, no. 9, pp. 2090–2100, 2015.

[28] M. Vafaei, A. Parhizgar, E. Abiri, and M. R. Salehi, "A low power and ultra-high input impedance analog front end based on fully differential difference inverter-based amplifier for biomedical applications," *AEU - International Journal of Electronics and Communications*, vol. 142, p. 154005, dec 2021.

[29] N. Heidmann, N. Hellwege, T. Hohlein, T. Westphal, D. Peters-Drolshagen, and S. Paul, "Modeling of an analog recording system design for ECoG and AP signals," in *Design, Automation and Test in Europe Conference and Exhibition (DATE)*, 2014, pp. 1–6.

[30] M. Kavitha, S. Akhila, and A. Kannan, "Flexible analog front end architecture for biomedical applications," in *2021 IEEE 3rd PhD Colloquium on Ethically Driven Innovation and Technology for Society, PhD EDITS 2021*. Institute of Electrical and Electronics Engineers Inc., 2021.

[31] T. Yang, J. Lu, M. S. Jahan, K. Griffin, J. Langford, and J. Holleman, "A configurable 5.9 μW analog front-end for biosignal acquisition," in *Proceedings of the Custom Integrated Circuits Conference*, vol. 2015-Novem. Institute of Electrical and Electronics Engineers Inc., nov 2015.

[32] J. Xu, M. Konijnenburg, H. Ha, R. van Wegberg, S. Song, D. Blanco-Almazán, C. Van Hoof, and N. Van Helleputte, "A 36µw 1.1mm2 reconfigurable analog front-end for cardiovascular and respiratory signals recording," *IEEE Transactions on Biomedical Circuits and Systems*, vol. 12, no. 4, pp. 774–783, 2018.

[33] R. Chebli, M. Ali, and M. Sawan, "High-CMRR low-noise fully integrated front-end for EEG acquisition systems," *Electronics*, vol. 8, no. 10, pp. 1–15, 2019.

[34] G. Scandurra, G. Cannatà, G. Giusi, C. Ciofi, D. Ingegneria, and U. Messina, "A new approach to DC removal in high gain , low noise voltage amplifiers," in *2017 International Conference on Noise and Fluctuations (ICNF)*, Vilnius, Lithuania, 2017, pp. 1–4.

[35] J. Ruiz-Amaya, A. Rodriguez-Perez, and M. Delgado-Restituto, "A low noise amplifier for neural spike recording interfaces," *Sensors (Switzerland)*, vol. 15, no. 10, pp. 25 313–25 335, 2015.

[36] S. Simmich, A. Bahr, and R. Rieger, "Noise efficient integrated amplifier designs for biomedical applications," *Electronics*, vol. 10, no. 13, pp. 1–17, 2021.

[37] J. Kim and H. Ko, "A dynamic instrumentation amplifier for low-power and low-noise biopotential acquisition," *Sensors*, vol. 16, no. 3, pp. 1–10, 2016.

[38] A. Farajidavar, J. L. Seifert, J. E. S. Bell, Y.-S. Seo, M. R. Delgado, S. Sparagana, M. I. Romero, and J.-C. Chiao, "A wireless system for monitoring transcranial motor evoked potentials." *Annals of biomedical engineering*, vol. 39, no. 1, pp. 517–23, 2011.

[39] C.-T. Lin, L.-W. Ko, M.-H. Chang, J.-R. Duann, J.-Y. Chen, T.-P. Su, and T.-P. Jung, "Review of wireless and wearable electroencephalogram systems and Brain-Computer Interfaces - a mini-review," *Gerontology*, vol. 56, no. 1, pp. 112–119, 2010.

[40] N. M. Neihart and R. R. Harrison, "Micropower circuits for bidirectional wireless telemetry in neural recording applications," *IEEE Transactions on Biomedical Engineering*, vol. 52, no. 11, pp. 1950–1959, 2005.

[41] A. M. Sodagar, K. D. Wise, and K. Najafi, "A wireless implantable microsystem for multichannel neural recording," *IEEE Transactions on Microwave Theory and Techniques*, vol. 57, no. 10, pp. 2565–2573, 2009.

[42] Y. M. Chi and G. Cauwenberghs, "Wireless non-contact EEG/ECG electrodes for body sensor networks," in *Body Sensor Networks, International Conference on*, 2010, pp. 297–301.

[43] T. Zhang, J. Lu, F. Hu, and Q. Hao, "Bluetooth Low Energy for wearable sensor-based healthcare systems," *2014 IEEE Healthcare Innovation Conference, HIC 2014*, pp. 251–254, 2014.

[44] E. Georgakakis, S. A. Nikolidakis, D. D. Vergados, and C. Douligeris, "An analysis of Bluetooth, Zigbee and Bluetooth Low Energy and their use in WBANs," *Lecture Notes of the Institute for Computer Sciences, Social-Informatics and Telecommunications Engineering*, vol. 55 LNICST, pp. 168–175, 2011.

[45] K. Shahzad and B. Oelmann, "A comparative study of in-sensor processing vs. raw data transmission using ZigBee, BLE and Wi-Fi for data intensive monitoring applications," in *2014 11th International Symposium on Wireless Communications Systems, ISWCS 2014 - Proceedings*. IEEE, 2014, pp. 519–524.

[46] N. V. R. Kumar, C. Bhuvana, and S. Anushya, "Comparison of ZigBee and Bluetooth wireless technologies-Survey," in *2017 International Conference on Information Communication and Embedded Systems (ICICES)*, 2017, pp. 1–4.

[47] K. Ragavan, R. Ramalakshmi, V. SrirengaNachiyar, G. Priya, and K. Jeyageetha, "Smart health monitoring system in Intensive Care Unit using Bluetooth Low Energy and message queuing telemetry transport protocol," *2023 5th International Conference on Smart Systems and Inventive Technology (ICSSIT)*, no. Icssit, pp. 284–291, 2023.

[48] A. Ali, G. A. Shah, M. O. Farooq, and U. Ghani, "Technologies and challenges in developing Machine-to-Machine applications: A survey," *Journal of Network and Computer Applications*, vol. 83, no. September 2016, pp. 124–139, 2017.

[49] H. Hayat, T. Griffiths, D. Brennan, R. P. Lewis, M. Barclay, C. Weirman, B. Philip, and J. R. Searle, "The state-of-the-art of sensors and environmental monitoring technologies in buildings," *Sensors (Switzerland)*, vol. 19, no. 17, 2019.

[50] Y. Yang, Y. Wang, Y. Lin, and L. Jia, "IoT system for collecting vital signs and geographic location data of mobile users," in *Proceedings - 2020 International Conference on Communications, Information System and Computer Engineering, CISCE 2020*. Institute of Electrical and Electronics Engineers Inc., jul 2020, pp. 163–168.

[51] D. Rajamohanan, B. Hariharan, and K. A. Unnikrishna Menon, "Survey on smart health management using BLE and BLE beacons," in *Proceedings of the 2019 International Symposium on Embedded Computing and System Design, ISED 2019*. Institute of Electrical and Electronics Engineers Inc., dec 2019, pp. 169–173.

[52] J. Malwade, S. Sayyed, J. Nasir, Y. Parab, G. Narayanan, and S. Gupta, "Wireless stethoscope with Bluetooth technology," in *2020 International Conference on Computational Performance Evaluation, ComPE 2020*, 2020, pp. 168–172.

[53] S. Y. Lee, Y. W. Hung, P. H. Su, I. P. Lee, and J. Y. Chen, "Biosignal monitoring clothing system for the acquisition of ECG and respiratory signals," *IEEE Access*, vol. 10, pp. 66 083–66 097, 2022.

[54] L. De Vito, E. Picariello, F. Picariello, S. Rapuano, and I. Tudosa, "A prototype of a wearable health device for mobile telemonitoring applications," *2022 IEEE International Symposium on Medical Measurements and Applications, MeMeA 2022 - Conference Proceedings*, no. i, 2022.

[55] S. Di Pascoli, D. Puntin, A. Pinciaroli, E. Balaban, and M. Pompeiano, "Design and implementation of a wireless In-Ovo EEG/EMG recorder," *IEEE Transactions on Biomedical Circuits and Systems*, vol. 7, no. 6, pp. 832–840, 2013.

[56] B. L.-d. Liao, C.-t. Lin, K. McDowell, A. E. Wickednden, K. Gramann, T.-p. Jung, L.-w. Ko, and J.-Y. Chang, "Biosensor technologies for augmented Brain-Computer Interfaces

in the next decades," *Proceedings of the IEEE*, vol. 100, no. Special Centennial Issue, pp. 1553–1566, 2012.

[57] E. Spanò, S. Di Pascoli, and G. Iannaccone, "Low-power wearable ECG monitoring system for multiple-patient remote monitoring," *IEEE Sensors Journal*, vol. 16, no. 13, pp. 5452–5462, jul 2016.

[58] F. Rossi, A. Mongardi, P. M. Ros, M. R. Roch, M. Martina, and D. Demarchi, "Tutorial: A versatile bio-inspired system for processing and transmission of muscular information," *IEEE Sensors Journal*, vol. 21, no. 20, pp. 22 285–22 303, 2021.

[59] R. J. Vetter, J. C. Williams, J. F. Hetke, E. A. Nunamaker, and D. R. Kipke, "Chronic neural recording using silicon-substrate microelectrode arrays implanted in cerebral cortex," *IEEE Transactions on Biomedical Engineering*, vol. 51, no. 6, pp. 896–904, 2004.

[60] G. R. Müller-Putz, R. Scherer, C. Neuper, and G. Pfurtscheller, "Steady-state somatosensory evoked potentials: Suitable brain signals for brain–computer interfaces?" *IEEE Transactions on Neural Systems and Rehabilitation Engineering*, vol. 14, no. 1, pp. 30–37, 2006.

[61] C.-T. Lin, L.-W. Ko, J.-C. Chiou, J.-R. Duann, R.-S. Huang, S.-F. Liang, T.-W. Chiu, and T.-P. Jung, "Noninvasive neural prostheses using mobile and wireless EEG," *Proceedings of the IEEE*, vol. 96, no. 7, pp. 1167–1183, 2008.

[62] C.-T. Lin, L.-W. Ko, C.-J. Chang, Y.-T. Wang, C.-H. Chung, F.-S. Yang, J.-R. Duann, T.-P. Jung, and J.-C. Chiou, "Wearable and wireless Brain-Computer Interface and its applications," in *Foundations of Augmented Cognition. Neuroergonomics and Operational Neuroscience: 5th International Conference*, San Diego, CA, 2009, pp. 741–748.

[63] R. Martins, S. Selberherr, and F. Vaz, "A CMOS IC for portable EEG acquisition systems," in *IEEE Instrumentation and Measurement Technology Conference*, St. Paul, Minnesota, 1998, pp. 1406–1410.

[64] C. A. Chestek, V. Gilja, P. Nuyujukian, R. J. Kier, F. Solzbacher, S. I. Ryu, R. R. Harrison, and K. V. Shenoy, "HermesC : Low-power wireless neural recording system for freely

moving primates," *IEEE Transactions on Neural Systems and Rehabilitation Engineering*, vol. 17, no. 4, pp. 330–338, 2009.

[65] H. Miranda, V. Gilja, C. A. Chestek, K. V. Shenoy, and T. H. Meng, "HermesD : A high-rate long-range wireless transmission system for simultaneous multichannel neural recording applications," *IEEE Transactions on Biomedical Circuits and Systems*, vol. 4, no. 3, pp. 181–191, 2010.

[66] J. Xu, B. Busze, H. Kim, K. Makinwa, C. V. Hoof, and R. F. Yazicioglu, "A 60nV/$\sqrt{Hz}$ 15-channel digital active electrode system for portable biopotential signal acquisition," *Solid-State Circuits Conference Digest of Technical Papers (ISSCC), 2014 IEEE International*, pp. 424–426, 2014.

[67] Y. M. Chi, P. Ng, E. Kang, J. Kang, J. Fang, and G. Cauwenberghs, "Wireless non-contact cardiac and neural monitoring," in *Wireless Health 2010*, ser. WH '10. New York, NY, USA: Association for Computing Machinery, 2010, p. 15–23.

[68] Y.-T. Wang, Y. Wang, and T.-P. Jung, "A cell-phone-based brain–computer interface for communication in daily life," *Journal of Neural Engineering*, vol. 8, no. 2, p. 025018, mar 2011.

[69] T. Torfs, V. Leonov, R. F. Yazicioglu, P. Merken, C. Van Hoof, R. J. Vullers, and B. Gyselinckx, "Wearable autonomous wireless electro-encephalography system fully powered by human body heat," in *Proceedings of IEEE Sensors*, 2008, pp. 1269–1272.

[70] A. Riera, S. J. Dunne, A. Riera, S. Dunne, I. Cester, and G. Ruffini, "STARFAST: a wireless wearable EEG/ECG biometric system based on the ENOBIO sensor," *Proceedings of the International Workshop on Wearable Micro and Nanosystems for Personalised Health*, 2008.

[71] R. Matthews, P. J. Turner, N. J. Mcdonald, K. Ermolaev, T. M. Manus, R. A. Shelby, and M. Steindorf, "Real time workload classification from an ambulatory wireless EEG system using hybrid EEG electrodes," 2008, pp. 5871–5875.

[72] L. Brown, J. van de Molengraft, R. F. Yazicioglu, T. Torfs, J. Penders, and C. Van Hoof, "A low-power, wireless, 8-channel EEG monitoring headset," in *2010 Annual International Conference of the IEEE Engineering in Medicine and Biology*, 2010, pp. 4197–4200.

[73] R. Joaquinito and H. Sarmento, "A wireless biosignal measurement system using a SoC FPGA and Bluetooth Low Energy," in *IEEE International Conference on Consumer Electronics - Berlin, ICCE-Berlin*, vol. 2016-Octob. IEEE, 2016, pp. 36–40.

[74] E. Avşar and M. N. Mowla, "Wireless communication protocols in smart agriculture: A review on applications, challenges and future trends," *Ad Hoc Networks*, vol. 136, no. April, 2022.

[75] D. Berezhnoy, T. Bergaliyev, and S. Sakhno, "Application of the Bluetooth protocol for data transfer from computer to the brain in active BCI-interfaces and development of the small Bluetooth neural stimulation device," in *2020 International Conference Engineering and Telecommunication, En and T 2020*, 2020, pp. 15–17.

[76] P. J. Langlois, N. Neshatvar, and A. Demosthenous, "A sinusoidal current driver with an extended frequency range and multifrequency operation for bioimpedance applications," *IEEE Transactions on Biomedical Circuits and Systems*, vol. 9, no. 3, pp. 401–411, 2015.

[77] J. Xu, S. Mitra, A. Matsumoto, S. Patki, C. Van Hoof, K. A. A. Makinwa, and R. F. Yazicioglu, "A wearable 8-channel active-electrode EEG/ETI acquisition system for body area networks," *IEEE Journal of Solid-State Circuits*, vol. 49, no. 9, pp. 2005–2016, 2014.

[78] D. Naranjo-Hernández, J. Reina-Tosina, and M. Min, "Fundamentals, recent advances, and future challenges in bioimpedance devices for healthcare applications," 2019.

[79] D. Buxi, S. Kim, N. Van Helleputte, M. Altini, J. Wijsman, R. F. Yazicioglu, J. Penders, and C. Van Hoof, "Correlation between electrode-tissue impedance and motion artifact in biopotential recordings," *IEEE Sensors Journal*, vol. 12, no. 12, pp. 3373–3383, 2012.

[80] M. Zamani, Y. Rezaeiyan, O. Shoaei, and W. A. Serdijn, "A 1.55 μw bio-impedance measurement system for implantable cardiac pacemakers in 0.18 μm CMOS," *IEEE Transactions on Biomedical Circuits and Systems*, vol. 12, no. 1, pp. 211–221, 2018.

[81] S. Rodriguez, S. Ollmar, M. Waqar, and A. Rusu, "A batteryless sensor ASIC for implantable bio-impedance applications," *IEEE Transactions on Biomedical Circuits and Systems*, vol. 10, no. 3, pp. 533–544, 2016.

[82] "ISO 60601-1:2015. Medical electrical equipment — Part 1-11: General requirements for basic safety and essential performance." International Organization for Standarization, 2015.

[83] "ISO 62304:2006. Medical device software - Software life cycle processes." International Organization for Standarization, 2006.

[84] E. Alonso, R. Giannetti, C. Rodríguez-Morcillo, J. Matanza, and J. D. Muñoz-Frías, "A novel passive method for the assessment of skin-electrode contact impedance in intraoperative neurophysiological monitoring systems," *Scientific Reports*, vol. 10, no. 1, pp. 1–11, 2020.

[85] E. Alonso Rivas, G. Scandurra, C. Ciofi, C. Rodríguez-Morcillo García, and R. Giannetti, "A novel approach for the design of fast-settling amplifiers for biosignal detection," *Electronics (Switzerland)*, vol. 10, no. 21, pp. 1–14, 2021. [Online]. Available: https://doi.org/10.3390/electronics10212631

[86] E. Jiménez-Carles Gil-Delgado, "Intraoperative Monitoring System," Patent WO 2018/011 439 Al, 2018.